

Instituto Tecnológico y de Estudios Superiores de Monterrey

Campus Monterrey

School of Engineering and Sciences



**A New Methodology for Inverse Kinematics and Trajectory Planning of
Humanoid Biped Robots**

A dissertation presented by

Alejandro Rodríguez Said

Submitted to the
School of Engineering and Sciences
in partial fulfillment of the requirements for the degree of

Doctor of Philosophy

in

Information Technologies and Communications

Major in Electronic Systems

Monterrey, Nuevo León, May 21th, 2019

Declaration of Authorship

I, Alejandro Rodríguez Said, declare that this dissertation titled, A New Methodology for Inverse Kinematics and Trajectory Planning of Humanoid Biped Robots and the work presented in it are of my own. I confirm that:

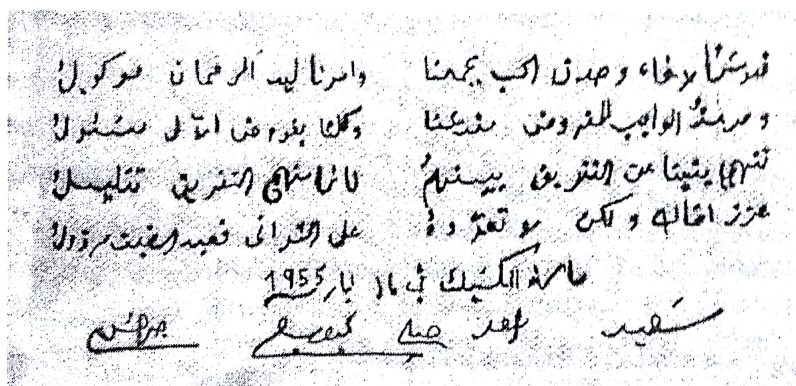
- This work was done wholly or mainly while in candidature for a research degree at this University.
- Where any part of this dissertation has previously been submitted for a degree or any other qualification at this University or any other institution, this has been clearly stated.
- Where I have consulted the published work of others, this is always clearly attributed.
- Where I have quoted from the work of others, the source is always given. With the exception of such quotations, this dissertation is entirely my own work.
- I have acknowledged all main sources of help.
- Where the dissertation is based on work done by myself jointly with others, I have made clear exactly what was done by others and what I have contributed myself.

Alejandro Rodríguez Said
Monterrey, Nuevo León, May 21th, 2019

©2019 by Alejandro Rodríguez Said
All Rights Reserved

Dedication

I want to dedicate this Dissertation to my friends who have been always there for me; to my professors who gave me all the knowledge I needed, and my parents for their moral and tireless support.



The sacred fraternity and the sincere love join us,
and our cause is entrusted to God.

And the inviolability of duty is our sanctuary,
and each one of us is responsible for the family commitments.

We prohibit the division among our children,
because the act of dividing is depreciating.

Support your brother but don't let him fall into laziness
because the slave of weakness is underestimated.

Roberto Said Lasserre.
México D.F., May 1955

Acknowledgements

I want to acknowledge the following people and institutions with whom I share this work.

- I want to thank Dr. Rogelio Soto for giving me the opportunity of studying a PhD, and believing in my intellect and knowledge. Also, for his unconditional academic support, as well as for managing the academic funding during my studies. I owe him the entrance to a new scientific world where I can now contribute for the rest of my life to transform the world I live in.
- I want to thank Dr. Ernesto Rodríguez Leal, for his support in the scientific publication process. Specially, due to his observations in the field of robotics and for sharing his experience in the English language and proof reading. I owe him the publication of my first scientific article.
- I want to thank Dr. José Luis Gordillo Moscoso, for sharing his knowledge in the field of robotics, as well as for his advice in the technical sessions. It is thanks to his perseverance that the mathematical procedures turned into real applications; and It is because of his devotion to do the things the right way, that my work accomplishes professional standards.
- I want to thank Dr. Leonardo Garrido Luna, for his support in the humanoid robotics laboratory, especially for his kindness in attending all of my needs regarding the experimentation platform. Thanks to his research team, I learned very important aspects about robot programming and operating systems.
- I want to thank Dr. Yasser Davizón Castillo for his help at reviewing my scientific work and for his valuable suggestions in the mathematical procedures.
- I want to thank Dr. Carlos Hernández Santos for his academic collaboration.
- I want to thank MSc. Héctor Colón for his friendship and for his advise where I found the moral support to finish this work.
- I want to thank my father and my mother for their endless love and understanding.
- I thank to Consejo Nacional de Ciencia y Tecnología (CONACYT), for his economic support which I used to sustain myself during the time I studied the PhD.
- I want to thank Tecnológico de Monterrey (ITESM) for giving me the necessary scholarship and economical support for studying the PhD, as well as all providing all academic resources I needed.
- I want to thank the Robotics Focus Group and the Laboratorio de Robótica del Área Noreste y Centro de México for their research funding, materials, books, and discussion meetings I needed to carry on this project.

A New Methodology for Inverse Kinematics and Trajectory Planning of Humanoid Biped Robots

by

Alejandro Rodríguez Said

Abstract

This dissertation presents a new methodology for Inverse Kinematics and Trajectory Planning for small-sized humanoid biped robots. Regarding the Inverse Kinematics, this study presents an explicit, omnidirectional, analytical, and decoupled closed-form solution for the lower limb kinematics of the humanoid robot NAO. It starts by decoupling the position and orientation analysis from the concatenation of Denavit-Hartenberg (DH) transformation matrices. Here, the joint activation sequence for the DH matrices is mathematically constrained to follow the geometry of a triangle. Furthermore, the implementation of a forward and a reversed kinematic analysis for the support and swing phase equations is developed to avoid the complexity of matrix inversion. The allocation of constant transformations allows the position and orientation end-coordinate systems to be aligned with each other. Also, the redefinition of the DH transformations and the use of constraints allows for the decoupling the shared Degree of Freedom (DOF) located between the legs and the torso; and which activates the torso and both of the legs when a single actuator (the *hip-yaw* joint) is activated. Furthermore, a three dimensional geometric analysis is carried out to avoid the singularities during the walking process. Numerical data is presented along with experimental implementations to prove the validity of the analytical results.

In relation to the trajectory planning, a method taken from manipulator robot theory is applied to humanoid walking. Fifth and seventh order polynomials are proposed to define the trajectories of the Center of Gravity (CoG) and the swing foot. The polynomials are designed so that the acceleration and jerk are constrained to be zero particularly at two moments: at the single support phase (when the robot is standing on a single foot), and at the foot landing (to prevent foot-to-ground impacts); thus, minimizing internal disturbance forces. Computer simulations are performed to compare the effects of the acceleration and jerk constraints.

In addition, the basics of the future work is given by providing a control model for robot equilibrium. First, the analysis of this model starts with a static equilibrium model which reacts to an ankle perturbation by using a hip actuation. Second, a dynamic model is proposed which incorporates the ground perturbations into the robot model by representing the ground tilt as an additional, passive, and redundant DOF located at the ankle. This procedure allows for two separate models (the one corresponding to the humanoid and the one corresponding to the ground) to be accounted into a single model, thus, minimizing complexity.

List of Figures

1.1	The robot NAO	1
1.2	Humanoid walking layer hierarchy	6
2.1	General manipulator having the last three revolute axes intersecting	9
2.2	Structure of a complex anthropomorphic kinematic chain	10
2.3	Area of allowable positions of ZMP in both: single support phase (solid contour) and double-support phase (shaded area)	10
2.4	Reduced problem: A two-link planar leg	11
2.5	Left: The joints of NAO. Right: The navigation coordinate system used in Graf et al. (2009)	12
2.6	Average fitness and maximum fitness during 28 generations	13
2.7	Kinematic configuration of the robot leg described by Hernández-Santos	13
2.8	Right leg inverse kinematics	14
2.9	Right leg of a HUBO KHR-4 robot. (a) Forward decoupling, (b) Reverse Decoupling	15
2.10	A HUBO KHR-4 humanoid robot	15
2.11	Link coordinate frames of the right leg of a Hubo KHR-4 robot	16
2.12	Using geometry in the triangle formed by the robot leg to derive the knee joint angle	16
2.13	Paths generated by the robot using two different ANNs.	18
2.14	Simple symmetric simulations without reaching singularities.	18
2.15	Front view of the right ankle joint.	19
2.16	A prototype of dual-arm robot with two decoupled manipulators.	20
2.17	Definition of Zero-Moment Point (ZMP)	21
2.18	Support leg exchange with a constant vertical distance	22
2.19	Walking pattern on flat floor based on 3D linear inverted pendulum	22
2.20	Coordinate frame gate trajectory	23
2.21	Controller block diagram for trajectory implementation	24
2.22	Swing-foot trajectory based in a cosine function	25
2.23	CoM trajectory consisting of a merging of a sine function $s(\varphi)$, the square root of a sine function $r(\varphi)$ and a linear function $l(\varphi)$	25
2.24	Cross section of the coordinate system used for the altered inverted pendulums	26
2.25	Two facing inverted pendulums	27
2.26	The inverted pendulum attached on a simulated model of the NAO. The red square indicates the plain on which the center of mass moves. The red dot is located in the position of the center of mass	27

2.27	Parameters used in the trajectory periodic functions	28
2.28	CoM up and down motion during walking	29
2.29	CoM up and down motion during walking	30
2.30	Cubic polynomial trajectory for the swing-foot.	30
2.31	Foot trajectory with respect to the world coordinate system.	31
2.32	Velocity recovery process.	32
3.1	Active joints of H21 NAO Robot	33
3.2	Sequence of joint activations in the forward analysis based in the triangular geometry	35
3.3	Forward position analysis of the humanoid leg	36
3.4	Forward orientation analysis of the humanoid leg	38
3.5	Sequence of joint activations in the reversed analysis based in the triangular geometry	39
3.6	Reversed position and orientation analysis of the humanoid leg	40
3.7	Turn-in-place movement orientation analysis	41
3.8	Position and orientation of the robot feet at the turn-in-place rotation	44
3.9	Geometric analysis in the estimation of the humanoid step size	45
3.10	Maximum theoretical distance z for a desired step size	46
3.11	Maximum practical distance z for a desired step size	46
3.12	Forward walking postures	50
3.13	Lateral walking postures	51
3.14	Turn-in-place walking postures	52
4.1	Position and acceleration of a sinusoidal CoG y -axis trajectory	55
4.2	Position of a sinusoidal CoG y -axis trajectory and a cycloidal-like swing-foot z -axis trajectory	55
4.3	Acceleration-constrained position trajectories for the CoG in the x and y axes	58
4.4	Acceleration-constrained trajectories: $y - axis$ (CoG) trajectory and $z - axis$ (swing-foot) trajectories	59
4.5	Acceleration profile of the acceleration-constrained CoG trajectory in the y -axis	60
4.6	Jerk profile of the acceleration-constrained CoG trajectory in the y -axis	61
4.7	Acceleration profile of the acceleration-constrained swing-foot trajectory in the z -axis	62
4.8	Jerk profile of the acceleration-constrained swing-foot trajectory in the z -axis	62
4.9	Jerk-constrained trajectories for the CoG in the x and y axes	65
4.10	Jerk-constrained trajectories: $y - axis$ (CoG) trajectory and $z - axis$ (swing-foot) trajectories	66
4.11	Acceleration profile of the jerk-constrained CoG trajectory in the y -axis	66
4.12	Jerk profile of the jerk-constraint CoG trajectory in the y -axis	67
4.13	Acceleration profile of the jerk-constrained swing-foot trajectory in the z -axis	67
4.14	Jerk profile of the jerk-constrained swing-foot trajectory in the z -axis	68
4.15	y -axis CoG trajectories	69
4.16	z -axis swing trajectory of the right foot	69

5.1	Static control model based on the double inverted pendulum with a hip strategy control	74
5.2	Dynamic control model based on the double inverted pendulum with a hip and ankle strategy control	75
A.1	Link and articulation nomenclature	77
A.2	Frame convention	78
A.3	Frame assignment	79
A.4	Planar geometry associated with a 3 DOF robot	83
A.5	Free motion	84
A.6	Joint Space Trajectory	85
A.7	(a) Cubic polynomial trajectory (b)Velocity profile (c) Acceleration profile . .	87
A.8	(a) Quintic polynomial trajectory (b)Velocity profile (c) Acceleration profile .	89

List of Tables

3.1	Joint motion ranges	34
3.2	Limb dimensions [mm]	34
3.3	Link parameters used in the forward position analysis	35
3.4	Link parameters used in the forward orientation analysis	37
3.5	Link parameters used for a turn-place movement	41
3.6	Forward walking end-effector coordinates (mm)	47
3.7	Forward walking angles (rad)	48
3.8	Lateral walking end-effector coordinates (mm)	48
3.9	Lateral walking angles (rad)	49
3.10	Turn-in-place coordinates (mm)	49
3.11	Turn-in-place angles (rad)	49
4.1	Initial and final time of the CoG walking stages	57
4.2	Acceleration-constrained coefficients for the CoG y-axis trajectory	57
4.3	Acceleration-constrained coefficients for the CoG x-axis trajectory	58
4.4	Initial and final times of the swing-foot walking stages	59
4.5	Acceleration-constrained coefficients for the swing-foot z-axis trajectory	60
4.6	Jerk-constrained coefficients for the CoG y-axis trajectory	64
4.7	Jerk-constrained coefficients for the CoG x-axis trajectory	64
4.8	Jerk-constrained coefficients for the swing-foot z-axis trajectory	65
A.1	Link parameters of a 3DOF mechanism	78

Contents

Abstract	v
List of Figures	viii
List of Tables	ix
1 Introduction	1
1.1 Motivation	4
1.2 Problem Statement	6
1.2.1 The Inverse Kinematic problem	6
1.2.2 The Trajectory Planning problem	7
1.3 Objectives	7
1.3.1 General Objectives	7
1.3.2 Particular Objectives	7
2 State of the Art on Humanoid Robotics	9
2.1 The State of the Art on Humanoid Inverse Kinematics	9
2.2 The State of the Art in Humanoid Trajectory Planning	21
3 Humanoid Inverse Kinematics	33
3.1 Joint and Dimension Nomenclature	33
3.2 Direct and Inverse Kinematics in the Forward Analysis	34
3.3 Direct and Inverse Kinematics in the Reversed Analysis	39
3.4 Turn-In-Place Analysis	41
3.5 Analysis of the Workspace of a Humanoid Step	45
3.6 Inverse Kinematics Experimentation	47
4 Humanoid Trajectory Planning	53
4.1 Acceleration and Jerk Constraints in Humanoid Trajectory Planning	53
4.2 Fifth order polynomial: Acceleration-constrained Humanoid Trajectories	56
4.3 Seventh-order Polynomials: Jerk-constrained Humanoid Trajectories	63
4.4 Comparison of the fifth-ordered and seventh-order polynomials	68
5 Conclusions and Future Work	70
5.1 Conclusions	70

5.2	Contrast of the Related Work in Humanoid Kinematics and Trajectory Planning	72
5.3	Future Work	73
5.3.1	Static Control Model for Humanoid Equilibrium	73
5.3.2	Dynamic Control Model for Humanoid Equilibrium with Ground Perturbations	74
A	Background Theory	76
A.1	Manipulator Kinematics	76
A.1.1	Direct Kinematics	77
A.1.2	Inverse Kinematics	79
A.2	Trajectory Planning	84
A.2.1	Cubic Polynomial Trajectories	85
A.2.2	Quintic Polynomial Trajectories	88
B	The Jacobian in Robotics	90
B.1	Inverse Kinematics Iterative Technique based in the Jacobian	90
	Bibliography	95

Chapter 1

Introduction

Humanoid robotics has become a highly important subject for the academic community in recent years due to its potential use in domestic, medical and industrial applications. Several sophisticated humanoid robots have been developed; for example, the ASIMO robot [Sakagami et al. (2002)], created by the Honda Motor Company; the QRIO robot [Ishida (2004)], manufactured by Sony; the HUBO robot [Park et al. (2012)], proposed by KAIST; and lastly, the Atlas robot designed by Google. On the other hand, although small-sized robots are provided with simpler actuation mechanisms, there is an increasing trend in their development because they are an accessible experimentation platform for students, researchers and hobbyists. There are some examples of this kind of robots: the DARwIn-OP [Robotis (2016)], manufactured by Robotis and the NAO robot [Aldebaran (2010)], created by Aldebaran Robotics (see Fig.1.1).

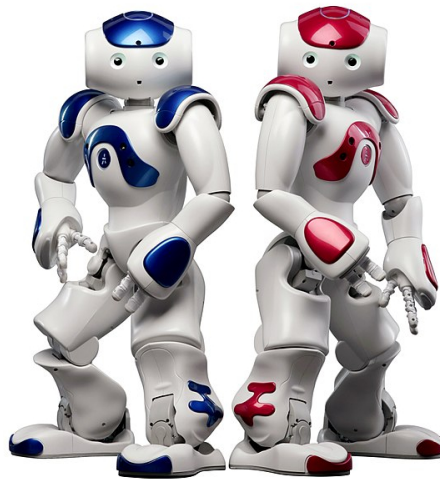


Figure 1.1: The robot NAO

It is well-known in literature that legged locomotion provides several advantages when compared to wheeled locomotion; for example, the length of the legs can be varied to match the surface geometry [Todd (2013)]. However, the design of complex dynamic motions for humanoids, is only achievable through the full understanding of kinematics [Kofinas et al. (2013)]; namely, the Forward and Inverse Kinematics. The first concept concerns with the determination of the position and orientation of the end-effector when the joint configurations are given; the second concept deals with the determination of the joint variables for a particular position and orientation of the end effector [Spong et al. (2006)].

In this study, new methodologies for the Inverse Kinematics and Trajectory Planning are proposed where the NAO robot is used as experimentation platform. Regarding the Inverse Kinematics, the Denavit-Hartenberg (DH) technique is used along with a geometrical procedure based in triangular arrangements to find a closed-form solution for the humanoid lower limb kinematics. This new procedure allows for the conciliation of both methods where simple solutions can be obtained for robot position and orientation. In particular, the mathematical decoupling of the joint shared by the two legs [Gouaillier et al. (2009)] is achieved. To accomplish this, the sequence of joint activations obtained by the geometrical procedure, is imposed to the DH approach. Furthermore, a local coordinate system is placed in the end effector (either the hip or the foot). This allows for the suppression of matrix inversion by solving the kinematic chain in forward and reversed orders as first shown in [Park et al. (2012)]. The insertion of constant DH matrices, allows for the end-effector coordinate systems of the foot and hip to be aligned with the navigation reference system of the robot, and allow for the DH joint activation sequence to coincide with the geometrical one. Finally, the motion constrains performed in the DH kinematic chains, allow for decreasing the mathematical complexity of the mechanical coupling, such that the humanoid is able to achieve the *turn-in-place* motion (as described in [Abdolmaleki et al. (2011)]), by using the proposed analytical method.

To deal with the challenges above described regarding the Inverse Kinematics, some authors have proposed different approaches. Donald Pieper in his PhD thesis [Pieper (1968)], has described a method to solve the configuration of robot chains, where in the special case of having three intersecting axes, the kinematics involves a reduced number of variables. Although the work of Donald Pieper is not concerned with humanoid robotics directly, his findings have helped in the analysis of humanoid robotic links. In addition, Miomir Vukobratović in [Vukobratovic et al. (1990)] described the humanoid kinematics for the first time introducing some important terms, such as the *Single Support Phase* and the *Double Support Phase*, which refer to the walking positions where the robot is standing over a single foot or both feet, respectively.

Some authors have proposed geometric approaches to deal with the direct decoupling of the position and orientation of the foot, such as Zannatha in [Zannatha and Limón (2009)] and Colin Graf in [Graf et al. (2009)] where the last author proposed to use a triangular arrangement along with a virtual ankle yaw joint to find the solution of the Inverse Kinematics of a humanoid leg; however, purely geometrical approaches miss out the advantages of the DH systematic procedures.

Some other authors have proposed the use of Artificial Intelligence; for example, Abbas Abdolmaleki in [Abdolmaleki et al. (2011)] has used Genetic Algorithms to achieve the turn-in-place movement where he optimized human data analyzed by the Fourier series; and Ahmed R. J. Almusawi in [Almusawi et al. (2016)] has used Neural Networks to learn robot

system characteristics and solve for the inverse kinematics of a 6 DOF robot arm.

Hernández-Santos in [Hernández-Santos et al. (2012)] has divided the humanoid body in frontal and sagittal and frontal planes and has designed a foot with a toe to provide for Inverse Kinematics redundancy. Hyungju Andy Park in [Park et al. (2012)] has solved the Inverse Kinematics of a humanoid leg by using the DH technique in the forward and reverse orders, which has allowed to obtain the position and orientation solution of the movement of the foot and the hips. Nicolaos Kofinas in [Kofinas et al. (2013)] and [Kofinas et al. (2014)] has used several techniques together such as: matrix elimination, manipulation of both sides, constant matrices and geometric approaches to solve for humanoid kinematics. Salman Faraji in [Faraji and Ijspeert (2017)] has analyzed the singularities when the hip, knee and ankle joints are aligned. Kenji Kaneko in [Kaneko et al. (2019)] have expanded the actuation range of the ankle joints, and Jiangping Wang in [Wang et al. (2019)] has proposed dual robotic arm with orientation constraints.

Regarding the trajectory planning of a humanoid robot; one of the main concerns, is how to move the Center of Gravity (**COG**, described in [Kaynov (2010)]) to accomplish the walking motion. The inverted pendulum model has been extensively used to achieve this kind of movement, as mentioned in [Kajita et al. (2002)]; however, one of the main drawbacks of this model, is the limitation of the step size. In this study, fifth and seventh order polynomials [Spong et al. (2006)] are proposed to define the trajectories of the center of gravity and the swing foot, (in the y -axis and the z -axis respectively). The polynomials are designed so that the acceleration and jerk are constrained to have zero value at the single support phase (the most unstable walking stage of the robot); and at the foot landing in order to minimize the impact of the foot on the ground [Kim et al. (2007)], thus, minimizing internal disturbances. The zero-acceleration (fifth polynomial) and the zero-jerk (seventh polynomial) trajectory profiles are compared and verified by means of computer simulations.

To deal with the design of the humanoid trajectory of the COG, some authors have proposed some concepts and techniques. For example, Miomir Vukobratović has defined the **ZMP** (*Zero Moment Point*) which refers to the point where the sum of all of the forces have a zero moment or torque. Shuuji Kajita in [Kajita et al. (2002)], has demonstrated that when the robot is standing over a single foot, its predominant dynamics can be modeled as a 3D linear inverted pendulum which connects the supporting foot with the **CoM** (Center of Mass). Later, in [Kajita et al. (2003)], the concept of ZMP was introduced into the inverted pendulum model to create a walking patten generator.

Ill-Woo Park in [Park et al. (2006a)] has proposed a cycloid function for the swing foot trajectory and a third degree polynomial for the movement of the CoG. A mixture of a sinusoid, a triangular wave and the square root of a sinusoid for the trajectory planning of the CoG have been proposed by Colin Graf in [Graf et al. (2009)]. Furthermore, the equations of the 3D inverted pendulum have been applied to design the CoG trajectory of the Robot NAO in [Graf and Röfer (2010)]. Hernández-Santos in [Hernández-Santos et al. (2012)] has used local sinusoidal functions over separated frontal and sagittal planes to guide the trajectory of humanoid lower-limb joints and links. Ren C. Luo in [Luo et al. (2013)] has designed a quasi-natural foot gate generator by varying the height of the CoG. Tzue-Hseng in [Li et al. (2017)] has provided for a foot trajectory in the swing phase using sections of sinusoidal functions. Chengju Liu, in [Liu et al. (2019)], has proposed a foot position compensator based in the

Lyapunov function to recalculate the CoM trajectory.

Finally, as part of the future research, static and dynamic robot models for Equilibrium Control have been developed. The static control model provides for a simple intuitive idea to know the limits for humanoid equilibrium. Here, inertial forces and ground perturbations have been neglected. On the other hand, the dynamic model mathematically describes the rotation of the robot about the ground by making use of the *IMU* (Inertial Measure Unit) readings and assuming that the foot height is negligible. This dynamic model considers the surface tilt disturbance as an additional sub-actuated D.O.F. belonging to the robot itself, thus, allowing for the external equilibrium disturbances to be included into the robot model in order to avoid the modeling of two separate subsystems, namely: the robot and the surface.

The remainder of the document is organized as follows: Chapter 1, Section 1.1, presents the motivation to develop this work, including the way it is subdivided. Section 1.2 expose the principal challenges related to the most representative state of the art. Section 1.3 declares the objectives to be reached in this study. In Chapter 2, the most relevant work is referenced. Section 2.1 cites the state of the art regarding the humanoid kinematics and Section 2.2 show the work related to humanoid trajectory planning. In Chapter 3 the mathematical approach to find the solutions for the new proposal of humanoid kinematics is presented. Section 3.2 presents the direct and inverse kinematics solution in the forward direction (i.e., the hip as seen by the base reference system at the ankle). Section 3.3 analyzes the direct and inverse kinematics in the reversed order (i.e., the ankle as seen as the base reference system at the hip). Section 3.4 reveals the analytical method to archive the rotation of the humanoid with respect the vertical axis; i.e., the turn-in-place motion. Section 3.5 analyzes the reachable workspace regarding humanoid walking, considering joint mechanical limitations. Section 3.6 shows the actual Cartesian end-effector coordinates and inverse kinematics angles that were loaded into robot NAO to validate the mathematical procedures; as well as pictures showing the walking postures. Chapter 4 presents the CoM and swing-foot trajectories proposed for humanoid robots. Section 4.2 exhibit the acceleration-constrained trajectories and Section 4.3 expose the jerk-constrained trajectories; then a comparison is given in Section 4.4. Finally, the conclusions are carried out in Chapter 5. Section 5.1 performs an analysis of the main contributions, Section 5.2 contrast the literature review with the present studies, and Section 5.3 suggest static and dynamic equilibrium control models. Additionally, Appendix A includes the background theory regarding robot kinematics, and Appendix B covers the theory of the matrix Jacobian.

1.1 Motivation

Regarding the Inverse Kinematics, although the Denavit-Hartenberg procedure has been extensively used, very often this method is so complicated that many authors prefer to find the solution by geometrical methods. However, is difficult for the geometrical procedures to be solved systematically. The motivation for this research work is to find a new method that combines the best of both worlds: the DH analytical approach and the geometrical one to find simple solutions. In addition, given the particular configuration of the hip joints of the NAO robot (where it is impossible to command a rotation for the hip joint without causing a torso

movement); the motivation is to find a mathematical way to correct this undesirable movement by performing an analytical compensation in the torso in order to correct the undesired pitch movement at the hip caused by the hip-yaw configuration. Here, a suitable pitch movement in the hip makes to look the torso and the hip to function independently although they are interrelated. This is possible because the entire kinematic system is available, and assuming that the hip-yaw movement is not necessary to perform neither the forward nor the lateral walking, some constraints were able to be made to achieve the turn-in-place motion using an analytical method.

Regarding the trajectory planning, although polynomial trajectories have been proposed in former studies, none of them compares the zero-acceleration and the zero-jerk trajectories. This analysis is particularly important to the swing movement because although the cycloidal trajectory has been proposed by some authors and claimed that it has a soft start and a soft end, this assumption relies on instantaneous velocity of the foot and not in the trajectory shape. It is obvious that the cycloidal function is discontinuous at the start and end points meaning that it has an intrinsic infinite velocity, acceleration, jerk, and *n-derivative* profile; for which in this case, it can be demonstrated mathematically that a higher-degree polynomial trajectory has a better performance.

Lastly, a dynamic control model is proposed as a future work to keep the equilibrium of the humanoid. It consists of integrating the dynamic model of the ground into the robot model itself. The motivation of this idea is to simplify the equilibrium control model of the robot by mathematically describing the ground perturbation as an additional sub-actuated robot joint.

Another motivation to state the structure of this dissertation, is the distinction among the topics regarding the humanoid walking: Inverse Kinematics, Trajectory Planning and Equilibrium Control. It is common to find in literature that these topics are presented in an interlaced manner which may complicate the understanding of the people once they are newly interested in humanoid robotics. In this study, the main logic is as follows: The Equilibrium Control is a Trajectory Planning modifier which adjusts the robot trajectory to preserve the equilibrium. However, in order to make the robot to follow a certain trajectory, the Inverse Kinematics is necessary to guide the robot end-effectors through the desired trajectory. In other words, there is a hierarchy as can be seen in Fig. 1.2 where the most important layer is the Inverse Kinematics layer, because without the Inverse Kinematics, the robot cannot simply move, whereas by guiding the robot with smooth movements over a perfectly flat surface, the Trajectory Planning design and the Equilibrium Control could be omitted. The proposal of a specific shape for the trajectory planning curves helps to increment the walking velocity, whereas the Equilibrium Control deals with the unexpected disturbances.

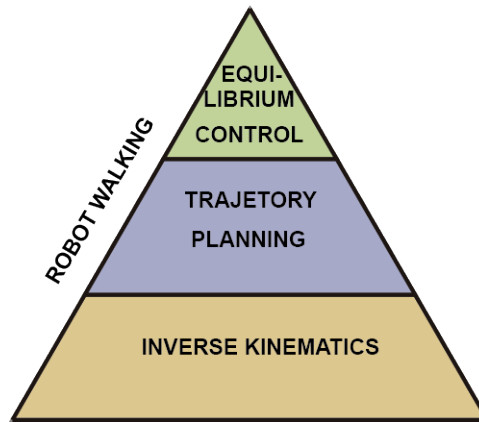


Figure 1.2: Humanoid walking layer hierarchy

1.2 Problem Statement

1.2.1 The Inverse Kinematic problem

One of the main problems about Inverse Kinematics, is the mathematical complexity to obtain closed-form analytic solutions. In general, closed-form solutions can only be obtained for 6 or less than 6-degree-of-freedom (DOF) systems with a specific structure [Ho et al. (2012)]. The computation of closed-form solutions require the performance of complex algebraic and geometric tasks, where the challenge consists in finding the configurations in which a reduced number of unknowns can be used to express the position and orientation of the end effector [Siciliano et al. (2009)]. Analytical solutions are preferred to numerical ones for real-time control applications because they are fast and reliable [Ho et al. (2012)]. A numerical method may use of the Jacobian matrix (see Appendix B), but common problems such as singularity, redundancy and computational complexity are the main drawbacks of using the inverse Jacobian matrix approach. Since the Jacobian method is velocity based instead of being position based, significant accumulation of error in position can result due to the iterative nature of the algorithm. Furthermore, the Jacobian matrix is singular when a limb of the humanoid robot is in a fully stretched position [Park et al. (2012)]; therefore, numerical methods may fail even if a solution exists [Kofinas et al. (2014)]. Another commonly adopted method for Inverse Kinematics is the geometric method [Graf et al. (2009); Zannatha and Limón (2009)]; however, the geometric method requires geometric intuition in solving the joint solution of a manipulator, and it may become more difficult to obtain the joint solution when more than five joints are involved [Park et al. (2012)].

Regarding the inverse kinematic problem, this work, aims to find analytic equations capable of making the humanoid robot reach a desired position and orientation in a fast and reliable manner in the walking process. The difference with previous works is that it inserts the geometrical inverse kinematics procedure into the DH method to find compact solutions. In addition, it finds an analytical hip compensation to undo the undesired hip yaw-pitch actuation due to the coupled joint; this is achieved by redefining and constraining the orientation matrix concatenations regarding the hip orientation.

1.2.2 The Trajectory Planning problem

There exist many kinds of planned trajectories in humanoid robotics; i.e., a series of points describing how a specific humanoid part must move in order to accomplish the walking process. Particularly, there are two trajectories of interest in the humanoid walking: the CoG and the swing-foot trajectories. In relation to the CoG trajectory, one of the most intuitive approach is based in sinusoidal functions and their variations, as can be seen in some works [Graf et al. (2009); Tay (2009)]. In addition, the inverted pendulum model has been described in [Kajita et al. (2014,0)] to model the trajectory of the CoG. Regarding the trajectory planing of the swing-foot, the cycloidal function has been used in some works [Olvera et al. (2009); Park et al. (2006a); Strom et al. (2010)]. The main feature of the cycloidal function is a slow start, a fast moving, and a slow stop; thereby reducing the speed burden of the actuators. However, there exist some disadvantages regarding the mentioned trajectories. For example, the main disadvantage of the trajectory planning based in sinusoidal functions, is that they have a maximum absolute value of acceleration in their crests and troughs. If this kind of movement is implemented for the CoG; then, a considerable acceleration will be present in the least-stable walking stages of the humanoid; i.e., when the robot is in the *single support phase* [Vukobratovic et al. (1990)], that is, when it is standing in a single foot. Moreover, if the inverted pendulum model is used; then, the limitation in the step size of the humanoid is the main drawback because it requires the double support phase to tend to a zero duration. In addition, if cycloidal functions are used, then, they must be restricted regarding velocity at the start and stop points, where the derivatives are infinite and may cause undesirable foot-to-ground impacts, and thus, robot imbalance.

1.3 Objectives

1.3.1 General Objectives

To provide a new mathematical procedure for the walking process of humanoid robots. These procedures include the analytical solution of the Inverse Kinematics of the lower limbs and the trajectory planning for the feet and the CoG.

1.3.2 Particular Objectives

The particular objectives can be summarized as follows:

1. To solve for the lower-limb Inverse Kinematics of a small-sized humanoid robot by providing analytic closed-form solutions.
 - (a) To conciliate both: the geometrical and the Denavit-Hartenberg procedures by inserting the sequence of joint activations provided by the geometrical arrangements (which are based on the shape of the triangle), into the DH matrices.
 - (b) To use constant transformation matrices to ensure the correct sequence of joint activations. Moreover, to use the constant transformations to align the coordinate systems of the end-effectors of the hip and the ankle with the navigation coordinate system of the robot.

- (c) To perform a forward kinematic analysis (which starts at the ankle and finishes at the hip), and a reversed kinematic analysis (which starts at the hip and finishes at the ankle) to avoid the mathematical complexity of matrix inversion.
 - (d) To manipulate the DH matrices by using a reduced number of unknowns to mathematically decouple the movement of the actuator shared by the two legs at the hip.
 - (e) To provide a simple three-dimensional geometric approach to avoid singularities in the walking process.
2. To provide functions for humanoid trajectories with zero-acceleration and zero-jerk at their end-points in order to restrict internal forces due to the presence of acceleration at the most unstable walking stages; and thus, contribute to robot equilibrium.
 - (a) To provide for polynomial CoG functions restricted to zero-acceleration at their end-points, in order minimize the internal disturbance forces at the single support phase.
 - (b) To provide for polynomial CoG functions restricted to zero-jerk at their end-points, in order minimize the internal disturbance forces at the single support phase.
 - (c) To provide for polynomial swing-foot functions restricted to zero-acceleration at their end-points, in order minimize the internal disturbance forces at foot landing.
 - (d) To provide for polynomial swing-foot functions restricted to zero-jerk at their end-points, in order minimize the internal disturbance forces at foot landing.
 - (e) To compare both: the effects of zero-acceleration versus zero-jerk trajectories for CoG and swing foot trajectories.
3. As a future work, to propose for a simple and efficient control model for humanoid robot equilibrium.
 - (a) To propose a dynamic hip and ankle control model to compensate for ground perturbations.
 - (b) To simplify the mathematical model of the ground perturbation by including it into the same robot model as an additional under-actuated D.O.F.

Chapter 2

State of the Art on Humanoid Robotics

This section presents the most relevant works about Inverse Kinematics, Trajectory Planning, and Balance Control that have been published regarding Humanoid Robotics and its related fields.

2.1 The State of the Art on Humanoid Inverse Kinematics

1968 Donald Lee Pieper, *The Kinematics of Manipulator under Computer Control*, Pieper (1968).

1. Several solutions are presented to the problem of finding the manipulator configuration leading to a specified position and orientation.
2. In the special case where the last three joints are revolute and their axes intersect, their point of intersection is only a function of the motion of the first three joints and the constant link parameters (see Fig. 2.1).

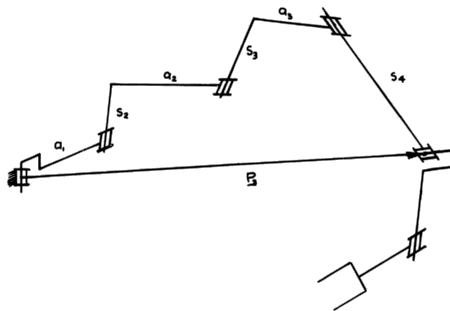


Figure 2.1: General manipulator having the last three revolute axes intersecting

1990 Miomir Vukobratović, *Biped Locomotion: Dynamics, Stability, Control and Application*, Vukobratovic et al. (1990)

1. The kinematics and dynamics of Humanoid Robots are first described. The structure of and anthropomorphic active mechanism is a complex kinematic chain, thus, it is partitioned into three kinematic chains. The first chain represents the legs; the second, the upper part of the body; and third, the hands. See Figure 2.2.
2. The *Single-support phase* and the *Double-support phase* are defined. When the robot is supported on one leg, the situation is recognized as single-support phase; and when both feet are on the ground, as double-support phase. See Fig. 2.3.

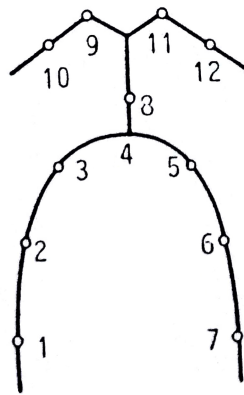


Figure 2.2: Structure of a complex anthropomorphic kinematic chain

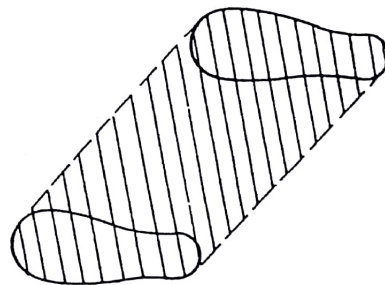


Figure 2.3: Area of allowable positions of ZMP in both: single support phase (solid contour) and double-support phase (shaded area)

2009 Ibarra Zannatha et. al., *Forward and Inverse Kinematics for a Small-sized Humanoid Robot*, Zannatha and Limón (2009).

1. A geometrical approach is presented to solve the Inverse Kinematics of a small-sized humanoid robot whose offset at the ankle joint prevents the direct decoupling of the position and orientation of the foot. Even for singularity-free mechanisms, the presence of some kinematic parameters (like offsets), prevents direct decoupling of the position and orientation in the inverse kinematics problem.

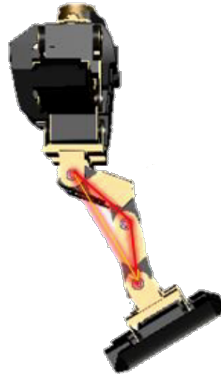


Figure 2.4: Reduced problem: A two-link planar leg

2009 Colin Graf et. al., *A Robust Closed-Loop Gait for the standart platform League Humanoid*, Graf et al. (2009).

1. A solution to the Inverse Kinematics of robot NAO is presented. Here, a geometrical approach is used to form triangular arrangements with the limbs of the leg. See Eqns. 2.1, 2.2, 2.3, 2.4, 2.5 and 2.6; where γ stands for the interior angle of the triangle formed by the thigh (upper leg) and the tibia (lower leg).
2. The computation assumes that there is an independent hip yaw joint for each leg, and leads to different computation values for the hip yaw joints of the left and right legs. Only one leg can realize the desired target. Normally, for stability, the support leg is supposed to reach the target.
3. A virtual foot yaw joint at the end of the kinematic chain of the leg was introduced to make the five-variable system reach a 6 DOF pose.

$$\gamma = \arccos \frac{l_{upperLeg}^2 + l_{lowerLeg}^2 - l_{trans}^2}{2 \cdot l_{upperLeg} \cdot l_{lowerLeg}} \quad (2.1)$$

$$\delta_{knee} = \pi - \gamma \quad (2.2)$$

$$\delta_{footPitch1} = \arccos \frac{l_{upperLeg}^2 + l_{lowerLeg}^2 - l_{trans}^2}{2 \cdot l_{lowerLeg} \cdot l_{trans}} \quad (2.3)$$

$$\delta_{footPitch2} = \arctan 2(x, \sqrt{y^2 + z^2}) \quad (2.4)$$

$$\delta_{footPitch} = \delta_{footPitch1} + \delta_{footPitch2} \quad (2.5)$$

$$\delta_{footRoll} = \arctan 2(y, z) \quad (2.6)$$

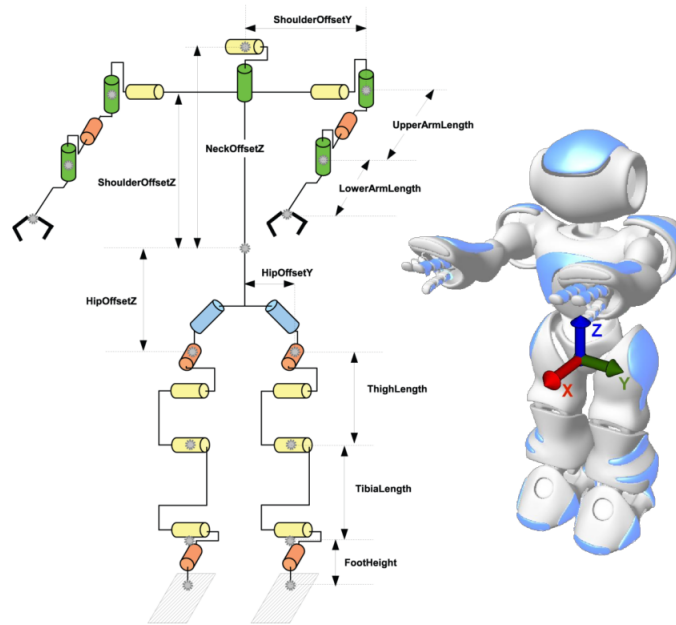


Figure 2.5: Left: The joints of NAO. Right: The navigation coordinate system used in Graf et al. (2009)

2011 Abbas Addolmaleki et. al., *Robust humanoid Turning - In - Place Using Fourier Series And Genetic Algorithm*, Abdolmaleki et al. (2011).

1. Data is captured from the human motion, and then modified to be applied to the humanoid robot. The data is analyzed using Fourier series and then, Fourier parameters are optimized using genetic algorithms.

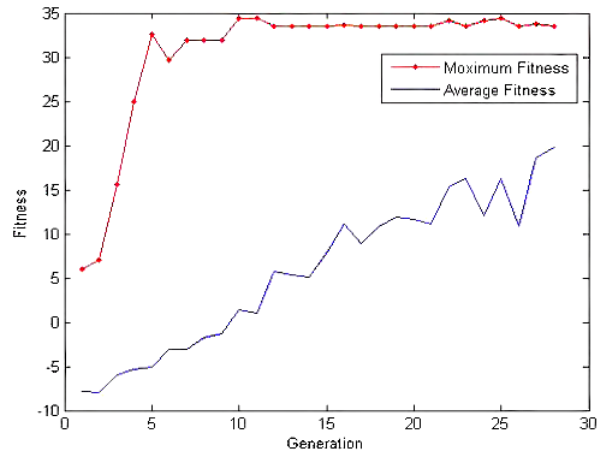


Figure 2.6: Average fitness and maximum fitness during 28 generations

2012 C. Hernández-Santos et. al., *Kinematics and dynamics of a new 16 DOF humanoid biped robot with active toe joint*, Hernández-Santos et al. (2012)

1. A novel humanoid leg architecture is proposed by adding an active toe joint, providing the necessary redundancy to avoid the singularity problem presented in humanoids (see Fig. 2.7).
2. Closed-form equations for forward and inverse kinematics are developed by dividing the walking gait into the sagittal and frontal planes. In particular, the sagittal plane is used to find inverse kinematics of the leg, see Fig. (2.8).

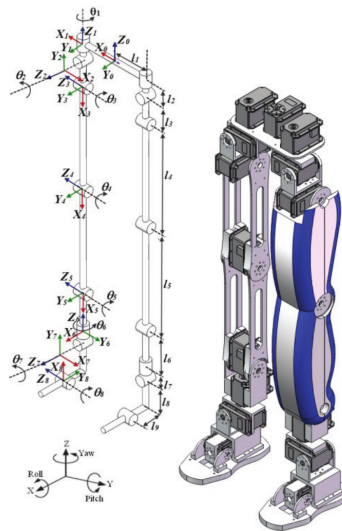


Figure 2.7: Kinematic configuration of the robot leg described by Hernández-Santos

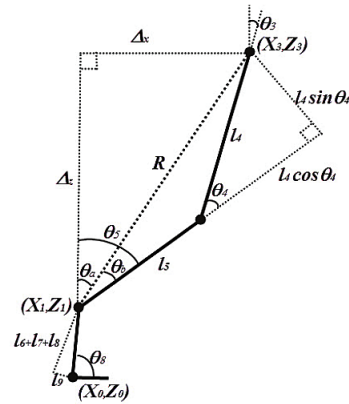


Figure 2.8: Right leg inverse kinematics

2012 Hyungju Andy Park et.al., *Close-Form Inverse Kinematic Position Solution for Humanoid Robots*, Park et al. (2012).

1. A novel reverse-decoupling method is developed by viewing the kinematic chain of a limb of a humanoid robot in reverse order and then decoupling it into the positioning and orientation mechanisms (see Fig. 2.9). Finally, the inverse-transform technique is used to derive a consistent joint solution.
2. The proposed approach is applied to a Hubo KHR-4 humanoid robot, and the proposed technique can also be applied to an ASIMO robot from Honda Motors, an HRP-2 robot from Kawada Industries, and a HOAP-2 robot from Fujitsu Automation with slight modifications. Unfortunately, for the limbs of these humanoid robots, the axes of the last three joints do not intersect at a point (see Fig. 2.10); however, a closer examination reveals that the joint axes of the first three joints do intersect at a point. This means that viewing the inverse kinematics problem with the joint angles in reverse order; that is, with the position/orientation of the base coordinate frame referenced to the end-effector coordinate frame, the position is a function of only the three joint angles. To solve the inverse kinematics problem in this reverse way, the inverse of the matrix multiplications is taken.

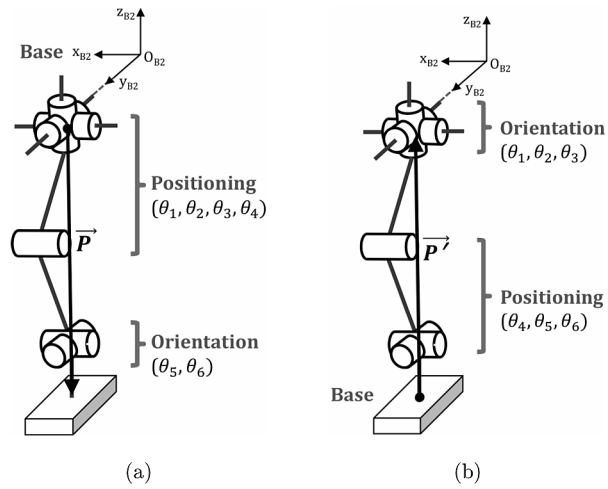


Figure 2.9: Right leg of a HUBO KHR-4 robot. (a) Forward decoupling, (b) Reverse Decoupling

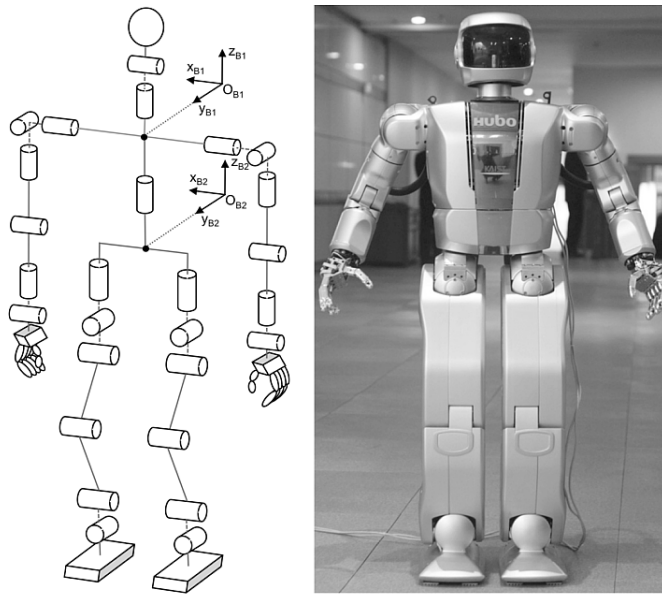


Figure 2.10: A HUBO KHR-4 humanoid robot

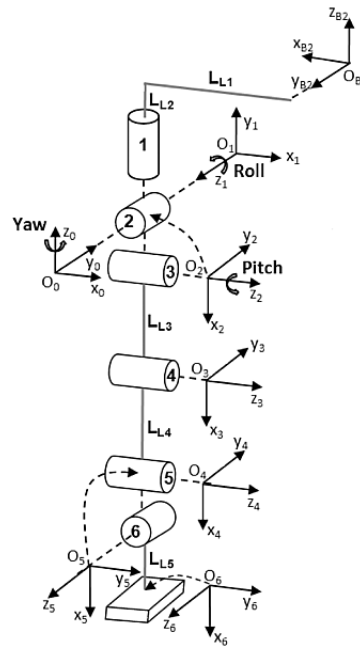


Figure 2.11: Link coordinate frames of the right leg of a Hubo KHR-4 robot

2014 Nikolaos Kofinas et. al., *Complete Analytical Forward and Inverse Kinematics for the NAO Humanoid Robot*, Kofinas et al. (2014).

1. A complete forward and inverse kinematics solution is presented by dividing the humanoid robot into five chains: the head, the two arms and the two legs. The Denavit-Hartenberg method is used along with the solution of the system of non-linear equations.
2. A summary of existent inverse kinematic techniques are used to provide analytical solutions for humanoid robotics. Matrix elimination, manipulation of both sides of matrix equations, constant matrices, and geometric approaches are used. The change in reference frame and matrix inversion are also applied; however, those techniques still led to a mathematical procedure with considerable complexity.

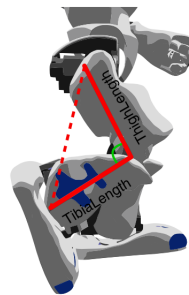


Figure 2.12: Using geometry in the triangle formed by the robot leg to derive the knee joint angle

2015 Alejandro Said et. al., *Decoupled Closed-Form Solution for Humanoid Lower Limb Kinematics*, Said et al. (2015)

1. The position analysis is approached using geometrical triangular arrangements. Furthermore, the joint activation sequence resulting from this geometry is inserted into the Denavit-Hartenberg analysis. This practice allows the conciliation of both analytical and geometrical equations in order to solve the system of non-linear equations.
2. End-effector coordinate frames are placed at the hip and the foot with the same orientation as the navigation frame of the robot. This allows the orientation functions to be obtained by equating the corresponding elements of the position and orientation matrix concatenations in a straight forward manner.
3. A forward and a reverse kinematic analysis are performed to avoid the use of matrix inversion; thus, decreasing the mathematical complexity of the kinematic chains for support and swing phases.
4. The kinematics of the joint that presents a mechanical dependency constraining the motion of the two legs and the torso, is solved analytically by means of a mathematical decoupling; thus, allowing the turn-in-place motion.
5. A simple geometrical approach is proposed to avoid in singularities in the walking postures. Theoretical and practical workspaces are analyzed considering mechanical actuation limitations.

2016 Ahmed R. J. Almusawi, L. Canan Dülger and Sadettin Kapucu. *A New Artificial Neural Network Approach in Solving Inverse Kinematics of Robotic Arm*, Almusawi et al. (2016)

1. An Artificial Neural Network (ANN) was used to learn the robot system characteristics rather than having to specify an explicit robot model.
2. An Artificial Neural Network trained with the Levenberg-Marquardt backpropagation algorithm is proposed to solve for the Inverse Kinematics of a 6-DOF robot arm. In addition to the target position and orientation, a feedback of the current joint angles configuration is included in the input pattern of the Neural Network. In Fig. 2.13, two paths are followed by the robot arm: the one using a traditional ANN, and the one proposed in this work.

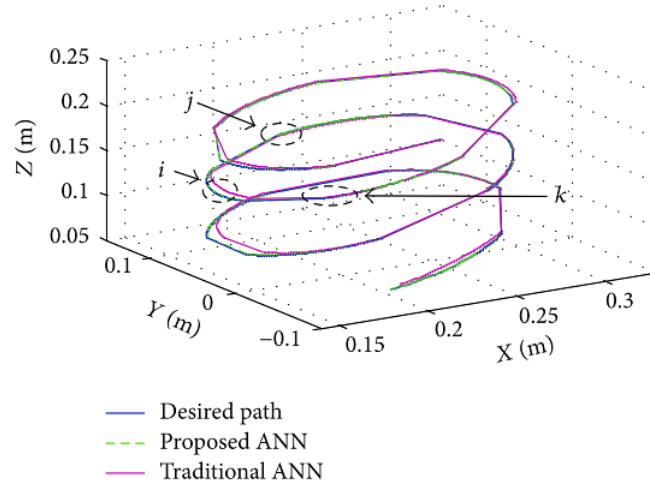


Figure 2.13: Paths generated by the robot using two different ANNs.

2017 Salman Faraji and Auke Jan Ijspeert. *Singularity-Tolerant Inverse Kinematics for Bipedal Robots: An Efficient Use of Computational Power to Reduce Energy Consumption*, Faraji and Ijspeert (2017)

1. Stretched-leg postures are more convenient for the mechanical hardware of humanoid robots, but they introduce two major difficulties to the control problem: 1) Singularities: which mainly refer to the alignment of the hip, knee and ankle joints leading to ill-conditioned Jacobians. 2) Joint position limits: which should be respected together with velocity limitations to avoid impacts.
2. In this study, a nonlinear inverse kinematics formulation to solve for positions is proposed. Compared to various other methods that integrate velocities, this formulation can better handle singular-postured balancing tasks. In addition, joint position and velocity boundaries are introduced as inequality constraints in order to ensure feasibility.

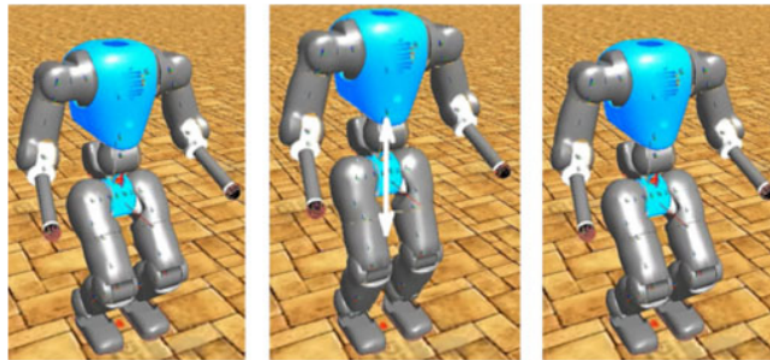


Figure 2.14: Simple symmetric simulations without reaching singularities.

2019 Kenji Kaneko, Hiroshi Kaminaga, Takeshi Sakaguchi, Shuuji Kajita, Mitsuharu Morisawa, Iori Kumagai, and Fumio Kanehiro. *Humanoid Robot HRP-5P: An Electrically Actuated Humanoid Robot With High-Power and Wide-Range Joints*, Kaneko et al. (2019)

1. Humanoid HRP-5P has been designed with electrically actuated high-power joints with wide movable range. In this new arrangement, the ankle joint has a lower height.
2. By adopting multiple motors instead of a huge motor with high power, the mounting is easier. To trace the belt path, a double-sided belt, rather than a single-side belt, is adopted.

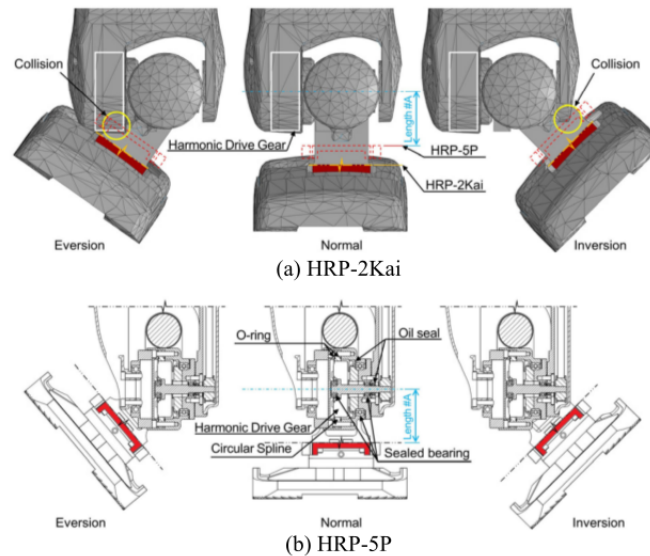


Figure 2.15: Front view of the right ankle joint.

2019 Jiangping Wang, Shirong Liu, Botao Zhang and Changbin Yu. *Inverse kinematics-based motion planning for dual-arm robot with orientation constraints*, Wang et al. (2019)

1. In this article, the focus relays on the dual-arm motion planning problem with end-effector orientation constraints; that is, computing a collision-free path for both arms between an initial state and a goal state while maintaining a specified orientation. It directly calculates the constraint-satisfying configuration by analytical IK instead of using the Jacobian pseudo-inverse projection methods.
2. Decoupled manipulators are frequently equipped with a humanoid spherical wrist from the viewpoint of the anthropomorphic arm structure, which allows decoupling motion of the position problem from the orientation problem. PR2 is designed with two 7-DOF decoupled manipulators, which allows us to decouple planning for the main arm joints (the first four joints) from the wrist joints (the last three joints).

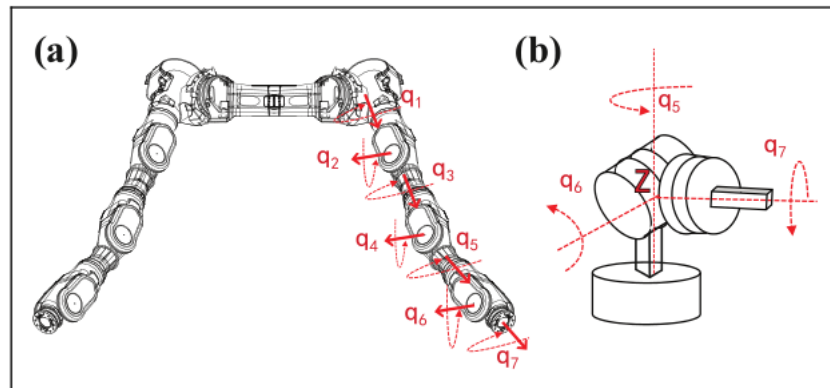


Figure 2.16: A prototype of dual-arm robot with two decoupled manipulators.

2.2 The State of the Art in Humanoid Trajectory Planning

1990, Miomir Vukobratović, *Biped Locomotion: Dynamics, Stability, Control and Application*, Vukobratovic et al. (1990).

1. *Zero Moment Point (ZMP)* is defined. ZMP refers to an equivalent reaction force acting at a certain point of the foot where the sum of all moments is equal to zero (see Fig. 2.17). Obviously, the ZMP in single support-phase cannot be out of the supporting area (are covered by the foot), while in double support phase, it can be anywhere inside the dashed area (see Fig. 2.3). Within these areas the ZMP can move continuously or not, depending on which gait type is performed.
2. A third characteristic is related to the periodical character of the mechanism motion in the walking process. The positions and velocities at the beginning and at the end of each step have to be the same, so that the walk can be performed continuously.

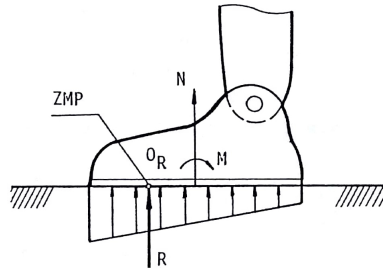


Figure 2.17: Definition of Zero-Moment Point (ZMP)

2002, Shuuji Kajita et. al., *A real time pattern generator for biped walking*, Kajita et al. (2002).

1. The dynamics of a 3D linear inverted pendulum (with zero input torques), is analyzed and used to provide the trajectories for a humanoid walking pattern generator. In this study, it is demonstrated that when a biped robot is supporting its body on one leg, its dominant dynamics can be represented by a single inverted pendulum which connects the supporting foot and the center of mass (CoM) of the whole robot.

The differential equations 2.7 and 2.8 show the dynamics of the CoM in the sagittal and lateral planes respectively. Using the solutions of the former differential equations, Fig. 2.19 shows a plot of the resulting trajectory described by the CoM and its projection onto the ground (from the standstill to a stop along three steps).

$$\ddot{x} = \frac{g}{z}x \quad (2.7)$$

$$\ddot{y} = \frac{g}{z}y \quad (2.8)$$

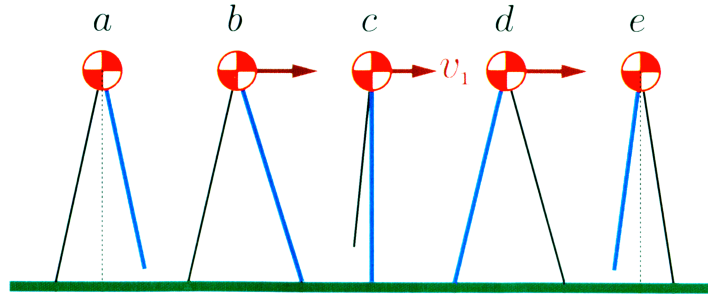


Figure 2.18: Support leg exchange with a constant vertical distance

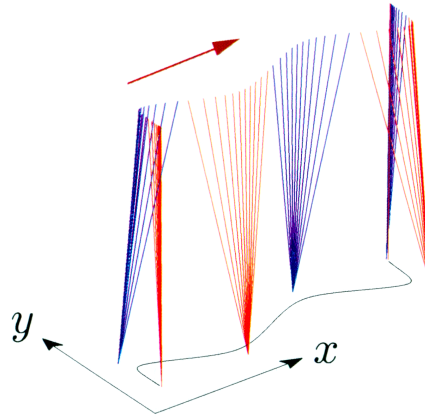


Figure 2.19: Walking pattern on flat floor based on 3D linear inverted pendulum

2003, Shuuji Kajita et. al., *Biped walking pattern generation by using preview control of zero-moment point*, Kajita et al. (2003).

1. A walking pattern generator that allows foot placements as a mixture of the ZMP and the inverted pendulum approaches is proposed; i.e., the equations for ZMP are substituted into the equations for the 3D linear inverted pendulum. The equations regarding the ZMP coordinates are shown in Eqns. 2.9 and 2.10.
2. The proposed equations for CoM trajectory generation are compared to a cart-table model yielding the same results.

$$p_y = y - \frac{z_c}{g}\ddot{y} \quad (2.9)$$

$$p_x = x - \frac{z_c}{g} \ddot{x} \quad (2.10)$$

2006, Ill-Woo Park et al., *Online free walking trajectory generation for biped humanoid robot KHR-3(HUBO)*, Park et al. (2006a).

1. A cycloid function is used in the generation of the gait trajectory used by the swing-leg ankle position. This function has a slow start, a fast moving and a slow stop. Figure 2.20 shows the coordinate frame used in the gate trajectory and sketch of of a cycloid trajectory.
2. A third order polynomial is used for the pelvis trajectory. This function is continuous in a defined time interval. Also, it is also easy to implement if the boundary conditions are well-defined.
3. The trajectory on each axis of the global coordinate system X - Y - Z , is decoupled of each other. Figure 2.21 shows the controller block diagram for the trajectory implementation.

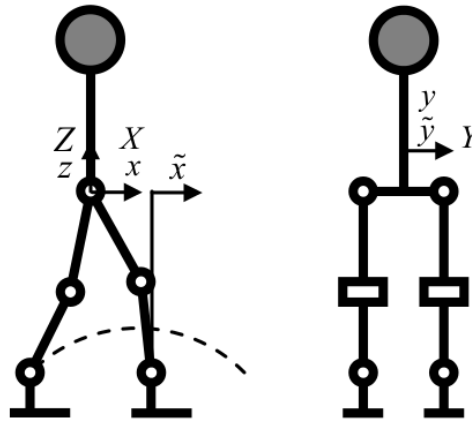


Figure 2.20: Coordinate frame gate trajectory

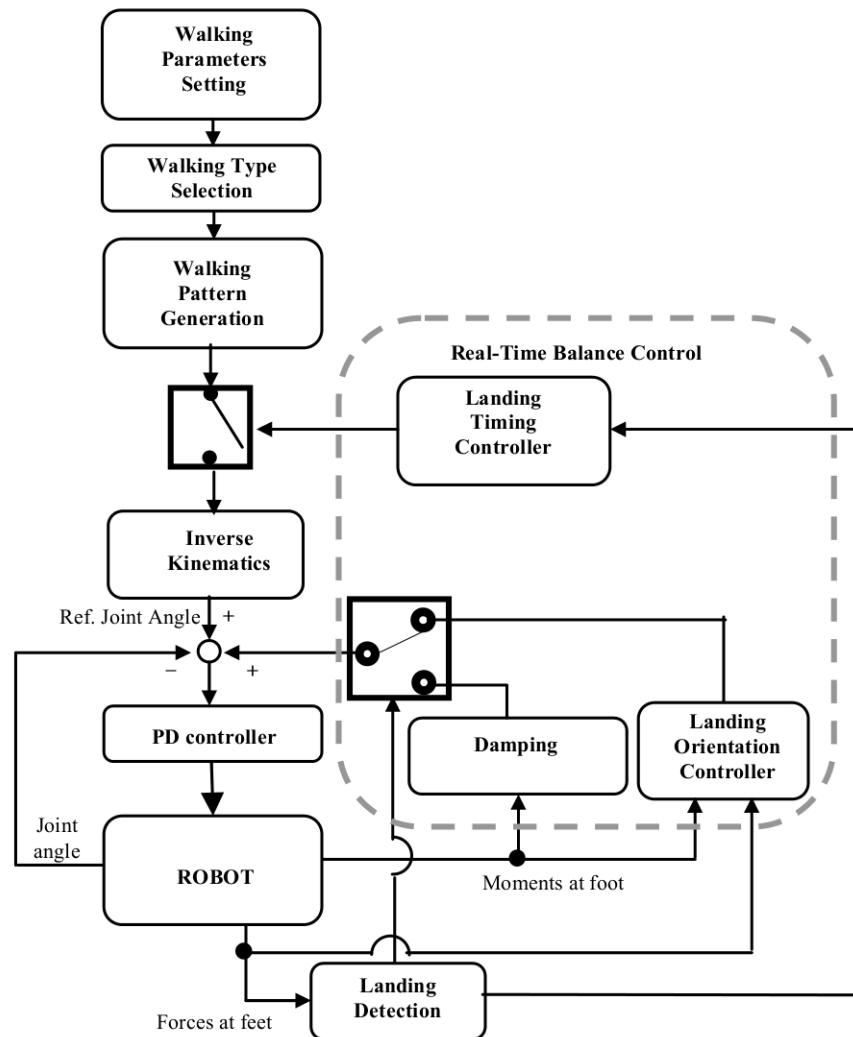


Figure 2.21: Controller block diagram for trajectory implementation

2009, Colin Graf et. al., *A Robust Closed-Loop Gait for the Standard Platform League Humanoid*, Graf et al. (2009).

1. Foot-lifting and step-advance trajectories are generated using cosine functions. The CoM movement is generated using a merging of a triangular, a sinusoidal and the square root of a sinusoidal function. Figure 2.22 shows the trajectory for the foot lifting, and Fig. 2.23 shows the trajectory for the CoM, where φ stands for parameterized units of time.

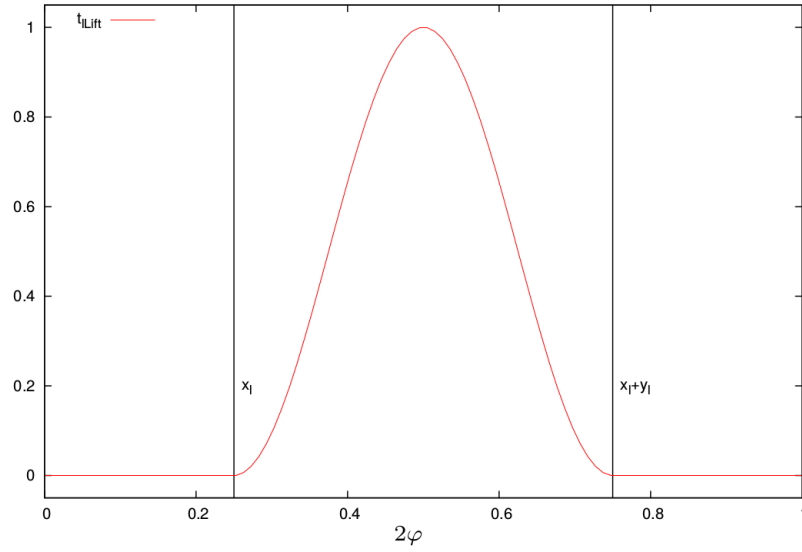


Figure 2.22: Swing-foot trajectory based in a cosine function

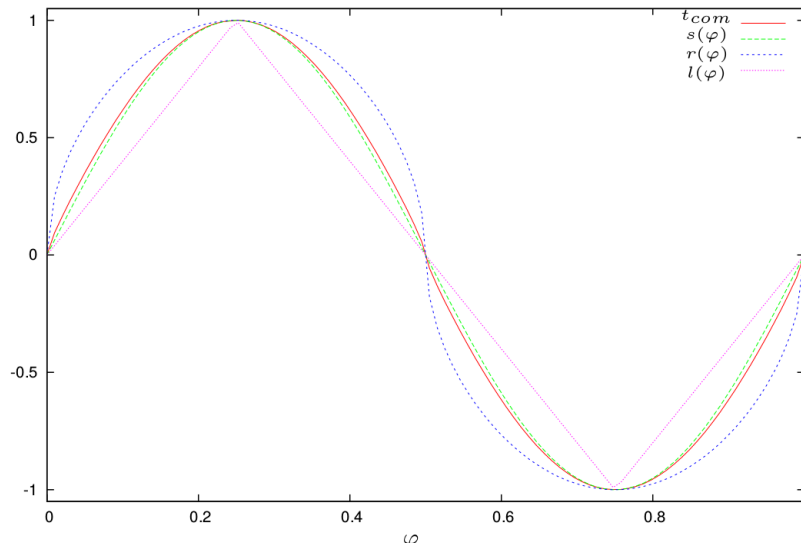


Figure 2.23: CoM trajectory consisting of a merging of a sine function $s(\varphi)$, the square root of a sine function $r(\varphi)$ and a linear function $l(\varphi)$

2010, Colin Graf et. al., *A Closed-loop 3D-LIPM Gait for the RoboCup Standard Platform League Humanoid*, Graf and Röfer (2010).

1. The approach in this study is the further development of the method first described in Kajita et al. (2003), in addition to the use of sensor feedback. The solutions of the differential equations for the 3D inverted pendulum have been applied to humanoid robot NAO. These solutions have the same mathematical form and they can be indicated by Eqns. 2.11, 2.12, and 2.13; where g is the gravitational acceleration, t is the time and z is the vertical distance from the supporting foot to the CoM assumed to be constant (see Fig. 2.18).
2. The need of the double support phase is eliminated by dynamically adjusting the point in time at which the support foot alternates. At the beginning of the single support phase, the position and the velocity of the center of mass should be in a state that leads to the proper position and velocity for the next single support phase, this problem is solved by using an iterative method.

$$x(t) = x(0) \cosh(t/T_c) + T_c \dot{x}(0) \sinh(t/T_c) \quad (2.11)$$

$$\dot{x}(t) = [x(0)/T_c] \sinh(t/T_c) + \dot{x}(0) \cosh(t/T_c) \quad (2.12)$$

$$T_c = \sqrt{z/g} \quad (2.13)$$

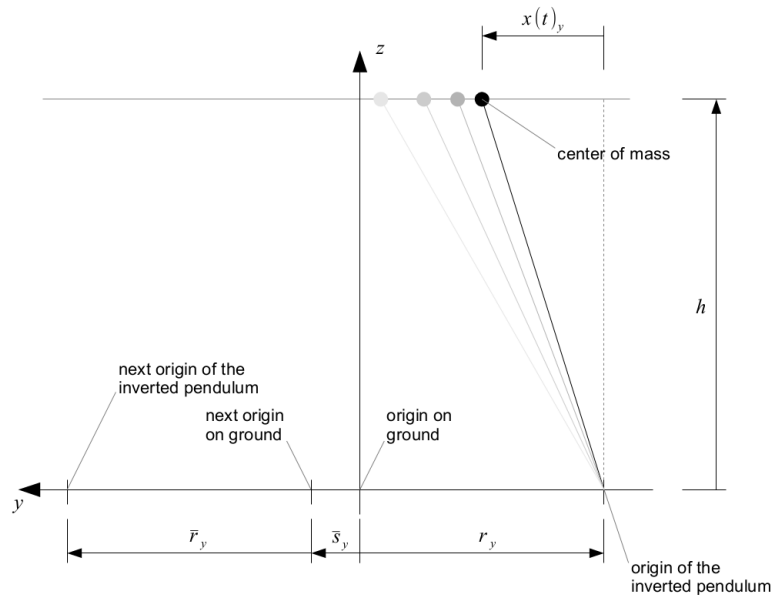


Figure 2.24: Cross section of the coordinate system used for the altered inverted pendulums

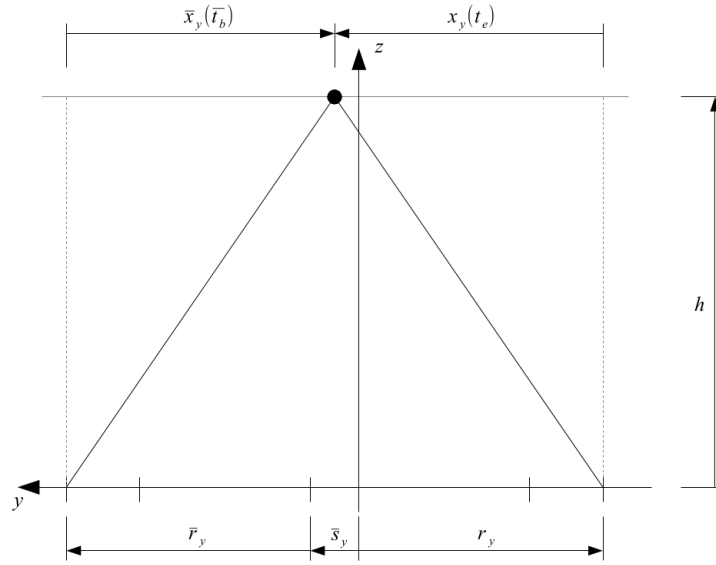


Figure 2.25: Two facing inverted pendulums

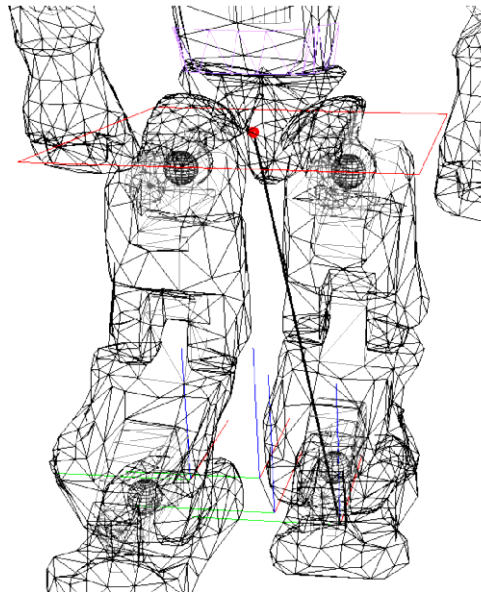


Figure 2.26: The inverted pendulum attached on a simulated model of the NAO. The red square indicates the plain on which the center of mass moves. The red dot is located in the position of the center of mass

2012, C.Hernández-Santos et al., *Kinematics and dynamics of a new 16 DOF humanoid biped robot with active toe joint*, Hernández-Santos et al. (2012).

1. Local sinusoidal trajectories where defined in the sagittal and frontal planes of a 16 DOF humanoid robot.

$$x_0(t) = \frac{s}{2\pi} \left(\frac{2\pi t}{T_s} - \sin \left(\frac{2\pi t}{T_s} \right) \right) \quad (2.14)$$

$$z_0(t) = \frac{s_h}{2} \left(\frac{2\pi t}{T_s} - \sin \left(\frac{2\pi t}{T_s} \right) \right) \quad (2.15)$$

$$x_1(t) = \frac{s}{2\pi} \left(\frac{2\pi t}{T_s} - \sin \left(\frac{2\pi t}{T_s} \right) \right) \quad (2.16)$$

$$z_1(t) = \frac{s_h}{2} \left(1 - \sin \left(\frac{2\pi t}{T_s} \right) \right) \quad (2.17)$$

$$x_3(t) = \frac{d}{2\pi} \left(\frac{2\pi t}{T_s} - \sin \left(\frac{2\pi t}{T_s} \right) \right) \quad (2.18)$$

$$z_3(t) = h \quad (2.19)$$

$$y = s \cdot \sin(T_s \pi t) \quad (2.20)$$

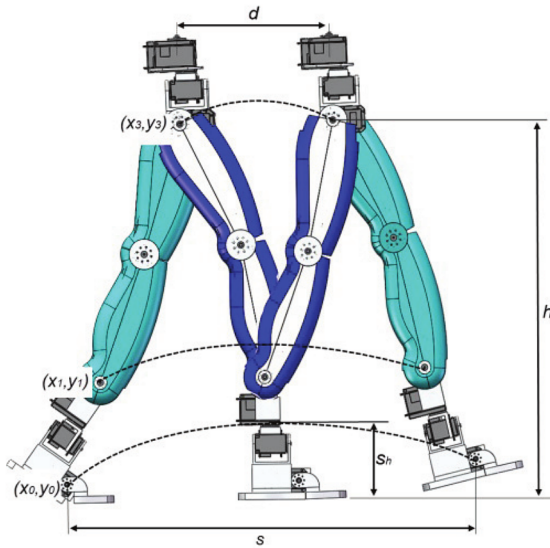


Figure 2.27: Parameters used in the trajectory periodic functions

2013, Ren C. Luo et. al., *Arbitrary Biped Robot Foot Gaiting Based on Variate CoM Height*, Luo et al. (2013).

1. A quasi-natural foot gait generator for biped walking with a varying CoM height is proposed. Walking gaits with constant low height permit large strides, but make the knees to bent heavily, so a large torque is required at the knees. Postures with a higher body condition, limit the length of step due to kinematics limitation. This trade-off can be solved by an up and down motion of the body. However, this method consumes more time in order to generate the trajectory based on the conventional preview control. To reduce time consumption, preview control with a particular design of COM height trajectory is proposed.
2. The approach creates a turning pattern by adopting trajectory mapping without pre-designing turning ZMP and foot trajectories.

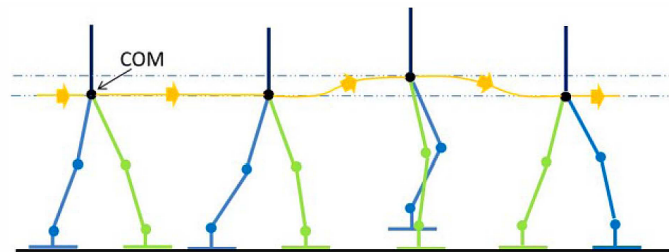


Figure 2.28: CoM up and down motion during walking

2015, Jung-Woo Heo et. al., *Biped Walking Pattern Generation Using an Analytic Method for a Unit Step With a Stationary Time Interval Between Steps*, Heo and Oh (2015).

1. An analytic solution for CoM trajectory is proposed using zero-velocity constraints at the initial and final step times. This CoM constraint allows for a stationary time interval between steps to stabilize the posture. The CoM trajectory was tested for providing long-stride walking with the DRC-HUBO robot.
2. In this study, a new and simple analytic solution is proposed for the unit step walking pattern. Analytic methods commonly share the disadvantage that the analytically obtained walking pattern cannot be changed during the unit step because it is already formulated in closed-form analytic solutions. In spite of this drawback, analytic solutions are still used for walking pattern generation because they do not require future information, as presented earlier, and they can be easily implemented since solutions are formulated in a closed form.



Figure 2.29: CoM up and down motion during walking

2016, Ravi Kumar Mandava and Pandu Ranga Vundavilli *Forward and Inverse Kinematic based Full Body Gait Generation of Biped Robot*, Mandava and Vundavilli (2016).

1. The full body gait generation of a 18-DOF two-legged robot was accomplished by using the concept of forward and inverse kinematics. The trajectories for upper and lower limbs are generated. The dynamic balance of the biped robot is determined by using the concept of the ZMP.
2. The gait generation was possible by constraining the swing-foot and the wrists trajectories to follow a cubic polynomial (see Fig. 2.30).

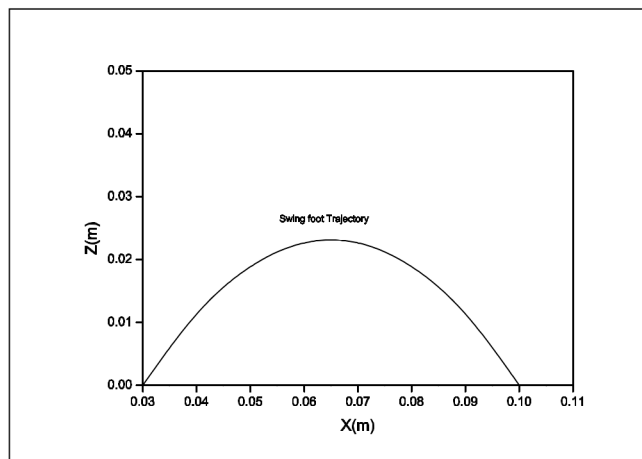


Figure 2.30: Cubic polynomial trajectory for the swing-foot.

2017, Tzoo-Hseng S. Li, Ya-Fang Ho, Ping-Huan Kuo, Yan-Ting Ye, and Li-Fan Wu *Natural Walking Reference Generation Based on Double-Link LIPM Gait Planning Algorithm*, Li et al. (2017).

1. This paper proposes a double-link LIPM (DLIPM) to eliminate the conflict about mass distribution. In addition, a gait planning algorithm is proposed for natural walking generation.
2. The foot trajectory generation can be divided into two parts according to the support phase. In the double support phase, both feet stay at fixed points. In the single support phase, the supporting foot stays at the fixed point and the swing foot trajectory is generated by sinusoidal functions (see Eqns. (2.21) and (2.22)).

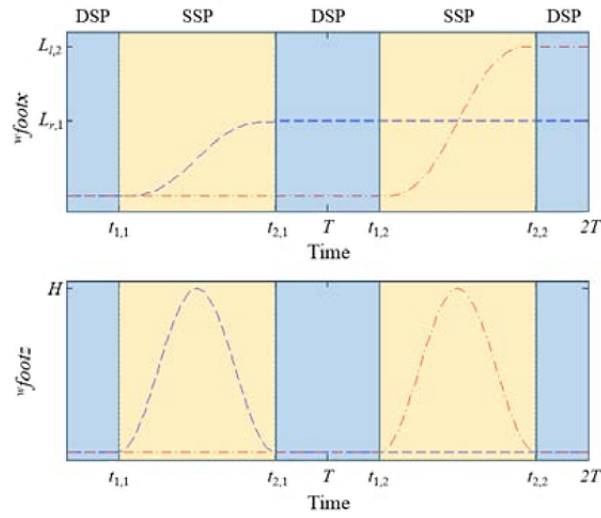


Figure 2.31: Foot trajectory with respect to the world coordinate system.

$$footX_{j,n}(t) = \begin{cases} 0 & \text{if } t \leq t_1 \\ \frac{L_{j,n}}{2\pi}(\theta - \sin \theta) & \text{if } t_1 < t \leq t_2 \\ L_{j,n} & \text{otherwise} \end{cases} \quad (2.21)$$

$$footZ_{j,n}(t) = \begin{cases} \frac{H}{2}(1 - \cos \theta) & \text{if } t_1 < t \leq t_2 \\ 0 & \text{otherwise} \end{cases} \quad (2.22)$$

2019, Chengju Liu, Tong Zhang, Changzhu Zhang, Ming Liu, and Qijun Chen, *Foot Placement Compensator Design for Humanoid Walking Based on Discrete Control Lyapunov Function*, Liu et al. (2019).

1. In this work, an online foot position compensator (FPC) is proposed for improving the robustness of humanoid walking based on orbital energy conservation and Discrete Control Lyapunov Function (DCLF), achieving foot placement. The online FPC is developed based on linear model predictive control (MPC) by replanning the trajectories of the center of mass (CoM) and properly placing the footsteps to resist external disturbances to recover the walking posture.
2. During humanoid walking, the single support phase duration is usually much longer than the double support phase and the supporting area is much smaller in the single support phase. Thus, the FPC is triggered during the single supporting phase. Since the foot of the robot already in contact with the ground cannot be changed, the FPC actuates in the next single supporting phase.

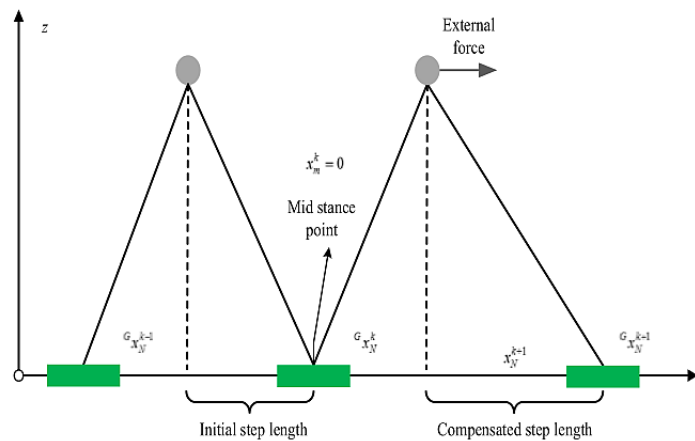


Figure 2.32: Velocity recovery process.

Chapter 3

Humanoid Inverse Kinematics

This study uses robot NAO model H21 manufactured by Aldebaran Robotics as an experimentation platform. Figure 3.1 shows the humanoid robot, including the navigation coordinate system, where the x -axis is pointing to the forward walking direction, the y -axis is pointing to the left side, and the z -axis is pointing upwards. Each leg of the robot has 5 DOF in addition to a special joint located between the hips; namely, the hip-yaw-pitch joint, where the hip-yaw and the hip-pitch movements are coupled by a gearbox; i.e, the hip-pitch movement is inevitable activated when a hip-yaw movement is executed. The results of this dissertation, are focused in solving for the inverse kinematics for each humanoid leg considering the above mentioned coupled joint. The problem of singularity is also addressed, by developing a simple geometric approach.

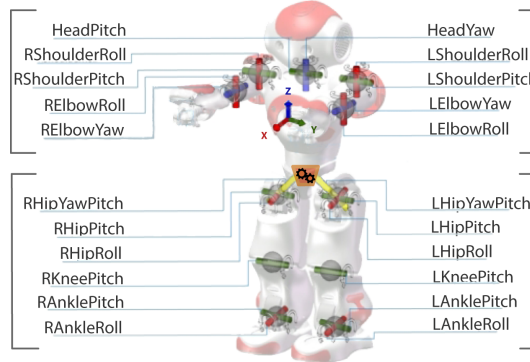


Figure 3.1: Active joints of H21 NAO Robot

3.1 Joint and Dimension Nomenclature

Consider θ_{ar} , θ_{ap} , θ_{kp} , θ_{hp} , θ_{hr} , and θ_{hy} denote the ankle roll, ankle pitch, knee pitch, hip pitch, hip roll, and hip yaw-pitch angles respectively. Table 3.1 includes the motion range used for each joint in this work. Table 3.2 includes the dimensional parameters of the humanoid robot where l_{ft} , l_{tb} and l_{tg} denote the foot height, the tibia length and the thigh length, respectively.

Table 3.1: Joint motion ranges

<i>Joint</i>	<i>Min</i>	<i>Max</i>
θ_{ar}	-22.27°	22.27°
θ_{ap}	-67.97°	52.86°
θ_{kp}	0°	121.04°

Table 3.2: Limb dimensions [mm]

<i>Limb</i>	<i>Dimension</i>
l_{ft}	45.11
l_{tb}	102.75
l_{tg}	100

From now on, following the same nomenclature as in [Wong and Liu (2013)], a letter L or R is added to the variables to indicate their location at the left or right leg, respectively. Also, a subscript s is added to the coordinates to indicate that they belong to the swing-leg analysis.

3.2 Direct and Inverse Kinematics in the Forward Analysis

The forward kinematic analysis describes the hip position and orientation at single and double support phases; i.e., the hip position as seen by the ankle. The solution for the inverse kinematics of the humanoid leg regarding position, can be obtained by following the geometric approach presented in [Graf et al. (2009)]. According to the above mentioned work, it is possible to define a position vector \mathbf{r} where the tibia, the thigh and the vector \mathbf{r} form a triangle which rotates an angular displacement θ_{ar} about the ankle roll articulation (see Fig. 3.2).

The forward kinematic chain in the robot leg, has been split into position and orientation formulations. According to [Pieper (1968)], breaking the kinematic analysis into position and orientation formulations, allows the position column of the DH matrix concatenation to consist of three equations, and thus, three unknowns; providing a solution to the kinematic problem. This approach has been followed by Park in [Park et al. (2012)] to solve for the kinematics of a humanoid leg. Additionally, in [Said et al. (2015)], the matrix inversion has been avoided to decrease the mathematical complexity while obtaining the solutions. Figure 3.3, shows the analytical assignment of the coordinate systems based in the DH procedure. Here, the hip joint variables have been not included; however, the distance from the knee joint to the intersection of the hip joints has been considered to determine the end-effector position.

In the present study, in relation with the position formulation; the joint activation sequence used in the analytical DH approach (see Fig. 3.3) uses the same activation sequence

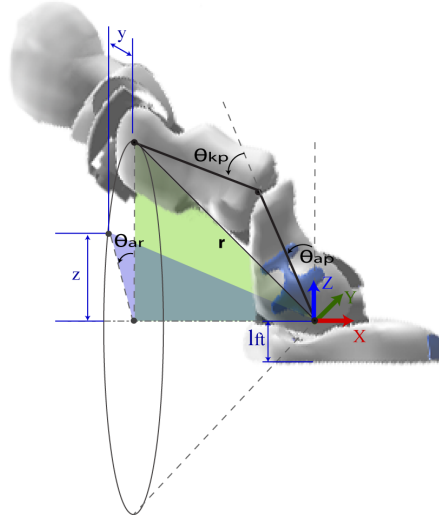


Figure 3.2: Sequence of joint activations in the forward analysis based in the triangular geometry

derived from the geometrical approach (see Fig. 3.2); i.e., the first joint variable to be activated is θ_{ar} , followed by θ_{ap} , while θ_{kp} is activated at the end.

The sequence of joint activations can also be observed in Table 3.3, where it is important to note that the constant coordinate systems number zero and six are aligned with the navigation coordinate system of the robot. Here, the constant coordinate system number six forces the kinematic chain to have the desired end-effector orientation, while constant coordinate system number one, obligates the kinematic chain to follow the desired joint activation order; i.e., the sequence given by the angles: θ_{ar} , θ_{ap} , θ_{kp} . In the forward analysis, the Z unit vector attached to the rotation center along every actuator, is pointing in the direction of a positive rotation relative to the ground.

Table 3.3: Link parameters used in the forward position analysis

i	α_{i-1}	a_{i-1}	θ_i	d_i
1	0	0	$-\pi/2$	0
2	$\pi/2$	0	$\theta_{ar} + \pi/2$	0
3	$\pi/2$	0	θ_{ap}	0
4	0	l_{tb}	θ_{kp}	0
5	$\pi/2$	l_{tg}	$\pi/2$	0
6	$\pi/2$	0	$\pi/2$	0

Using the parameters presented in Table 3.3, the position coordinates of the hip (as seen by the ankle) can be extracted from the fourth column of the DH matrix concatenation, leading

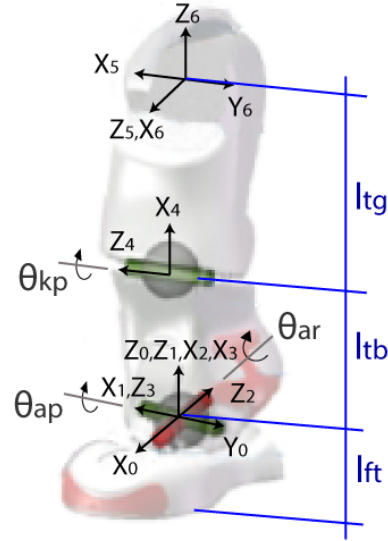


Figure 3.3: Forward position analysis of the humanoid leg

to Eqns. 3.1, 3.2 and 3.3. The software used for mathematical manipulation of matrices is *Maple* [Maplesoft (2019)].

$$x = -l_{tg} \left[S(\theta_{ap} + \theta_{kp}) + \left(\frac{l_{tb}}{l_{tg}} \right) S\theta_{ap} \right] \quad (3.1)$$

$$y = l_{tg} S\theta_{ar} \left[C(\theta_{ap} + \theta_{kp}) + \left(\frac{l_{tb}}{l_{tg}} \right) C\theta_{ap} \right] \quad (3.2)$$

$$z = l_{tg} C\theta_{ar} \left[C(\theta_{ap} + \theta_{kp}) + \left(\frac{l_{tb}}{l_{tg}} \right) C\theta_{ap} \right] \quad (3.3)$$

Thus, the inverse kinematics regarding the hip position can be obtained by solving the system of non-linear equations given by Eqns. 3.1, 3.2 and 3.3. The ankle roll angle θ_{ar} is obtained by dividing Eq. 3.2 by Eq. 3.3, (see Eq. 3.4).

$$\theta_{ar} = \arctan \left(\frac{y}{z} \right) \quad (3.4)$$

Squaring and adding Eqns. 3.1, 3.2 and 3.3 results in Eq. (3.5)

$$x^2 + y^2 + z^2 = 2 \cdot l_{tg} \cdot l_{tb} \cdot C\theta_{kp} + l_{tg}^2 + l_{tb}^2 \quad (3.5)$$

Solving for the knee pitch angle θ_{kp} gives Eq. (3.6)

$$\theta_{kp} = \arccos \left[\frac{x^2 + y^2 + z^2 - l_{tg}^2 - l_{tb}^2}{2 \cdot l_{tb} \cdot l_{tg}} \right] \quad (3.6)$$

Dividing Eq. (3.1) by the square root of the sum of the squares of Eqs. (3.2) and (3.3) results in Eq. (3.7).

$$\frac{x}{\sqrt{y^2 + z^2}} = \frac{-S(\theta_{ap} + \theta_{kp}) + (l_{tb}/l_{tg})S\theta_{ap}}{C(\theta_{ap} + \theta_{kp}) + (l_{tb}/l_{tg})C\theta_{ap}} \quad (3.7)$$

Solving for the ankle pitch angle θ_{ap} gives Eq.(3.8).

$$\theta_{ap} = -\arctan \left[\frac{\sqrt{y^2 + z^2}S\theta_{kp} + xC\theta_{kp} + (l_{tb}/l_{tg})x}{\sqrt{y^2 + z^2}C\theta_{kp} + (l_{tb}/l_{tg})\sqrt{y^2 + z^2} - xS\theta_{kp}} \right] \quad (3.8)$$

After determining the hip position, the torso orientation must be solved. In the forward orientation analysis, due to the fact that the hip yaw-pitch joint does not play any role during the forward and the sideways gaits, the analysis of this joint is removed to reduce the number of variables affecting the orientation equations. The chosen coordinate systems can be seen in Fig. 3.4. The DH parameters used in the forward orientation analysis are shown in Table 3.4.

Table 3.4: Link parameters used in the forward orientation analysis

i	α_{i-1}	a_{i-1}	θ_i	d_i
7	$\pi/2$	0	$\theta_{hp} + \pi/2$	0
8	$-\pi/2$	0	$\theta_{hr} + \pi/2$	0
9	$\pi/2$	0	$-\pi/2$	0

To maintain the torso upright Eq. (3.9) is used to solve for θ_{hp} in Eq. (3.10). Also, Eq. (3.11) is used to solve for θ_{hr} in Eq. (3.12).

$${}^7\mathbf{T}_9(1, 1) = -{}^0\mathbf{T}_6(1, 1) \quad (3.9)$$

$$\theta_{hp} = -(\theta_{ap} + \theta_{kp}) \quad (3.10)$$



Figure 3.4: Forward orientation analysis of the humanoid leg

$${}^7\mathbf{T}_9(2,2) = -{}^0\mathbf{T}_6(2,2) \quad (3.11)$$

$$\theta_{hr} = -\theta_{ar} \quad (3.12)$$

3.3 Direct and Inverse Kinematics in the Reversed Analysis

In this subsection, the reversed kinematic analysis [Park et al. (2012)] describes the position of the foot as it moves across the air; i.e., the foot position at the swing phase. Regarding the present study, this means that the ankle position is analyzed as seen by the hip. Following a similar approach as mentioned in the forward analysis, the reversed geometric analysis can be obtained as shown in Fig. 3.5. Gathering the information about position and orientation into a single figure, Fig. 3.6 shows the assignment of the coordinate systems used in the reversed analysis. Here, the Z unit vector along every actuator is aligned in the direction of a positive rotation relative to the hip. The angles from the inverse kinematics solution are shown in Eqns. (3.13), (3.14) and (3.15); and they take the position coordinates x_s , y_s and z_s as inputs, where the subscript s indicates that they describe the swing phase movement. The orientation inverse kinematics solutions are shown in Eqns. (3.16) and (3.17).

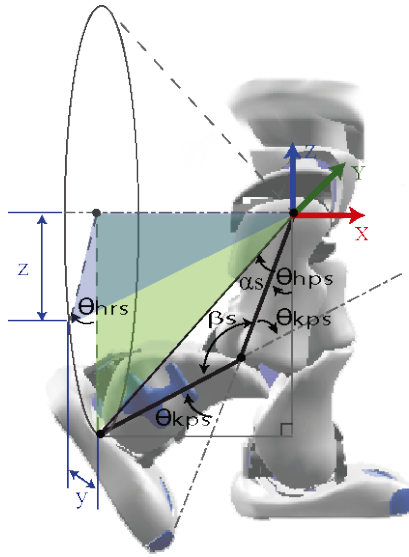


Figure 3.5: Sequence of joint activations in the reversed analysis based in the triangular geometry

$$\theta_{hr} = \arctan\left(-\frac{y_s}{z_s}\right) \quad (3.13)$$

$$\theta_{kp} = \arccos\left[\frac{x_s^2 + y_s^2 + z_s^2 - l_{tb}^2 - l_{tg}^2}{2 \cdot l_{tb} \cdot l_{tg}}\right] \quad (3.14)$$

$$\theta_{hp} = -\arctan\left[\frac{\sqrt{y_s^2 + z_s^2}S\theta_{kp} + x_sC\theta_{kp} + (l_{tg}/l_{tb})x_s}{\sqrt{y_s^2 + z_s^2}C\theta_{kp} + (l_{tg}/l_{tb})\sqrt{y_s^2 + z_s^2} - x_sS\theta_{kp}}\right] \quad (3.15)$$

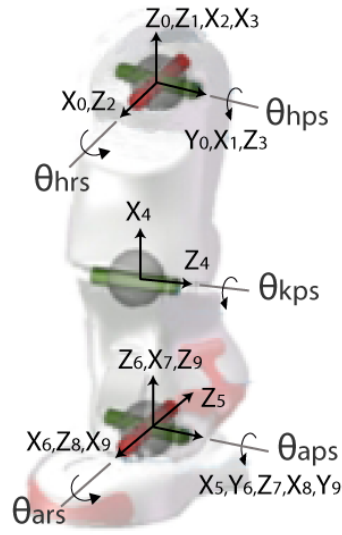


Figure 3.6: Reversed position and orientation analysis of the humanoid leg

Solving for the orientation joint variables θ_{ap} and θ_{ar} results in

$$\theta_{ap} = -(\theta_{hp} + \theta_{kp}) \quad (3.16)$$

$$\theta_{ar} = -\theta_{hr} \quad (3.17)$$

Notice that the joint angles θ_{ap} and θ_{ar} have changed their roles from variables used for position in the forward analysis to variables used for orientation in the reversed analysis.

3.4 Turn-In-Place Analysis

To activate the hip yaw movement, the robot NAO includes a special mechanism located in the hips, where only one actuator is needed for both legs, resulting in a reduction of the building costs and space [Gouaillier et al. (2009)]. This special joint is called the *hip-yaw-pitch* joint. The collateral effect caused by the configuration of this joint, is a hip pitch rotation affecting both legs, when only a hip yaw rotation is desired.

In this section, the solutions for the mathematical decoupling the hip yaw and of the hip pitch movements are presented, allowing the robot to perform a *turn-in-place* movement; i.e., a rotation about the navigation z -axis while maintaining the torso in a vertical position [Abdolmaleki et al. (2011); Zorjan and Hugel (2013)]. Figure 3.7 presents the joint activation sequence including the *hip-yaw-pitch* joint, and Table 3.5 shows the corresponding link parameters. Note that the transformation 8T_9 used in Table 3.4, has been modified from the forward analysis to include the hip yaw-pitch into the kinematic chain.



Figure 3.7: Turn-in-place movement orientation analysis

Table 3.5: Link parameters used for a turn-place movement

i	α_{i-1}	a_{i-1}	θ_i	d_i
9	$\pi/2$	0	$\pi/2$	0
10	$-\pi/4$	0	θ_{hy}	0
11	$\pi/4$	0	$-\pi/2$	0
12	0	0	$-\pi/2$	0

The matrix concatenation of Euler angles $\mathbf{R}_x\mathbf{R}_y\mathbf{R}_z$ is used in order to describe the hip motion, as in [Graf et al. (2009)] and [Nunez et al. (2012)]. Note that the leg position is not

considered in this section, therefore $\theta_{ar} = \theta_{ap} = \theta_{kp} = 0$. Since the hip yaw-pitch joint produces undesired motion only in the hip pitch axis, the constraint $\theta_{hr} = 0$ is considered to reduce the complexity of the equations. Multiplying the matrices of the forward kinematic analysis (including the hip yaw-pitch joint) and considering the above mentioned constraints results in Eq. 3.18.

$${}^0\mathbf{R}_{12} = \begin{bmatrix} r_{11} & r_{12} & r_{13} \\ r_{21} & r_{22} & r_{23} \\ r_{31} & r_{32} & r_{33} \end{bmatrix} \quad (3.18)$$

Where the elements of the matrix are described by the following equations.

$$r_{11} = C\theta_{hp}C\theta_{hy} - \left(\frac{\sqrt{2}}{2}\right) S\theta_{hp}S\theta_{hy} \quad (3.19)$$

$$r_{12} = -\left(\frac{\sqrt{2}}{2}\right) \left[C\theta_{hp}S\theta_{hy} + \left(\frac{\sqrt{2}}{2}\right) S\theta_{hp}C\theta_{hy} \right] + \left(\frac{1}{2}\right) S\theta_{hp} \quad (3.20)$$

$$r_{13} = -\left(\frac{\sqrt{2}}{2}\right) \left[C\theta_{hp}S\theta_{hy} + \left(\frac{\sqrt{2}}{2}\right) S\theta_{hp}C\theta_{hy} \right] - \left(\frac{1}{2}\right) S\theta_{hp} \quad (3.21)$$

$$r_{21} = \left(\frac{\sqrt{2}}{2}\right) S\theta_{hy} \quad (3.22)$$

$$r_{22} = \left(\frac{1}{2}\right) + \left(\frac{1}{2}\right) C\theta_{hy} \quad (3.23)$$

$$r_{23} = -\left(\frac{1}{2}\right) + \left(\frac{1}{2}\right) C\theta_{hy} \quad (3.24)$$

$$r_{31} = S_{hp}C\theta_{hy} + \left(\frac{\sqrt{2}}{2}\right) C\theta_{hp}S\theta_{hy} \quad (3.25)$$

$$r_{32} = -\left(\frac{\sqrt{2}}{2}\right) \left[S\theta_{hp}S_{hy} - \left(\frac{\sqrt{2}}{2}\right) C\theta_{hp}C_{hy} \right] - \left(\frac{1}{2}\right) C\theta_{hp} \quad (3.26)$$

$$r_{33} = - \left(\frac{\sqrt{2}}{2} \right) \left[S\theta_{hp}S\theta_{hy} - \left(\frac{\sqrt{2}}{2} \right) C\theta_{hp}C\theta_{hy} \right] + \left(\frac{1}{2} \right) C\theta_{hp} \quad (3.27)$$

Making $\mathbf{R}_x\mathbf{R}_y\mathbf{R}_z = {}^0\mathbf{R}_{12}$ leads to Eqn 3.28.

$$\frac{r_{21}}{r_{22}} = \frac{S_z C_x}{C_z C_x} = \frac{(\sqrt{2}/2)S\theta_{hy}}{(1/2) + (1/2)C\theta_{hy}} = \tan(\theta_z) \quad (3.28)$$

Where θ_z represents the turn-in-place rotation. The equation 3.29 is solved for θ_{hy} in order to determine the yaw rotation to be performed by the robot.

$$\theta_{hy} = \arctan \left[\frac{2\sqrt{2} \tan(\theta_z)}{\tan^2(\theta_z) + 2}, \frac{\tan^2(\theta_z) - 2}{\tan^2(\theta_z) + 2} \right] \quad (3.29)$$

Equation 3.30 is needed to correct the undesired pitch rotation θ_y

$$\frac{r_{13}}{r_{33}} = \frac{C_x S_y}{C_x C_y} = \frac{-(\sqrt{2}/2) \left[C\theta_{hp}S\theta_{hy} + (\sqrt{2}/2)S\theta_{hp}C\theta_{hy} \right] - (1/2)S\theta_{hp}}{-(\sqrt{2}/2) \left[S\theta_{hp}S\theta_{hy} - (\sqrt{2}/2)C\theta_{hp}C\theta_{hy} \right] + (1/2)C\theta_{hp}} = \tan(\theta_y) \quad (3.30)$$

The consideration in Eq. 3.31 is made to remove the navigation pitch rotation θ_y when the hip yaw-pitch θ_{hy} is activated.

$$\tan \theta_y = 0 \quad (3.31)$$

Equation 3.31 ensures that $\theta_y = 0$ is valid. Furthermore, a compensation parameter ϕ_{hp} is obtained from Eq. 3.30 by solving for θ_{hp} and rewriting it as ϕ_{hp} . The parameter ϕ_{hp} is defined in Eq. 3.32 and it must be added to the hip pitch angle in order to eliminate the undesired pitch motion due to the coupled hip yaw-pitch rotation.

$$\phi_{hp} = - \arctan \left[\frac{\sqrt{2}S\theta_{hy}}{1 + C\theta_{hy}} \right] \quad (3.32)$$

Thus, the compensated pitch angle θ_{hpc} for a turn-in-place rotation is denoted by Eq. 3.33, where the subscript c refers to the compensation.

$$\theta_{hpc} = \theta_{hp} + \phi_{hp} \quad (3.33)$$

Certain practical aspects were considered for achieving the turn-in-place rotation. If the analysis is made over the right foot as the support foot, then, θ_{hy} and θ_{hp} must have opposite signs in their respective solutions. Also, the position of the swing foot should be considered to achieve an effective robot rotation as can be seen in Fig. 3.8.

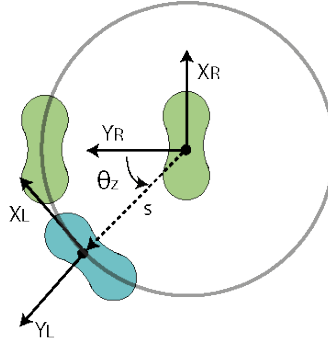


Figure 3.8: Position and orientation of the robot feet at the turn-in-place rotation

In addition, the motion at the turn-in-place rotation should be small in order to prevent the legs of the robot from knocking against each other. Furthermore, Eq. 3.34 should be used when it is desired that the sole of the swing foot remains parallel to the ground, where θ_{apc} is the compensated ankle pitch angle of the swing foot. Finally, it is recommended to organize the joint commands in tuples of right and left leg angles of the same kind of articulation, in order to achieve optimal positioning.

$$\theta_{apc} = \theta_{ap} + \phi_{hp} \quad (3.34)$$

3.5 Analysis of the Workspace of a Humanoid Step

According to [Ogawa and Kanada (2010)], in the direct kinematics problem, the existence, uniqueness and stability of the solution is guaranteed; in the case of the inverse kinematics problem, however, it may be difficult to obtain a solution because these conditions are not guaranteed. In this work, a simple 3D geometrical approach is presented to avoid singularities in order to ensure the existence of a solution of a humanoid step. To achieve this goal, the Center of Mass (CoM) is maintained at a defined height. Here, the coordinates of the swing foot, x_s and y_s , are projected into a plane which is parallel to the ground and which intersects the ankles of the support feet, as shown in Fig. 3.9. It can be easily shown that the step size s is given by Eq. (3.35).

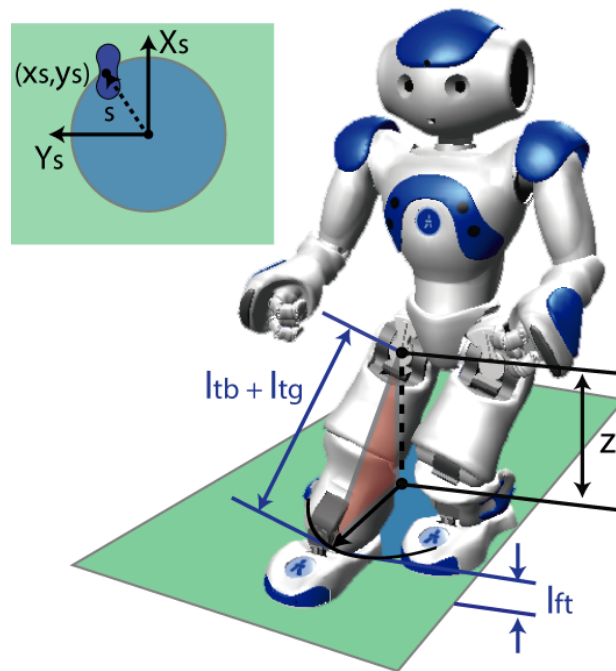


Figure 3.9: Geometric analysis in the estimation of the humanoid step size

$$s = \sqrt{x_s^2 + y_s^2} \quad (3.35)$$

From Fig. 3.9, it can be seen that the distance z , the thigh, the tibia, and the step s form a triangle which restricts the height of z (in Eq. 3.3), to the condition indicated by Eq. (3.36).

$$z \leq \sqrt{(l_{tb} + l_{tg})^2 - s^2} \quad (3.36)$$

Fig 3.10 shows the theoretical plot of the maximum displacement z that the robot must satisfy in order to produce a step size s , i.e., the step workspace without considering the mechanical joint limits. It can be seen that the longer the step is desired to be, the lower the height of the hips must be. Considering the joint limitations, the practical workspace

is shown in Fig. 3.11, where there is an important limitation at the lateral displacements. In both workspace graphs, there is no dexterous workspace because only one possible robot orientation is assumed [Jiang et al. (2009)], where the foot soles remain parallel to the ground and the torso resides upright.

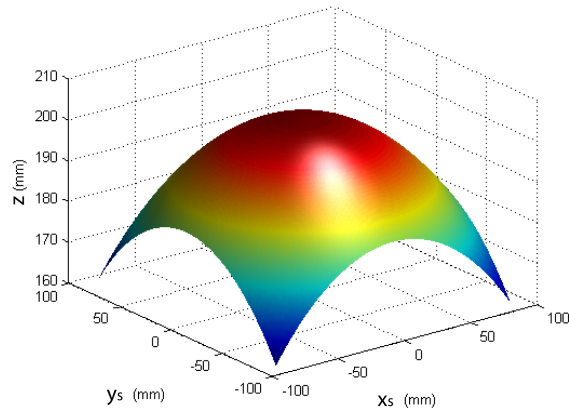


Figure 3.10: Maximum theoretical distance z for a desired step size

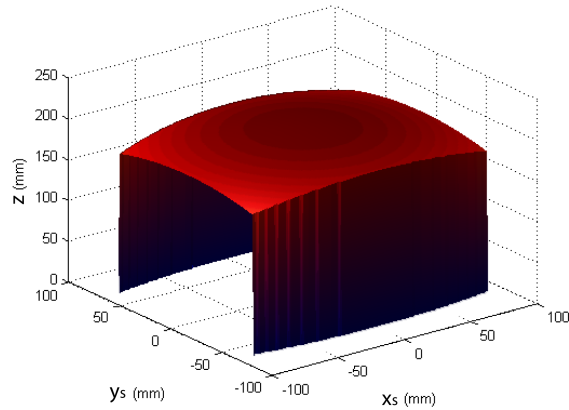


Figure 3.11: Maximum practical distance z for a desired step size

3.6 Inverse Kinematics Experimentation

The validation of the formulas is accomplished by executing three basic motions: (1) Forward Walking (see Fig. 3.12), (2) Lateral Walking (see Fig. 3.13) and (3) Turn-in-place motion (see Fig.3.14).

For each kind of movement (i.e., forward walking, lateral walking and turn-in-place movement), there are two types of tables. The first type, contains the end-effector Cartesian coordinates which the NAO robot is requested to reach (see Tables 3.6, 3.8, and 3.10). The second type, contains the solution angles that were found by using the inverse kinematic equations obtained in Sections 3.2, 3.3, and 3.4; and solved using the *Maple* software package. The NAO robot was programmed to execute the solution angles; i.e., it was not requested to solve for the inverse kinematics equations (see Tables 3.7, 3.9, and 3.11).

The joint angles given by the formulas proposed in this work, have been written in a table to form a sequence of walking postures. Then, the walking postures are executed to perform a quasi-static walking [Kanoun et al. (2010)], i.e; the position of the CoG, is always enclosed within the support polygon. The end effector coordinates are divided into two kind of movements: the hip movement (using x , y , z coordinates), and the swing-foot movement (using x_s , y_s , and z_s coordinates). The end-effector coordinates used in the forward walking are presented in Table 3.6, and the corresponding joint angles are shown in Table 3.7. For the lateral walking, the end-effector coordinates are presented in Table 3.8 and the corresponding joint angles are shown in Table 3.9. Regarding the turn-in-place motion, the movement is performed counterclockwise, the end-effector coordinates are presented in Table 3.10, and the corresponding joint angles are shown in Table 3.11.

Table 3.6: Forward walking end-effector coordinates (mm)

Stage	R_x	R_y	R_z	L_x	L_y	L_z	R_{x_s}	R_{y_s}	R_{z_s}	L_{x_s}	L_{y_s}	L_{z_s}	Description
0	0	0	185.75	0	0	185.75							Bends down
1	0	62	185.75	0	62	185.75							Moves to left
2							50	-62	-155.85				Moves the right foot forward
3							50	-62	-185.75				Lands the right foot
4	0	-62	185.75	50	-62	185.75							Moves hips to the right and forward
5										-50	62	-155.75	Lifts the left foot from behind
6										50	62	-155.75	Moves the lifted left foot forward
7										50	62	-185.75	Lands the left foot
8	50	62	185.75	0	62	185.75							Moves hips to the left and forward
9							-50	-62	-155.75				Lifts the right foot from behind
10							50	-62	-155.75				Moves the lifted right foot forward
*													Repeat stages 3,4 and 5
11										0	62	-155.75	Aligns the left foot
12										0	62	-185.75	Lands the aligned left foot

Table 3.9: Lateral walking angles (rad)

<i>Stage</i>	$R\theta_{ar}$	$L\theta_{ar}$	$R\theta_{ap}$	$L\theta_{ap}$	$R\theta_{kp}$	$L\theta_{kp}$	$R\theta_{hp}$	$L\theta_{hp}$	$R\theta_{hr}$	$L\theta_{hr}$
0	0.0	0.0	-0.368	-0.368	0.747	0.747	-0.379	-0.379	0.0	0.0
1	0.317	0.317	-0.198	-0.198	0.401	0.401	-0.203	-0.203	-0.317	-0.317
2	0.337	0.317	-0.385	-0.198	0.785	0.401	-0.398	-0.203	-0.337	-0.317
3	0.234	0.317	-0.290	-0.198	0.588	0.401	-0.298	-0.203	-0.234	-0.317
4	-0.317	-0.234	-0.198	-0.290	0.401	0.588	-0.203	-0.298	0.317	0.234
5	-0.317	-0.386	-0.198	-0.339	0.401	0.688	-0.203	-0.349	0.317	0.386
6	-0.317	-0.364	-0.198	-0.083	0.401	0.170	-0.203	-0.086	0.317	0.364
7	0.364	0.317	-0.083	-0.198	0.170	0.401	-0.086	-0.203	-0.364	-0.317
8	0.386	0.317	-0.339	-0.198	0.688	0.401	-0.349	-0.203	-0.386	-0.317
9	-0.317	-0.337	-0.198	-0.387	0.401	0.785	-0.203	-0.398	0.317	0.337
10	-0.317	-0.317	-0.198	-0.198	0.401	0.401	-0.203	-0.203	0.317	0.317

Table 3.10: Turn-in-place coordinates (mm)

<i>Stage</i>	R_x	R_y	R_z	L_x	L_y	L_z	R_{x_s}	R_{y_s}	R_{z_s}	L_{x_s}	L_{y_s}	L_{z_s}	<i>Description</i>
0	0	0	191.75	0	0	191.75							Bends down
1	0	-62	191.75	0	-62	191.75							Moves to right
2										0	62	-179.75	Lifts the left foot
3										-10.766	61.058	-179.75	Positions the left foot
4													Rotates the left foot 10° ccw
5										-10.766	61.058	-191.75	Lands the left foot
6	14.772	-59.396	191.75	15	-62	191.75							Moves the hips forward
7	4.005	63.662	191.75	15	62	191.75							Moves hips to the left
8							-4.005	63.662	-179.75				Lifts the right foot
9	0	62	191.75				0	-62	-173.75				Aligns the right foot
10							0	-62	-191.75				Lands the right foot

Table 3.11: Turn-in-place angles (rad)

<i>Stage</i>	$R\theta_{ar}$	$L\theta_{ar}$	$R\theta_{ap}$	$L\theta_{apc}$	$R\theta_{kp}$	$L\theta_{kp}$	$R\theta_{hpc}$	$L\theta_{hp}$	$R\theta_{hr}$	$L\theta_{hr}$	$L\theta_{hy}$
0	0.0	0.0	-0.326	-0.326	0.661	0.661	-0.335	-0.335	0.0	0.0	0.0
1	-0.312	-0.312	-0.108	-0.108	0.220	0.220	-0.111	-0.111	0.312	0.312	0.0
2	-0.312	-0.332	-0.108	-0.349	0.220	0.709	-0.111	-0.359	0.312	0.332	0.0
3	-0.312	-0.327	-0.108	-0.406	0.220	0.709	-0.111	-0.302	0.312	0.327	0.0
4	-0.312	-0.327	-0.108	-0.406+0.174	0.220	0.709	-0.111+0.174	-0.302	0.312	0.327	-0.248
5	-0.312	-0.308	-0.108	-0.161+0.174	0.220	0.220	-0.111+0.174	-0.058	0.312	0.308	-0.248
6	-0.300	-0.312	-0.192	-0.154+0.174	0.239	0.162	-0.046+0.174	-0.008	0.300	0.312	-0.248
7	0.320	0.312	-0.099	-0.154+0.174	0.162	0.162	-0.062+0.174	-0.008	-0.320	-0.312	-0.248
8	0.340	0.312	-0.362	-0.154+0.174	0.692	0.162	-0.329+0.174	-0.008	-0.340	-0.312	-0.248
9	0.342	0.312	-0.421	-0.108	0.855	0.220	-0.434	-0.111	-0.342	-0.312	0.0
10	0.312	0.312	-0.108	-0.108	0.220	0.220	-0.111	-0.111	-0.312	-0.312	0.0

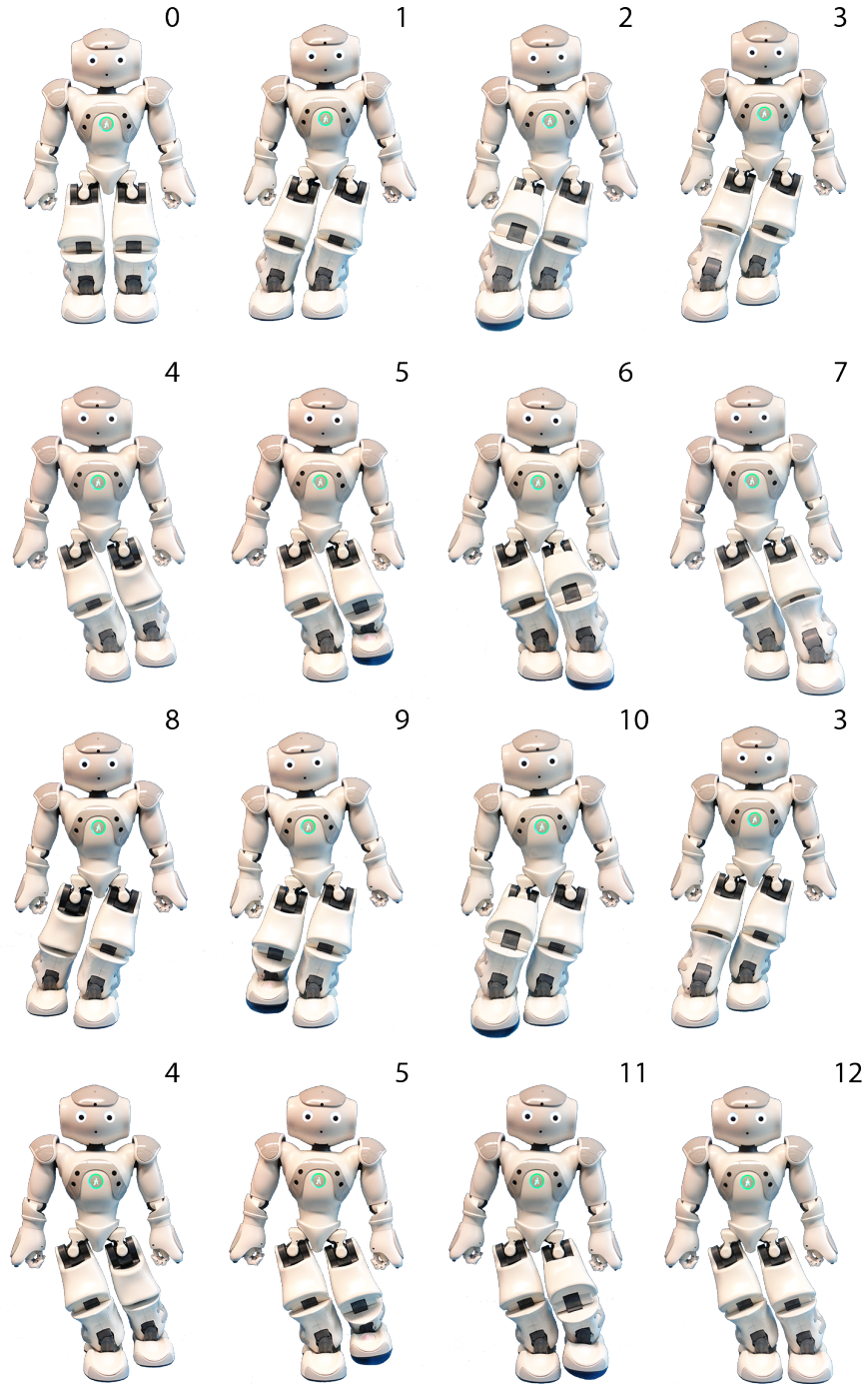


Figure 3.12: Forward walking postures

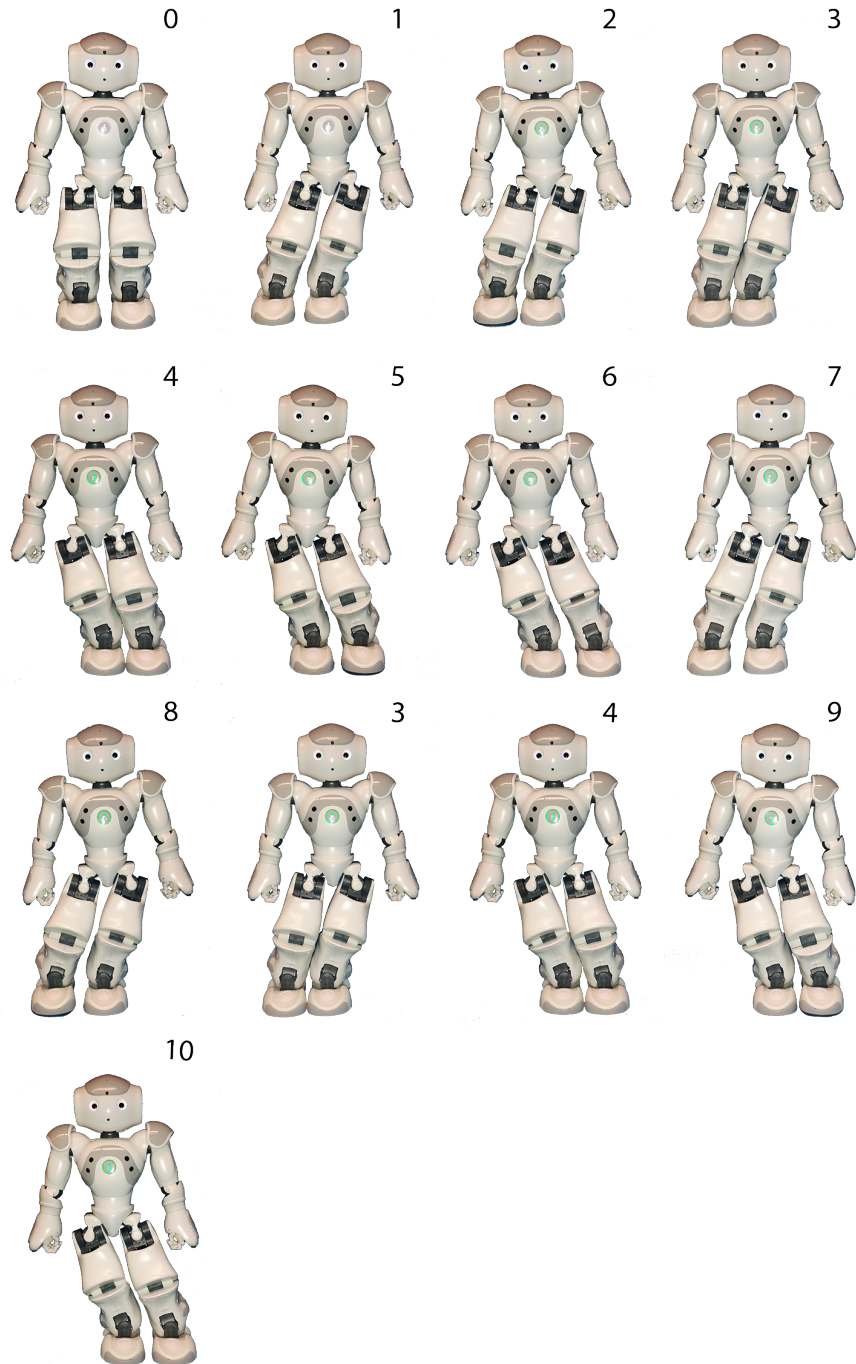


Figure 3.13: Lateral walking postures

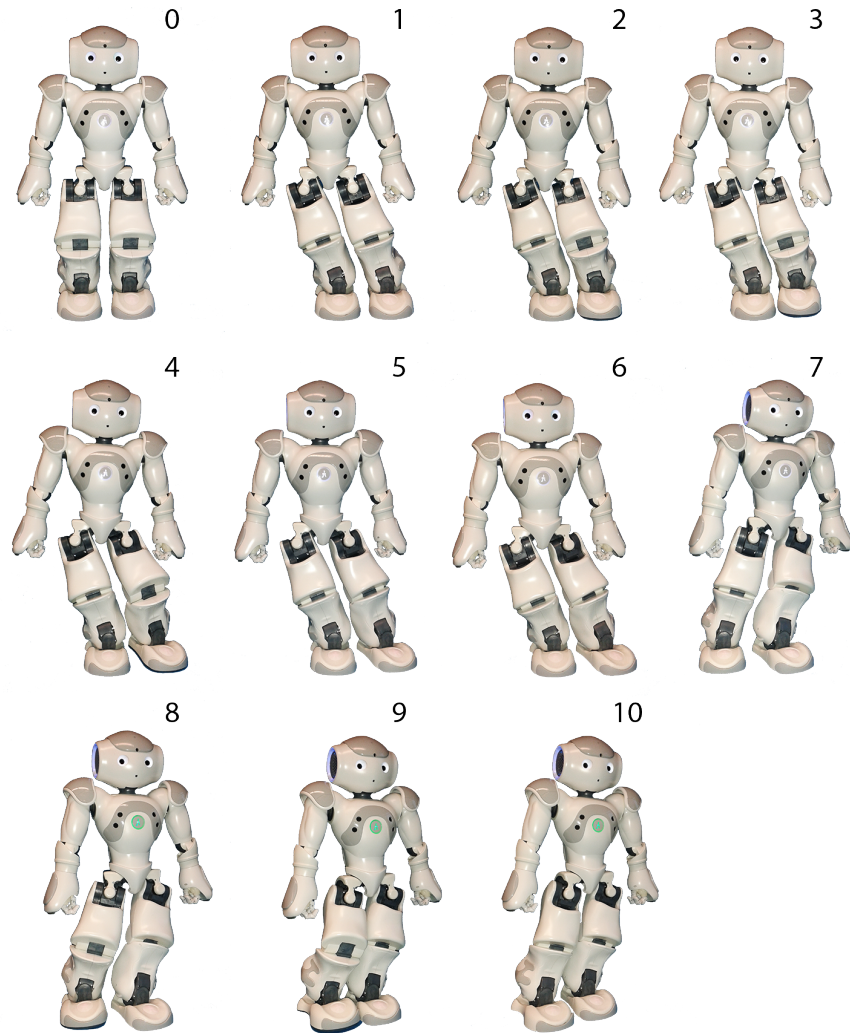


Figure 3.14: Turn-in-place walking postures

Chapter 4

Humanoid Trajectory Planning

In this work, a method taken from manipulator robot theory is applied to humanoid walking. Fifth and seventh order polynomials are proposed to define the trajectories of the center of gravity and the swing foot. The polynomials are designed so that the acceleration and jerk are constrained to have a zero value particularly at two moments: at the single support phase and at the foot landing, thus, minimizing internal disturbance forces.

These trajectories have been programmed using the numerical software package provided by [ESI-Group (2019)], which allowed to compare the acceleration and jerk waveforms of both: the acceleration-constrained and jerk-constrained trajectories, where the acceleration waveform is the most critical, because (as the force is proportional to it) abrupt changes in its shape, can conduce to internal robot destabilization. These proposed trajectories were designed from a mathematical point of view, i.e., they were not loaded into the robot NAO.

4.1 Acceleration and Jerk Constraints in Humanoid Trajectory Planning

The trajectory planning is used to find the series of points that connects an initial and a final configuration while satisfying the specified constraints at the endpoints [Spong et al. (2006)]. There exist several kinds of planned trajectories in humanoid robotics describing how a specific humanoid part must move in order to accomplish the walking process. Particularly, there are two trajectories of interest in the humanoid walking: the Center of Gravity (CoG) and the *swing-foot* trajectories [Kaynov (2010); Vukobratovic et al. (1990)]. In relation to the CoG trajectory, one of the easiest and most intuitive approach is based in the sinusoidal function and its variations, as can be seen in some works [Graf et al. (2009); Tay (2009)]. In addition, the inverted pendulum model has been used in [Kajita et al. (2014,0)] to describe the trajectory of the CoG.

Regarding the trajectory planing of the swing-foot, the cycloidal function has been studied in [Olvera et al. (2009); Park et al. (2006a); Strom et al. (2010)] where it has been claimed that the features of the cycloidal function include a slow start, a fast moving, and a slow stop; thereby reducing the speed burden of the actuators.

Consider that in this work, the x-axis, the y-axis and the z-axis trajectories refer to the forward, lateral, and swing-foot movements of the humanoid robot; in accordance with the

right-hand rule. Consider also that the *double support phase* refers to the instant when the robot is supported by both feet, and the *single support phase*, the instant when it stands over one foot [Vukobratovic et al. (1990)].

Figure 4.1, shows a sinusoidal CoG *y-axis* trajectory simulated using the software *SciLab* [ESI-Group (2019)], i.e., the lateral movement of the CoG. Here, as in work described in [Said et al. (2015)], a lateral amplitude of 6.2 cm has been chosen. It can be observed that the CoG position must go from side to side due to the need of the robot to transfer its center of gravity from one foot to the other (see [Park and Lee (2013)]). It can be seen that the sinusoidal function has the maximum absolute acceleration in its crests and troughs, which are the least-stable walking stages of the robot, because in those moments, the robot is standing on just one foot.

Figure 4.2, shows an elliptical trajectory, (i.e., a modified cycloidal function) which allows for the step size to have a different magnitude than its height. Here a maximum foot elevation of 2.99 cm has been used. If a cycloidal-like function is used to execute the *swing-foot* trajectory, then, the foot-to-ground impact [Park et al. (2006b)] could be aggravated by the infinite n -derivatives at the start and stop points (as can be seen at 0.2, 0.3, 0.7, and 0.8 seconds in Fig. 4.2), thus, leading to robot imbalance.

Finally, although a fast walking speed can be reached by using the inverted pendulum model [Graf and Röfer (2010)]; the small available time to perform the *double support phase*, the limitation in the step size, and the knee bending (in order to keep the CoM with a constant height), are the main drawbacks [Shin and Kim (2015)].

In contrast, with the aforementioned advantages of trajectories based in sinusoidal and cycloidal functions, as well as those based in the inverted pendulum model; the objective of this study is to analyze fifth-order and a seventh-order polynomial trajectories, which allow for the acceleration to be constrained particularly at the single support phase, and at the foot landing; this, in order to reduce the internal forces which result in robot imbalance. This approach can be applied particularly to affordable humanoid robots whose sensors, high precision actuators, and computational power are limited [Missura and Behnke (2014)].

Fifth-order polynomials allow for constraining the acceleration, whereas seventh-order polynomials allow for constraining both: acceleration and jerk. Although third-order polynomials have already been used in literature for humanoid trajectories [Park et al. (2006a,0)], in this work, a comparison of the effects of acceleration and jerk constraints is provided by means of computer simulations to analyze the CoG and the swing-foot trajectories, i.e., the movements in the *y-axis* and the *z-axis*.

This chapter begins by presenting the fifth-order polynomials in Section 4.2 where the acceleration and the jerk profiles are compared for the acceleration-constrained trajectories of the CoG and the swing foot. Then, in Section 4.3 seventh-order polynomials are shown, where the acceleration and the jerk profiles of the jerk-constrained trajectories are studied. Finally, in Section 4.4 a comparison between the fifth and seventh order polynomials is carried out.

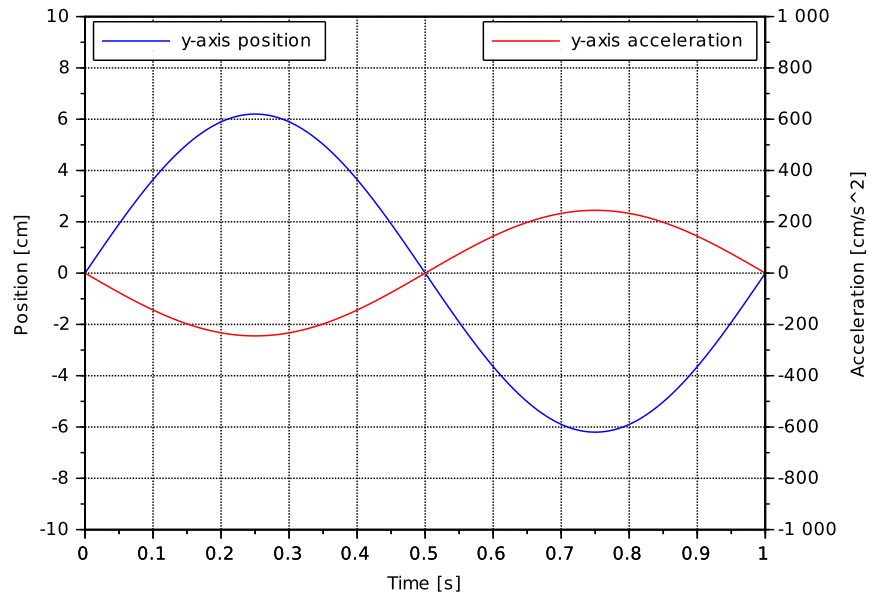


Figure 4.1: Position and acceleration of a sinusoidal CoG y-axis trajectory

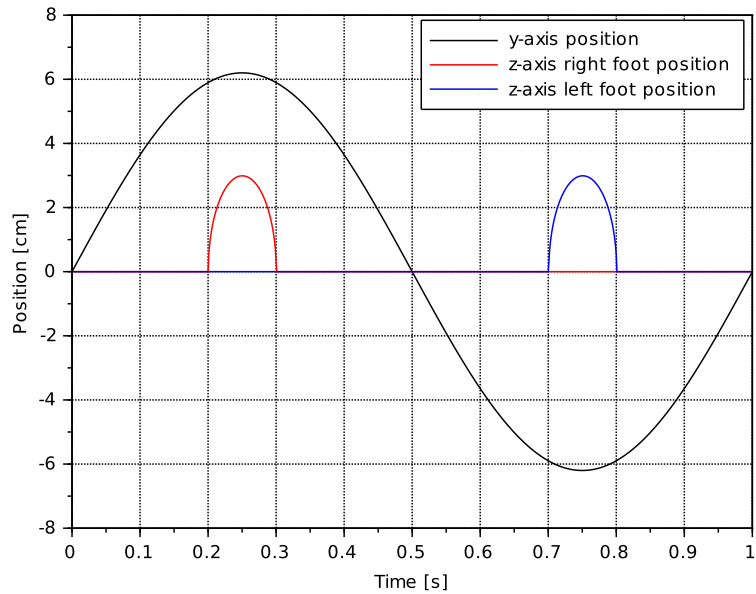


Figure 4.2: Position of a sinusoidal CoG y-axis trajectory and a cycloidal-like swing-foot z-axis trajectory

4.2 Fifth order polynomial: Acceleration-constrained Humanoid Trajectories

According to Newton's second law, the force is proportional to the mass and the acceleration. Given the mass of a certain robot part, it is possible to make the assumption that the greater its acceleration, the larger the internal force generated by that part. In consequence, by constraining the CoG trajectory to have zero acceleration at the *single-support phase* (lapses from 0.2 to 0.3 and from 0.7 to 0.8 in Fig. 4.5), then, the internal disturbance forces are minimized at unstable robot configurations, thus, contributing to robot equilibrium.

The required fifth order polynomial $q(t)$ to ensure that the acceleration can be restricted is shown in Eq. (4.1), where $a_0, a_1, a_2, a_3, a_4, a_5$ are the polynomial coefficients, and t is the time.

$$q(t) = a_0 + a_1(t) + a_2(t)^2 + a_3(t)^3 + a_4(t)^4 + a_5(t)^5 \quad (4.1)$$

Considering the initial conditions, such as the initial position $q(t_0)$, the initial velocity $v(t_0)$, and the initial acceleration $\alpha(t_0)$; as well as the final conditions, such as the final position $q(t_f)$, the final velocity $v(t_f)$, and the final acceleration $\alpha(t_f)$; and writing the appropriate number of derivatives, we obtain the set of Eqns. in (4.2); where t_0 and t_f refer to the initial and final times, respectively.

$$\begin{aligned} q(t_0) &= a_0 + a_1(t_0) + a_2(t_0)^2 + a_3(t_0)^3 + a_4(t_0)^4 + a_5(t_0)^5 \\ v(t_0) &= a_1 + 2a_2(t_0) + 3a_3(t_0)^2 + 4a_4(t_0)^3 + 5a_5(t_0)^4 \\ \alpha(t_0) &= 2a_2 + 6a_3(t_0) + 12a_4(t_0)^2 + 20a_5(t_0)^3 \\ q(t_f) &= a_0 + a_1(t_f) + a_2(t_f)^2 + a_3(t_f)^3 + a_4(t_f)^4 + a_5(t_f)^5 \\ v(t_f) &= a_1 + 2a_2(t_f) + 3a_3(t_f)^2 + 4a_4(t_f)^3 + 5a_5(t_f)^4 \\ \alpha(t_f) &= 2a_2 + 6a_3(t_f) + 12a_4(t_f)^2 + 20a_5(t_f)^3 \end{aligned} \quad (4.2)$$

The set of Eqns. in (4.2) can be written in matrix form:

$$\begin{bmatrix} 1 & t_0 & t_0^2 & t_0^3 & t_0^4 & t_0^5 \\ 0 & 1 & 2t_0 & 3t_0^2 & 4t_0^3 & 5t_0^4 \\ 0 & 0 & 2 & 6t_0 & 12t_0^2 & 20t_0^3 \\ 1 & t_f & t_f^2 & t_f^3 & t_f^4 & t_f^5 \\ 0 & 1 & 2t_f & 3t_f^2 & 4t_f^3 & 5t_f^4 \\ 0 & 0 & 2 & 6t_f & 12t_f^2 & 20t_f^3 \end{bmatrix} \begin{bmatrix} a_0 \\ a_1 \\ a_2 \\ a_3 \\ a_4 \\ a_5 \end{bmatrix} = \begin{bmatrix} q_0 \\ v_0 \\ \alpha_0 \\ q_f \\ v_f \\ \alpha_f \end{bmatrix} \quad (4.3)$$

Matrix Eq. (4.3) can be written in compact form as shown in Eq. (4.4), where \mathbf{M} is the coefficient matrix regarding time, \mathbf{a} contains the vector of coefficients; and \mathbf{b} consists of the initial and final conditions. Finally, vector \mathbf{a} is solved by using the *Gauss-Jordan reduction* procedure, which can be found in [Nakos et al. (1999)].

Table 4.1: Initial and final time of the CoG walking stages

stage	t_0 [s]	t_f [s]
s_1	0.00	0.199
s_2	0.20	0.299
s_3	0.30	0.699
s_4	0.70	0.799
s_5	0.80	0.999

Table 4.2: Acceleration-constrained coefficients for the CoG y-axis trajectory

	s_1	s_2	s_3	s_4	s_5
a_0	0	6.2	136.22	- 6.2	- 67384.06
a_1	0	0	- 1617.61	0	380678.64
a_2	0	0	7706.23	0	- 856908.01
a_3	7867.42	0	- 17380	0	960516.68
a_4	- 59302.17	0	18374.43	0	- 536103.61
a_5	119200.36	0	- 7357.13	0	119200.36

$$\mathbf{M} \cdot \mathbf{a} = \mathbf{b} \quad (4.4)$$

Figure 4.3 shows the y-axis and the x-axis CoG trajectories while the humanoid robot is taking a single step. The y-axis trajectory has an oscillatory behavior because the robot's weight has to be supported by the left and right feet intermittently. In the other hand, the x-axis trajectory is the one responsible of an effective forward movement. This humanoid step has been divided into 5 stages whose initial and final times can be seen in Table 4.1. The sampling period has been chosen to be 0.001 seconds. Following the work in [Said et al. (2015)], the lateral amplitude has been chosen to be 6.2 *cm* regarding the y-axis trajectory, and 5 *cm* for the step size, regarding the x-axis trajectory.

In relation to Figure 4.3, stage s_1 corresponds to the time where the CoG moves from a standstill position (on both feet) towards the left foot. In stage s_2 the CoG remains over center of the left foot while the right foot is lifted and moved forwards (see swing trajectories in Fig. 4.4). In stage s_3 the CoG moves from the center of the left foot towards the center of the right foot; in addition, CoG also moves forwards. In stage s_4 the CoG remains over the center of the right foot while the left foot is lifted and moved forwards (see swing trajectories in Fig. 4.4). In stage s_5 the CoG moves from the center of the right foot to a standstill position on both feet. Tables 4.2 and 4.3 show the specific polynomial coefficients for the y-axis and the x-axis CoG trajectories, respectively.

Regarding Fig. 4.4, the swing-foot trajectory has been subdivided into four walking

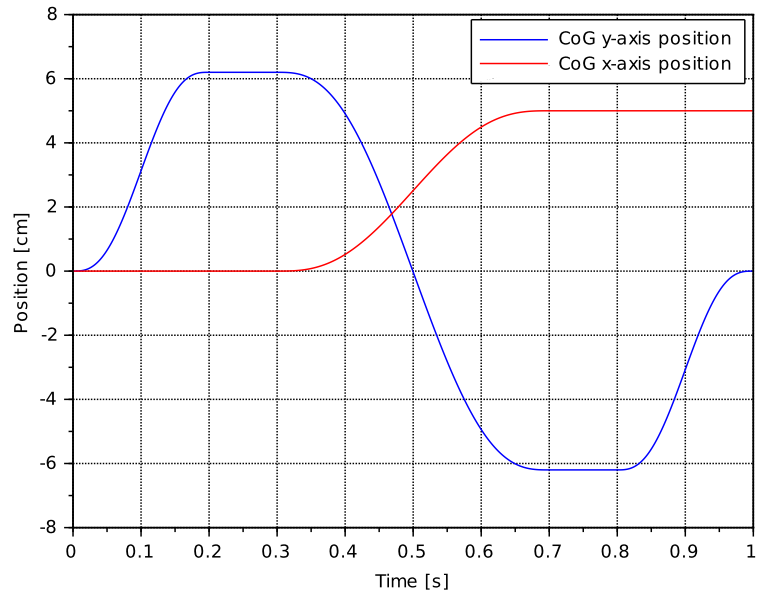


Figure 4.3: Acceleration-constrained position trajectories for the CoG in the x and y axes

Table 4.3: Acceleration-constrained coefficients for the CoG x-axis trajectory

	s_1	s_2	s_3	s_4	s_5
a_0	0	0	- 52.43	5	5
a_1	0	0	652.26	0	0
a_2	0	0	- 3107.35	0	0
a_3	0	0	7008.06	0	0
a_4	0	0	- 7409.04	0	0
a_5	0	0	2966.58	0	0

Table 4.4: Initial and final times of the swing-foot walking stages

Foot	stage	t_0 [s]	t_f [s]
right	s_a	0.20	0.249
	s_b	0.25	0.299
left	s_c	0.7	0.749
	s_d	0.75	0.799

stages: two for the right foot and two for the left one. The initial and final times of these stages can be seen in Table 4.4. It can be seen that stage s_a has the same initial time as stage s_2 , that is, the right foot begins to be lifted when the robot starts to be supported by the left foot. In the other hand, the end of stage s_b coincides with the end of stage s_2 , that is, the right foot lands when the robot stops to be supported only by the left foot. The movement for the left foot is defined similarly to the right foot swing trajectory,

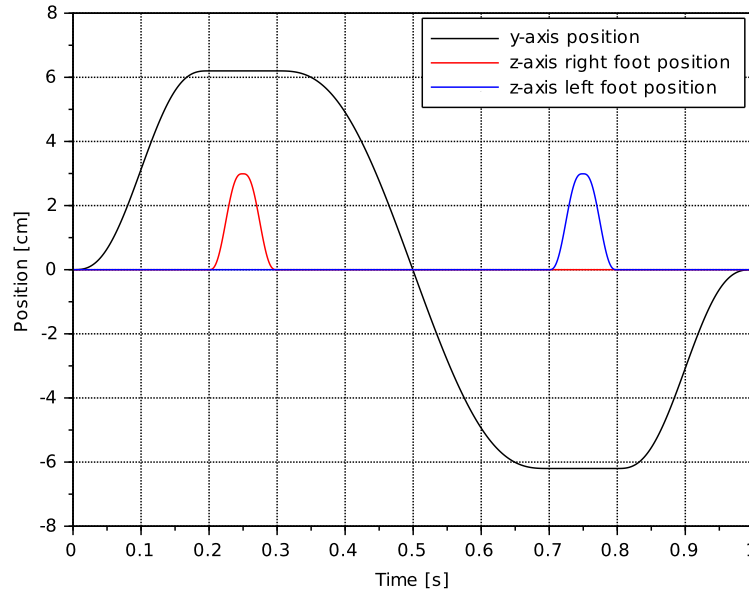


Figure 4.4: Acceleration-constrained trajectories: y - axis (CoG) trajectory and z - axis (swing-foot) trajectories

Figure 4.5 shows the acceleration profile of the CoG position trajectory when it is restricted to be zero in the single support phase, particularly, at stages s_2 and s_4 . It can be seen that although the acceleration has been effectively constrained to be zero at these stages, there still remain sudden changes in acceleration at 0.2, 0.3, 0.7, and 0.8 seconds. Here, a sudden change in acceleration represents an impact that contributes to robot imbalance.

Table 4.5: Acceleration-constrained coefficients for the swing-foot z-axis trajectory

	s_a	s_b	s_c	s_d
a_0	-34804.32	0	-12629268	17640071
a_1	787536.57	0	87291460	-1.140×10^8
a_2	-7100480.3	0	-2.412×10^8	2.948×10^8
a_3	31882120	2.99	3.332×10^8	-3.808×10^8
a_4	-71289963	0	-2.301×10^8	2.459×10^8
a_5	63509989	0	63509989	-63509988

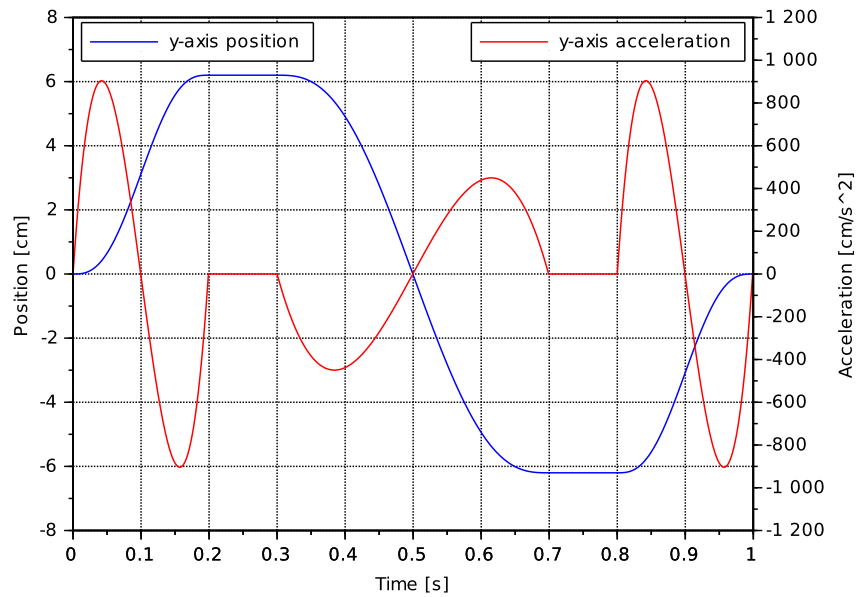


Figure 4.5: Acceleration profile of the acceleration-constrained CoG trajectory in the y-axis

Figure 4.6 describes the jerk profile when the acceleration is constrained to be zero at the single support phase (as shown in Fig. 4.5). Here jerk discontinuities can be observed at 0.2, 0.3, 0.7 and 0.8, which belong to the same places where sudden changes in the acceleration take place.

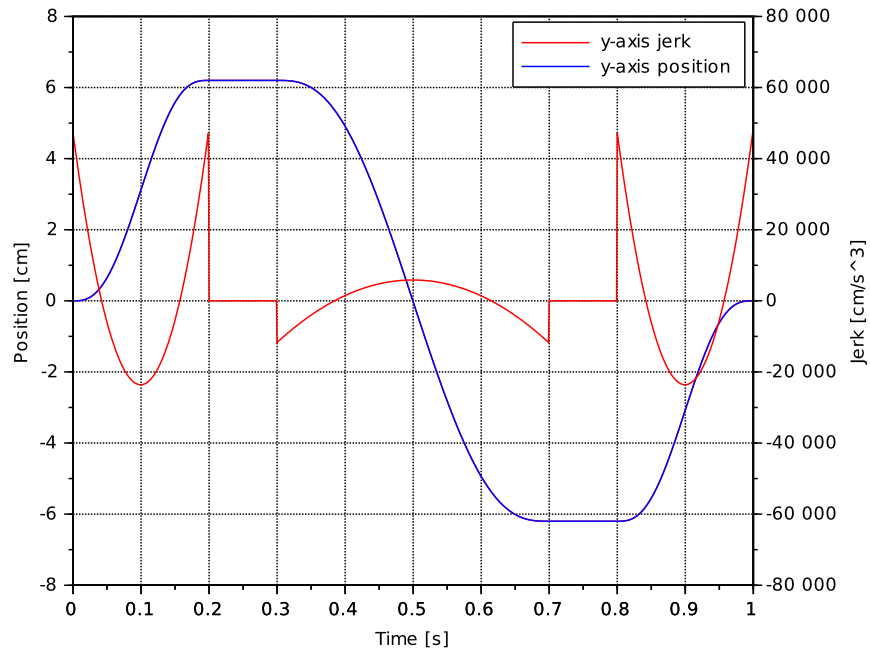


Figure 4.6: Jerk profile of the acceleration-constrained CoG trajectory in the y-axis

Figures 4.7 and 4.8, show respectively the acceleration and jerk profiles of the swing trajectory of the right foot when the fifth-order polynomial is used. In this trajectory, the acceleration has been restricted to be zero at three points: first, at the beginning of the swing movement; second, when the foot reaches its maximum height; and third, when it lands. It can be seen that both profiles show acceleration and jerk discontinuities which contribute to robot instability when the foot reaches its maximum height.

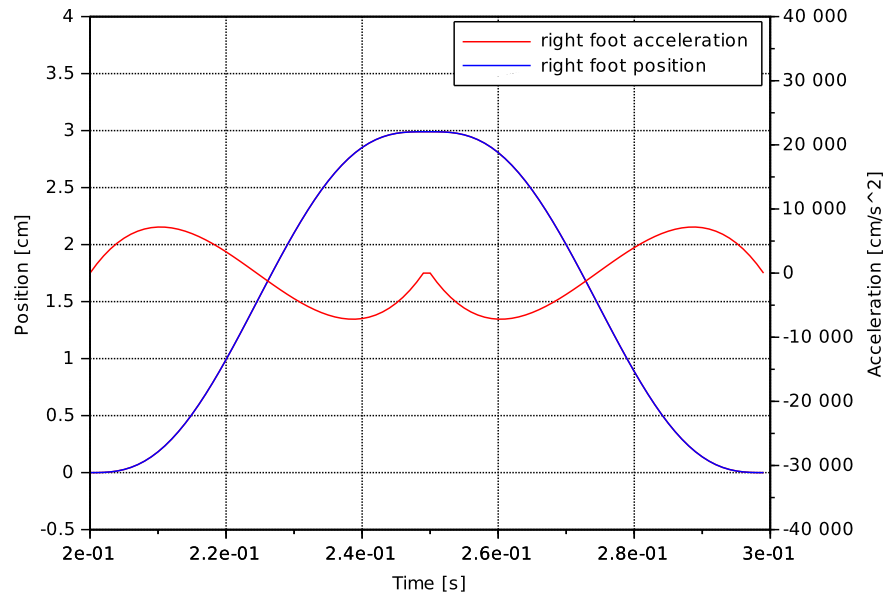


Figure 4.7: Acceleration profile of the acceleration-constrained swing-foot trajectory in the z-axis

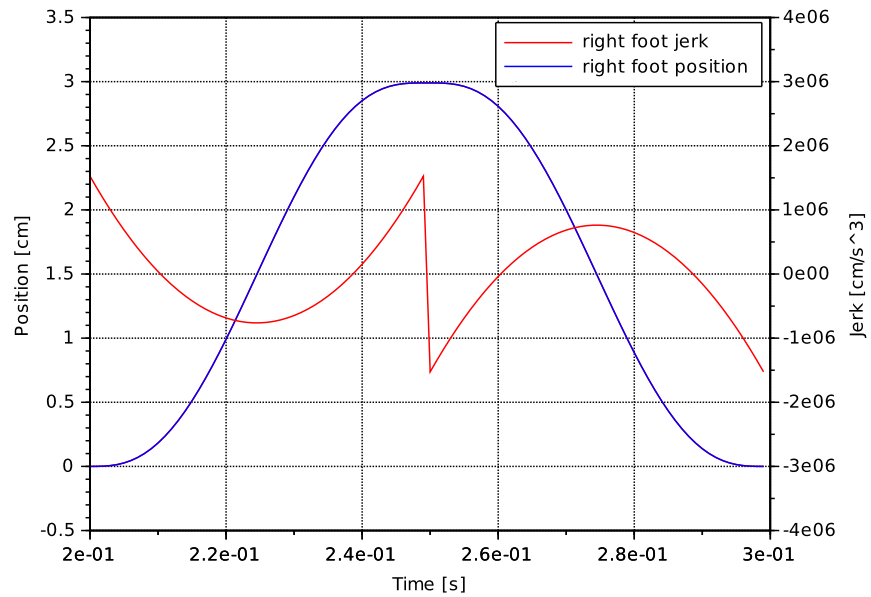


Figure 4.8: Jerk profile of the acceleration-constrained swing-foot trajectory in the z-axis

4.3 Seventh-order Polynomials: Jerk-constrained Humanoid Trajectories

Although using a fifth order polynomial is effective to eliminate the acceleration at the single support phase as well as for reducing the foot-to-ground impact at landing, the problem of the acceleration discontinuities still remains. To solve this problem, it is possible to constrain the jerk of the humanoid trajectories by using a seventh order polynomial, as in shown in Eq. (4.5).

$$q(t) = a_0 + a_1(t) + a_2(t)^2 + a_3(t)^3 + a_4(t)^4 + a_5(t)^5 + a_6(t)^6 + a_7(t)^7 \quad (4.5)$$

Considering the initial and final conditions of the jerk, $\gamma(t_0)$ and $\gamma(t_f)$, respectively; and taking the appropriate number of derivatives, we obtain the Eqns. in (4.6).

$$\begin{aligned} q(t_0) &= a_0 + a_1(t_0) + a_2(t_0)^2 + a_3(t_0)^3 + a_4(t_0)^4 + a_5(t_0)^5 + a_6(t_0)^6 + a_7(t_0)^7 \\ v(t_0) &= a_1 + 2a_2(t_0) + 3a_3(t_0)^2 + 4a_4(t_0)^3 + 5a_5(t_0)^4 + 6a_6(t_0)^5 + 7a_7(t_0)^6 \\ \alpha(t_0) &= 2a_2 + 6a_3(t_0) + 12a_4(t_0)^2 + 20a_5(t_0)^3 + 30a_6(t_0)^4 + 42a_7(t_0)^5 \\ \gamma(t_0) &= 6a_3 + 24a_4(t_0) + 60a_5(t_0)^2 + 120a_6(t_0)^3 + 210a_7(t_0)^4 \\ q(t_f) &= a_0 + a_1(t_f) + a_2(t_f)^2 + a_3(t_f)^3 + a_4(t_f)^4 + a_5(t_f)^5 + a_6(t_f)^6 + a_7(t_f)^7 \\ v(t_f) &= a_1 + 2a_2(t_f) + 3a_3(t_f)^2 + 4a_4(t_f)^3 + 5a_5(t_f)^4 + 6a_6(t_f)^5 + 7a_7(t_f)^6 \\ \alpha(t_f) &= 2a_2 + 6a_3(t_f) + 12a_4(t_f)^2 + 20a_5(t_f)^3 + 30a_6(t_f)^4 + 42a_7(t_f)^5 \\ \gamma(t_f) &= 6a_3 + 24a_4(t_f) + 60a_5(t_f)^2 + 120a_6(t_f)^3 + 210a_7(t_f)^4 \end{aligned} \quad (4.6)$$

Equations in (4.6) can be written in matrix form as shown in Eq. (4.7), whose vector of coefficients \mathbf{a} is also obtained by performing a *Gauss-Jordan reduction*.

$$\begin{bmatrix} 1 & t_0 & t_0^2 & t_0^3 & t_0^4 & t_0^5 & t_0^6 & t_0^7 \\ 0 & 1 & 2t_0 & 3t_0^2 & 4t_0^3 & 5t_0^4 & 6t_0^5 & 7t_0^6 \\ 0 & 0 & 2 & 6t_0 & 12t_0^2 & 20t_0^3 & 30t_0^4 & 42t_0^5 \\ 1 & t_f & t_f^2 & t_f^3 & t_f^4 & t_f^5 & t_f^6 & t_f^7 \\ 0 & 1 & 2t_f & 3t_f^2 & 4t_f^3 & 5t_f^4 & 6t_f^5 & 7t_f^6 \\ 0 & 0 & 2 & 6t_f & 12t_f^2 & 20t_f^3 & 30t_f^4 & 42t_f^5 \end{bmatrix} \begin{bmatrix} a_0 \\ a_1 \\ a_2 \\ a_3 \\ a_4 \\ a_5 \\ a_6 \\ a_7 \end{bmatrix} = \begin{bmatrix} q_0 \\ v_0 \\ \alpha_0 \\ \gamma_0 \\ q_f \\ v_f \\ \alpha_f \\ \gamma_f \end{bmatrix} \quad (4.7)$$

Figure 4.9 shows the CoG y-axis trajectory when the jerk is constrained to be zero at the single support phase. In addition, the CoG x-axis trajectory is also shown, where the jerk has been restricted to be zero at the beginning and ending of the forward movement. Figure 4.10 shows the y-axis trajectory along with the swing trajectories of the right and left feet,

Table 4.6: Jerk-constrained coefficients for the CoG y-axis trajectory

	s_1	s_2	s_3	s_4	s_5
a_0	0	6.2	- 573.30	- 6.2	4539611
a_1	0	0	9943.39	0	- 35852101
a_2	0	0	- 71054.74	0	1.211×10^8
a_3	0	0	273084.66	0	$- 2.265 \times 10^8$
a_4	138371.75	0	- 607606.95	0	2.537×10^8
a_5	- 1668805	0	781358.12	0	$- 1.701 \times 10^8$
a_6	6988295.7	0	- 538610.66	0	63175597
a_7	- 10033447	0	154042.8	0	- 10033447

Table 4.7: Jerk-constrained coefficients for the CoG x-axis trajectory

	s_1	s_2	s_3	s_4	s_5
a_0	0	0	233.67	5	5
a_1	0	0	- 4009.43	0	0.
a_2	0	0	28651.10	0	0.
a_3	0	0	- 110114.78	0	0.
a_4	0	0	245002.8	0	0.
a_5	0	0	- 315063.76	0	0.
a_6	0	0	217181.72	0	0.
a_7	0	0	- 62114.03	0	0.

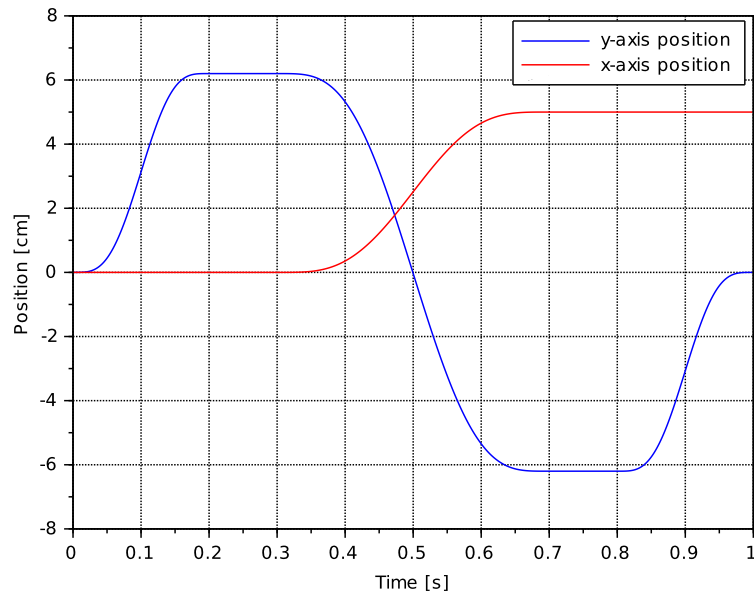
where the jerk has been constrained to be zero at the beginning and at the ending of the swing movement, as well as when the feet reach their maximum height.

The acceleration profile of the jerk-constrained CoG y-axis trajectory is shown in Fig. 4.11. Here, the acceleration discontinuities have been effectively removed. Figure 4.12 shows the jerk profile of the jerk-constrained CoG y-axis trajectory, where it can be seen that the jerk discontinuities have been reduced. Figures 4.13 and 4.14, show the acceleration and the jerk profiles of the jerk-constrained swing trajectories of the right foot. It can be noticed that the acceleration discontinuities have been effectively removed in Fig. 4.13, and that the jerk discontinuities have been reduced in Fig. 4.14.

Tables 4.6 and 4.7 show the y-axis and the x-axis polynomial coefficients for the CoG trajectory. Similarly, Table 4.8 shows the z-axis polynomial coefficients for the swing trajectory of the right foot.

Table 4.8: Jerk-constrained coefficients for the swing-foot z-axis trajectory

	s_a	s_b	s_c	s_d
a_0	2409937.5	0	9.194×10^9	-1.468×10^{10}
a_1	-76228029	0	-8.895×10^{10}	1.328×10^{11}
a_2	1.031×10^9	0	3.688×10^{11}	-5.150×10^{11}
a_3	-7.727×10^9	0	-8.491×10^{11}	1.109×10^{12}
a_4	3.467×10^{10}	2.99	1.173×10^{12}	-1.433×10^{12}
a_5	-9.310×10^{10}	0	-9.717×10^{11}	1.111×10^{12}
a_6	1.386×10^{11}	0	4.472×10^{11}	-4.780×10^{11}
a_7	-8.817×10^{10}	0	-8.817×10^{10}	8.817×10^{10}

Figure 4.9: Jerk-constrained trajectories for the CoG in the x and y axes

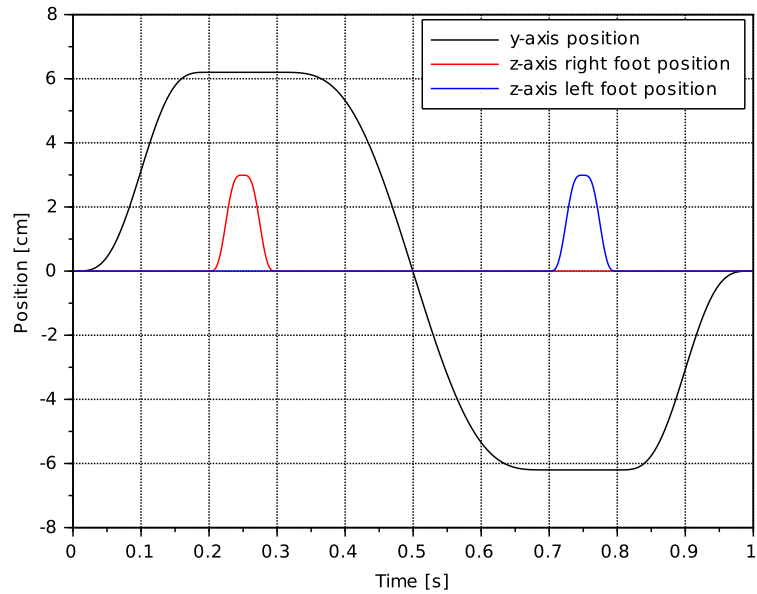


Figure 4.10: Jerk-constrained trajectories: y -axis (CoG) trajectory and z -axis (swing-foot) trajectories

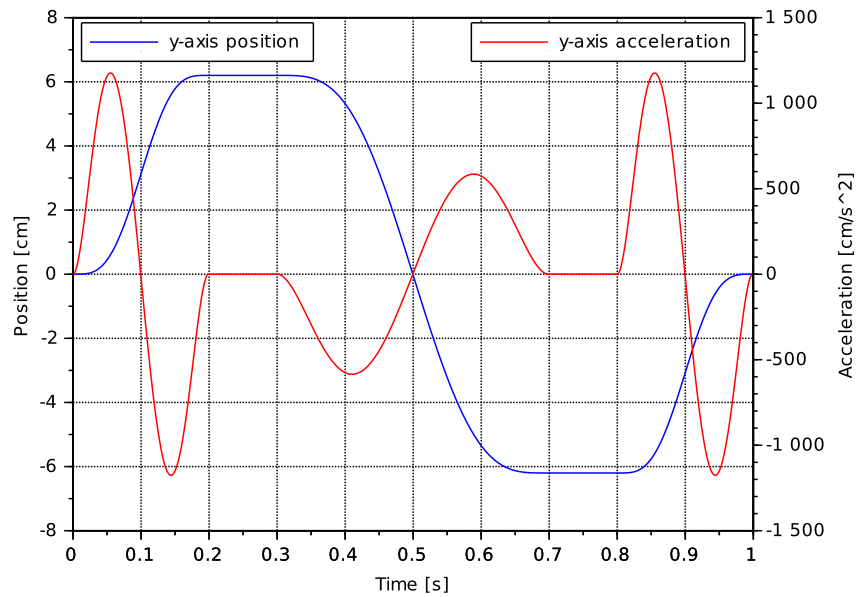


Figure 4.11: Acceleration profile of the jerk-constrained CoG trajectory in the y -axis

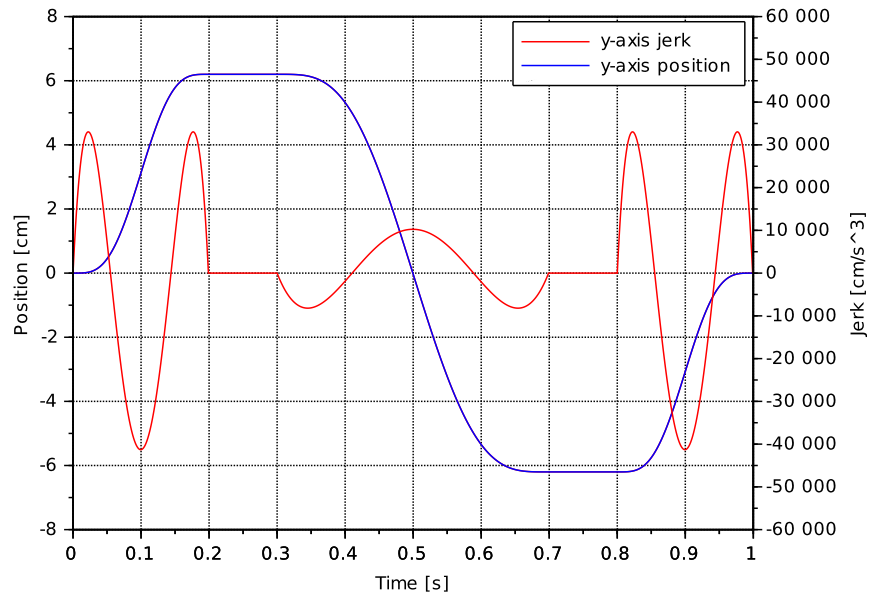


Figure 4.12: Jerk profile of the jerk-constraint CoG trajectory in the y-axis

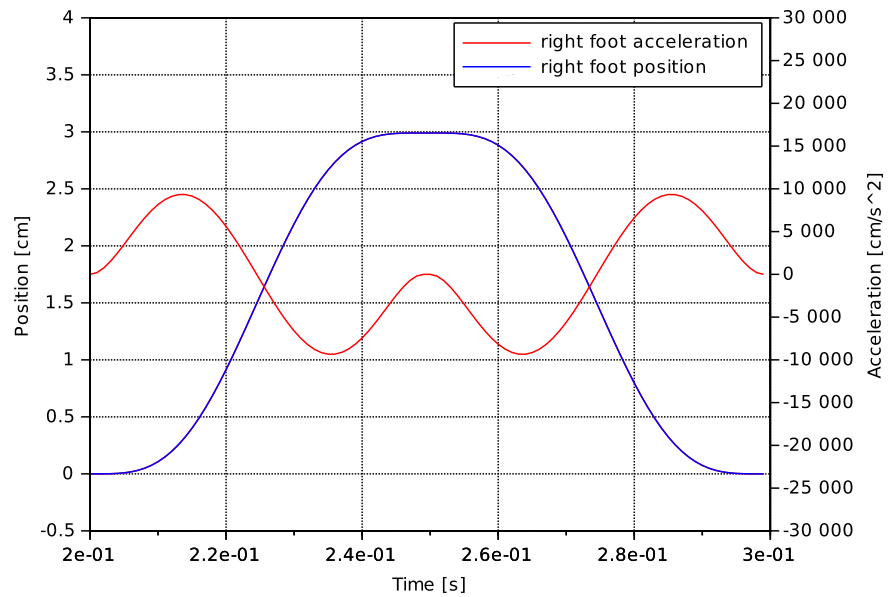


Figure 4.13: Acceleration profile of the jerk-constrained swing-foot trajectory in the z-axis

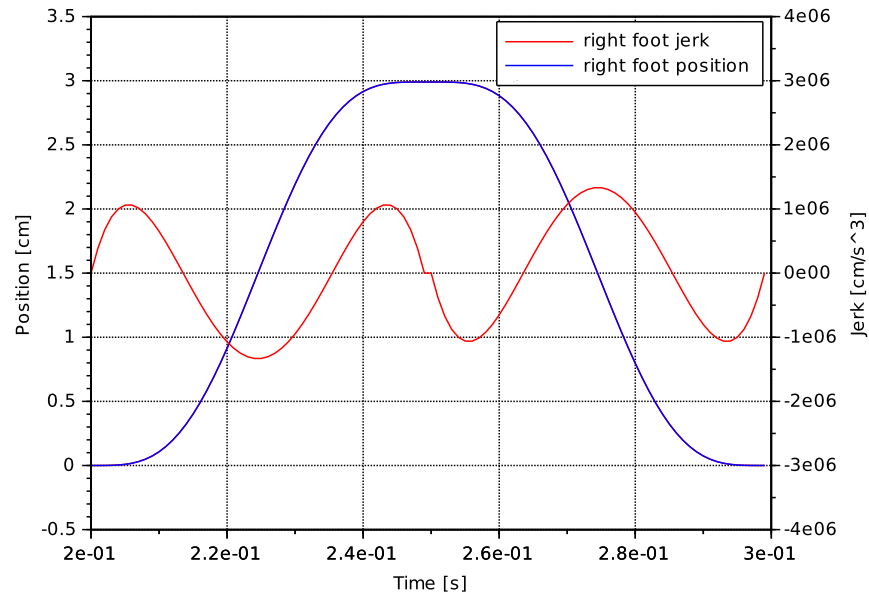


Figure 4.14: Jerk profile of the jerk-constrained swing-foot trajectory in the z-axis

4.4 Comparison of the fifth-order and seventh-order polynomials

In this section a comparison of the proposed fifth-order and seventh-order polynomials is performed; i.e., the acceleration-constrained and the jerk-constrained trajectories. The trajectory regarding the CoG movement in the y-axis is shown in Fig. 4.15. Figure 4.16, shows the swing trajectory in the z-axis of the right foot.

From figures 4.15 and 4.16, it can be seen that although the acceleration-constrained and the jerk-constrained trajectories are similar, the inclusion of higher degree terms in the polynomial function has a severe impact when removing the acceleration discontinuities in Figs. 4.5 and 4.7. In this manner, the internal destabilizing forces can be reduced. See Eqns. (4.1) and (4.5).

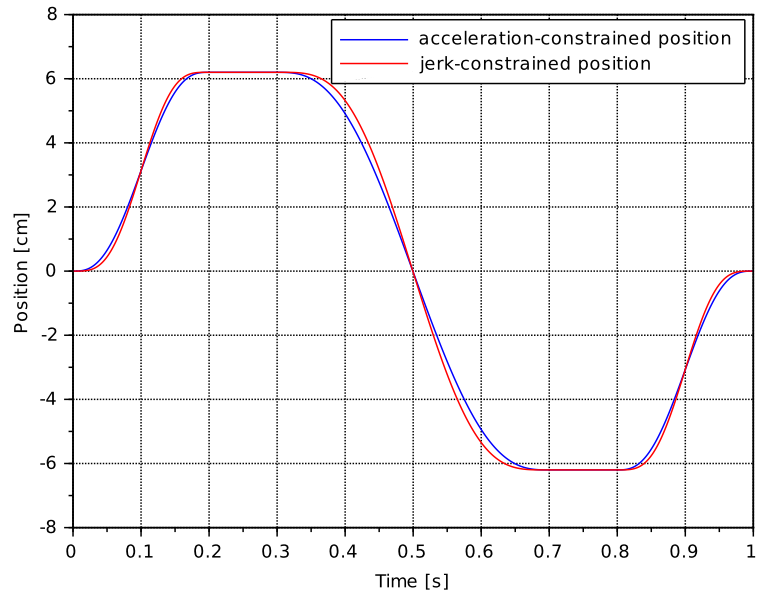


Figure 4.15: y-axis CoG trajectories

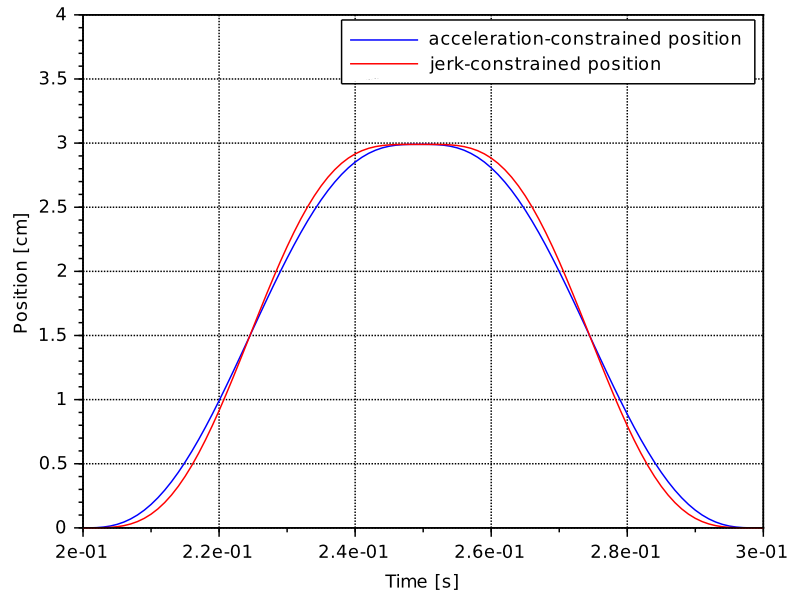


Figure 4.16: z-axis swing trajectory of the right foot

Chapter 5

Conclusions and Future Work

5.1 Conclusions

In regards to the **humanoid kinematics**, the following achievements and observations were made:

- This dissertation has presented an **analytical, omnidirectional, and closed-form** solution for the lower limb kinematics for the small-sized humanoid robot NAO. The kinematics are analytical in the sense that the Denavit-Hartenberg matrix concatenations rather than a pure geometrical procedure have been used; this allowed for the position and orientation terms to be mathematically determined. Because the kinematic equations allow for the humanoid to go forwards, sideways and to perform a turn-in place motion, they are omnidirectional. Finally, because there are no iterative approaches, the kinematics are also in a closed-form.
- This study has determined the **direct and inverse kinematics**, as well as the **forward and reverse kinematics** for the swing phase and the support phase. Here, the end-effector coordinates were calculated for a specific set of joint angles (direct kinematics), and the joint angles were calculated for a set of end-effector coordinates (inverse kinematics). In the forward kinematic analysis, the position and orientation of the robot hips were described as seen by the ankle, allowing for the body of the humanoid to be moved. In the reversed kinematic analysis, the ankle was described as seen by the hips, allowing for the foot to be moved across the air in the swing phase. The forward and reversed kinematic analysis allowed to **avoid the matrix inversion** operations which add mathematical complexity to the inverse kinematic equations.
- In this work, the **position and orientation** equations have been **solved separately** by taking advantage of the fact that the robot leg has three joint axes intersecting at the end-effectors (either the ankle or the hips). In the forward kinematic analysis, the kinematic chain of the robot leg was solved up to the location of the hips without considering the movement of the hip joints, allowing for the position matrix concatenations to be obtained. After that, the orientation matrix concatenations were obtained by a kinematic chain analysis which considered only the hip joints. That is, the forward kinematic analysis, uses the joints of the ankle and the knee as position parameters; while the

joints of the hips, are used as orientation parameters. A similar approach was followed in the reversed kinematic analysis, where the joints of the hips and the knee were used as position parameters, meanwhile the joints of the ankle, as orientation parameters.

- The inclusion of the joint order used in the **triangular geometrical analysis within the DH procedure** helped to compact the position equations analytically. The constant matrix transformations were crucial for this task because they allowed for the joint coordinate systems in the matrix concatenations to be aligned in exactly the same order and orientation as they would have had in a purely the geometrical analysis.
- Furthermore, the DH parameters were redefined and constrained in order to include the hip-yaw-pitch joint, which is an articulation which is shared among both of the legs and the hips; this method allowed for obtaining the solutions for the **turn-in-place** rotation in an **analytical** manner. This procedure was carried out in the forward kinematic analysis. Here, the position parameters such as the joint angles of the ankle and the knee, were constrained to be equal to zero because they do not interfere with the turn-in-place orientation analysis. In addition, the hip roll actuation was also set to zero because the coupling only takes place in the yaw and pitch movements at the hip. After this, the procedure consisted in matching a general Euler's angle matrix concatenation to the kinematic forward chain analysis which included the hip yaw-pitch (the coupled joint) in order to solve for a hip pitch compensation to cancel the unwanted pitch movement.
- The insertion of constant coordinate systems allowed for the **navigation** and the **end-effector** coordinate systems at the ankle and hips to be **aligned** with each other. In addition, the end-effector reference system corresponding to the turn-in-place analysis, is also aligned with the navigation coordinate system. This method, allowed for the terms in the position and orientation matrix concatenations to match mathematically in order to be equated directly and easily.
- The simple **3D geometric approach** allowed for the **singularities** to be avoided regarding the maximum possible humanoid step. The analysis was constructed from a triangle which was formed by considering the height of the robot hips, the maximum length of the leg when is fully stretched, and the size of the step. For a desired step size, the hips of the robot have to be lowered so that the swing leg is able to reach the soil. The **workspace for a humanoid step** is then described mathematically by the resulting formulas.

In regards to the **trajectory planning for humanoids**, the following achievements and observations were made:

- This dissertation has analyzed fifth-order and seventh-order polynomials to cancel the **acceleration and jerk** of the center of gravity when the robot is **standing on a single foot**, which is in fact, the most unstable stage of humanoid walking.
- These polynomials also removed the acceleration and jerk at **foot landing**, thus, reducing the **foot-to-ground impact** to contribute to robot equilibrium. Unlike cycloidal functions, polynomial trajectories do not have infinite derivatives at the start and stop points, so that the foot can reach the soil smoothly.

- It has been shown that although fifth-order polynomials can prevent the acceleration disturbances during the single support phase and foot landing, the sudden modifications in the function shape produces **abrupt changes in acceleration** which can degrade stability. However, by using seventh-order polynomials; i.e., considering jerk restrictions, the sudden changes in acceleration can be reduced. As the force is proportional to the mass and to the acceleration, by cancelling of the acceleration discontinuities, the force discontinuities are also eliminated.
- From the presented graphical analysis, it can be concluded that despite the **similarities** between the fifth-order and seventh-order polynomial trajectories, the inclusion of higher-order terms has a great impact in the smoothness of the acceleration profiles. In Addition, polynomial trajectories allowed for the allocation of a **rest time**, contributing to **human-like** step movement.

5.2 Contrast of the Related Work in Humanoid Kinematics and Trajectory Planning

To achieve the results in this dissertation, the related work has been crucial in the generation of new ideas; for example, the work provided by Donald Lee Pieper in [Pieper (1968)], has made possible to conceive the idea of the decoupling of position and orientation of a kinematic chain. Although the problem of humanoid robotic limbs is not addressed in his PhD thesis, the general idea was able to be applied to the lower limbs of humanoid NAO because the legs have intersecting rotational axis at the end-effectors located and the ankle and hips. The work done by Colin Graf in [Graf et al. (2009)] helped to realize that the geometry of the humanoid leg of NAO could be analyzed by matching the geometry of a triangle with the angles formed by the hip, the knee and the ankle. In the cited work, the position analysis was carried out from a pure geometrical point of view. However, in the dissertation presented here, this geometry was inserted into the Denavit-Hartenberg analysis, which allowed to manage the position and orientation equations from a pure analytical point of view, thus, simplifying the kinematic solutions. One of the most important related works, has been the one developed by Hyungju Andy Park in [Park et al. (2012)] which decoupled the position and orientation kinematic equations. To achieve this, they have analyzed the kinematic chain of a humanoid leg in two directions: the forward and the reversed. However, they still had to implement decision equations and some matrix inversion operations, adding complexity to the solutions. In the present dissertation, the matrix inversion operations were able to be completely avoided. The inverse kinematics procedure provided by Nikolaos Kofinas in [Kofinas et al. (2014)] makes use of the entire kinematic chain of the leg of the robot NAO, leading to solutions which are not explicit. In the present dissertation, we only have two base reference systems: the one situated at the ankle (which depends on the x , y , z coordinates), and the one located at the hip, (which depends on the x_s , y_s , z_s coordinates). Although the work presented by [Kaneko et al. (2019)] was presented after the publication of the work presented by Alejandro Said in [Said et al. (2015)], it is important to notice that they have addressed the problem of the limited range of actuation of the ankle joints by redesigning them to perform more human-like tasks. It was mentioned in Chapter 3, Section 3.5 that the workspace for humanoid step has

principally reduced by the limited actuation range of the ankle joints.

The work presented by Shuuji Kajita in [Kajita et al. (2002) and Kajita et al. (2003)], present a walking patten generator based on a simplified model regarding an inverted pendulum. The model is based in differential equations which have sinusoidal solutions dependable of the initial conditions (see also [Graf and Röfer (2010)]). With this model, humanoid have demonstrated to walk very fast, so it is the preferred choice for soccer games. However, the limitation in the step size is the mayor drawback, since sinusoidal trajectories do not provide for a rest stance lapse to perform large steps. In this dissertation, polynomial trajectories are proposed which provide for sufficient rest time to perform a large step. The work presented by Ill-Woo Park in [Park et al. (2006b)] 3rd order polynomials and cycloidal functions are proposed for the CoM and swing-foot trajectories, respectively. However, in this dissertation it has been demonstrated that polynomials which do not contemplate jerk constraints, tend to have acceleration discontinuities affecting the balance of the robot. Similarly, although cycloidal functions are simple to implement (see also [Mandava and Vundavilli (2016)]), they limit the velocity of the swing-foot since they have infinite derivatives at the start and stop points, which may produce foot-to-ground impacts. The jerk-constrained trajectories in this dissertation do provide for mathematical certainty regarding the acceleration limitation (and thus velocity), of the swing foot. In the work presented by Colin Graf in [Graf et al. (2009)], a mixture of a sinusoid, a triangular function, and the square root of a sinusoid have been used as a walking pattern generator. For the swing foot trajectory, they have proposed a cosine function (as it was also proposed in [Li et al. (2017)]); however, in the case of the mixture of functions, mathematical certainty is unavailable, while when using cosine functions with a rest time, mathematical acceleration discontinuities are present.

5.3 Future Work

5.3.1 Static Control Model for Humanoid Equilibrium

A static control model approach for humanoid equilibrium is useful because it provides a simple idea about the control strategy at small waking speeds because the inertial forces and ground perturbations are neglected. This model can be represented by Figure 5.1.

In the static double inverted pendulum model of Figure 5.1, q_1 represents the ankle angle, q_2 is the hip angle, m_1 is the mass of both legs, m_2 is the mass of the torso (including head, arms and shoulders), L_1 is the length of the legs (measured from the ground to the hips; i.e. neglecting the foot height), L_{c1} is the distance from the ground to the center of mass of the legs, L_{c2} is the distance from hips to the center of mass of the torso. The hip control strategy is assumed to be able of being applied to both: the sagittal and frontal planes; i.e. the ankle and hip angles can use rather the pitch or roll joints according to the plane being considered. Here, the *hip control strategy* refers to the ability of the system to compensate equilibrium perturbations by manipulating the hip joint angles; thus, modifying the torso inclination.

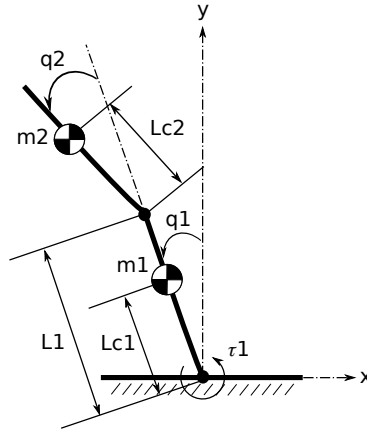


Figure 5.1: Static control model based on the double inverted pendulum with a hip strategy control

5.3.2 Dynamic Control Model for Humanoid Equilibrium with Ground Perturbations

The Inertial Measure Unit **IMU** is a device capable of sensing the tilt of a humanoid robot. Assuming the robot does not take off both feet at the same time, a tilt reading may be caused by the actuation of the joints of the lower limbs or by the ground perturbations. Commonly, an IMU comprises a collection of gyroscopes and accelerometers, which can provide velocity and acceleration readings respectively. Position readings are also possible by using estimation algorithms. These readings can be used to achieve a corrective action in the ankle and hip joints of the robot against ground perturbations. Here, the knee joints are not used, because they are only useful in the sagittal plane, whereas the goal is to design a universal controller which is useful in both planes: sagittal and frontal.

The robot inclination, can be modeled including a rotation of the robot about the ground, under the assumption that the foot height is negligible, as can be seen in Fig. 5.2. Because the IMU is located in the chest of the NAO robot, the IMU angle reading q_m includes the angle of inclination of the ground q_g , the angle of the ankle q_1 and the angle of the hip q_2 , as shown by Eq. 5.1.

$$q_m = q_g + q_1 + q_2 \quad (5.1)$$

To estimate the angle of the ground, Eq. 5.2 has to be considered.

$$q_g = q_m - (q_1 + q_2) \quad (5.2)$$

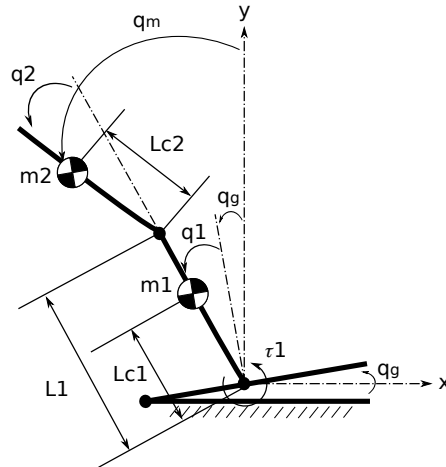


Figure 5.2: Dynamic control model based on the double inverted pendulum with a hip and ankle strategy control

Appendix A

Background Theory

In this section, the mathematical fundamentals necessary to understand the work in this dissertation are reviewed. The background theory regarding the direct and inverse kinematics as well as the trajectory planning are revised.

A.1 Manipulator Kinematics

Information in the following section can be found in [Craig (2005)]. The kinematics is the science which analyzes the movement without considering the forces that causes it. To understand the complicated geometry of the manipulator, typically, frames are added to the parts of the mechanism and then relations among the frames are described. The central topic, is the calculus of the position and orientation of the end-effector relative to the base, as a function of the variables of the articulations.

A manipulator can be considered as a set of links connected into a chain-like form by means of articulations. Generally, the articulations are designed to have only one degree of freedom, but they can be modeled as n articulations with a single degree of freedom if they have n degrees of freedom.

The links are named from the stationary base which can be named link 0. The first mobile link is named link 1, and so on up to link n . To locate an end-effector into the 3D space, six degrees of freedom are required as a minimum.

Figure A.1 shows the line mutually perpendicular over which the distance a_{i-1} of the link is measured. The torsion of link $i - 1$, i.e., α_{i-1} can be measured by projecting axes $i - 1$ and i into a plane whose normal direction is over the line a_{i-1} and estimating the angle between such projections using the right-hand rule from axis $i - 1$ towards axis i . In the especial case of having perpendicular axes, the torsion is measured in the plane containing both axes, but the sign of α_{i-1} is lost. If so, we are free to choose the sign of α_{i-1} arbitrarily.

The signed displacement over the i axis is called d_i , and it is variable if the articulation i is prismatic. The angle of the articulation θ_i , describes the amount of rotation over the i axis between link a_{i-1} and a_i .

In the case of an angular articulation, θ_i is variable and the other parameters are fixed. There exists a convention to assign these quantities called the **Denavit-Hartenberg** convention.

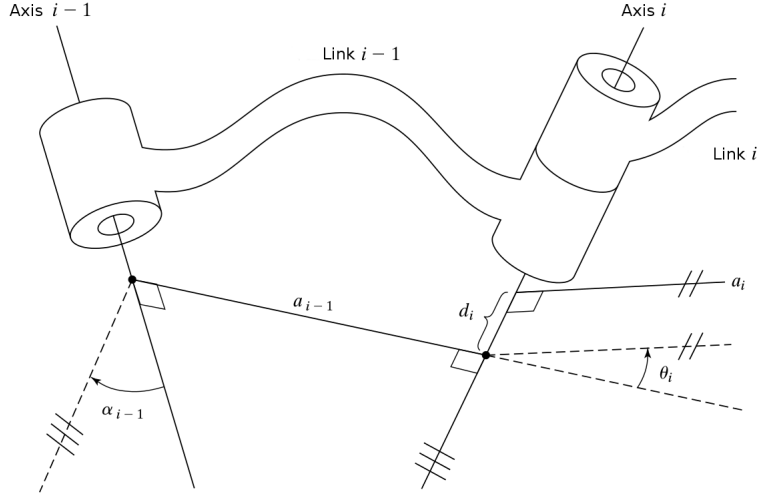


Figure A.1: Link and articulation nomenclature

A.1.1 Direct Kinematics

The information in the following subsection can be found in [Craig (2005)]. To be able to describe the location of each of the links and their adjacent links, we define a frame for each link. The chosen convention is defined as follows: The \hat{Z}_i axis of the frame i , called \hat{Z}_i , is coincident with the articulation i axis. The origin of frame i is located where the perpendicular line a_i intersects with the axis of articulation i . \hat{X}_i is directed towards a_i from articulation i to articulation $i + 1$. We define α_i by measuring it in the sense of the right-hand rule over the \hat{X}_i . Axis \hat{Y}_i is chosen to follow the right-hand rule to complete the i -th frame. Figure A.2 shows the location of frames $i - 1$ and i for a general manipulator.

If the frames are assigned according to the Denavit-Hartenberg convention, the following definitions are valid:

- a_i = The distance from \hat{Z}_i to \hat{Z}_{i+1} measured along \hat{X}_i .
- α_i = The angle from \hat{Z}_i to \hat{Z}_{i+1} measured along \hat{X}_i .
- d_i = The distance from \hat{X}_{i-1} to \hat{X}_i measured along \hat{Z}_i .
- θ_i = The angle from \hat{X}_{i-1} to \hat{X}_i along \hat{Z}_i .

Generally, we chose $a_i > 0$; however, α_i , d_i and θ_i are quantities with sign. The convention used in here, does not represent the only way to assign frames to the links. First of all, when we align \hat{Z}_i with the articulation i axis, there are two possible directions in which \hat{Z}_i

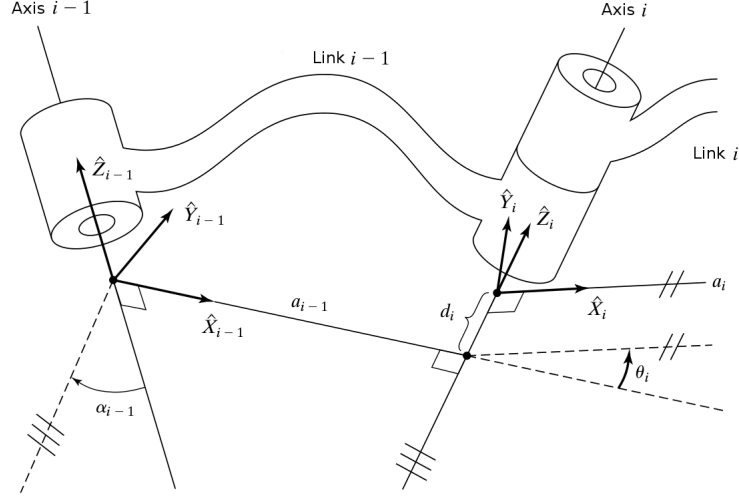


Figure A.2: Frame convention

could be pointing. Even more, in the case of having two intersecting articulation axes (i.e., $a_i = 0$) there are two options to choose of the direction of \hat{X}_i .

As an example, Figure A.3 can be considered. It shows a planar arm comprised of three links. As all articulations are angular, it is known as a RRR mechanism. We start by defining the reference frame, which it is called frame $\{0\}$. This frame is fixed to the base and it is aligned with the frame $\{1\}$ when the first articulation variable is θ_1 is zero. Axis \hat{Z}_0 is aligned with the articulation 1. As the arm is located into a plane, all axes \hat{Z} are parallel and all d_i are zero. When all articulations are set in zero degrees, all axes \hat{X} must be aligned. Table A.1.1 shows the link parameters.

Table A.1: Link parameters of a 3DOF mechanism

i	α_{i-1}	\mathbf{a}_{i-1}	θ_i	\mathbf{d}_i
1	0	0	θ_1	0
2	0	L_1	θ_2	0
3	0	L_2	θ_3	0

If it is desired to build the transformation which defines frame $\{i\}$ relative to frame $\{i-1\}$, then, each one of these transformations will be a function on only one parameter and simple enough so it can be written by inspection, as shown by Eq. (A.1).

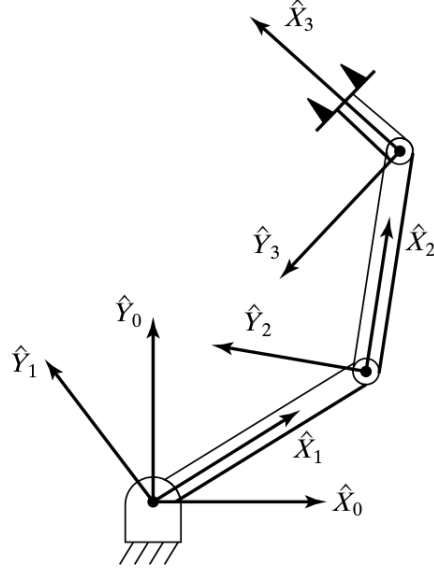


Figure A.3: Frame assignment

$${}^i{}_{i-1}T = R_X(\alpha_{i-1})D_X(a_{i-1})R_Z(\theta_i)D_Z(d_i) \quad (\text{A.1})$$

Carrying out the multiplication in Eq. (A.1) the general form of ${}^i{}_{i-1}T$ is shown in Eq. (A.2).

$${}^i{}_{i-1}T = \begin{bmatrix} C\theta_i & -S\theta_i & 0 & a_{i-1} \\ S\theta_i C\alpha_{i-1} & C\theta_i C\alpha_{i-1} & -S\alpha_{i-1} & -S\alpha_{i-1}d_i \\ S\theta_i S\alpha_{i-1} & C\theta_i S\alpha_{i-1} & C\alpha_{i-1} & C\alpha_{i-1}d_i \\ 0 & 0 & 0 & 1 \end{bmatrix} \quad (\text{A.2})$$

Once all frames and link parameters have been defined, the link transformations can be multiplied to find the relation of frame $\{N\}$ to frame $\{0\}$, as shown in Eq. (A.3).

$${}^0{}_N T = {}^0{}_1 T {}^1{}_2 T {}^2{}_3 T \dots {}^{N-1}{}_N T \quad (\text{A.3})$$

A.1.2 Inverse Kinematics

Information in this subsection is taken from reference [Craig (2005)]. Here, the problem of finding the set of variables which accomplish a given position and orientation of the end-effector is addressed. The resulting equations are not-linear and transcendental, so they are difficult to solve. Given the numeric value of ${}^0{}_N T$, we try to find values for $\theta_1, \theta_2, \dots, \theta_N$. We

must worry about the existence of the solutions, the case of multiple solutions and the solving method.

The *workspace* is defined as the volumetric space in which is possible to drive the end-effector. In order for the existence of a solution, the destiny location must relay into the workspace. There are tow kinds of workspace: the *dexterous* and the *reachable* workspace. The dexterous workspace refers to the space that the end-effector can reach with all possible orientations. The reachable workspace is the space that the end-effector can reach with at least one orientation.

Another possible problem is having multiple solutions because the system has to be prepared to chose one. The criteria over the decision of taking one to other solution vary, but a wise solution would be to chose the closest one. The presence of obstacles would imply choosing the farthest solution. The physical limitations of the real articulations can also be a problem; for example, the workspace of a robot can be limited when their rotational articulations can not rotate up to 360 degrees.

Unlike linear equations, there are no general algorithms that can be applied to solve a set of non-linear equations. The solutions of those equations can be divided into tow groups: Analytic (closed-form solutions) and numeric. In the case of multiple solutions, the numerical methods do not guarantee the finding of all the solutions; and because of their iterative nature, the numeric solutions are slower. Consider that an analytic solution is the one which is based on polynomial form with the need of no iteration. The analytic solutions can be sub-divided into two methods: the algebraic and the geometric. They are similar in the sense that the geometric approach make use of algebraic expressions. Only in special cases, the robots with six degrees of freedom can be solved analytically. One sufficient condition so that the manipulator has a solution in a closed form, is that three adjacent axes intersect in one point.

As an example, consider the manipulator in Fig. A.3. The link parameters can be used to find the kinematic equation of this arm, as shown by Eq. (A.4).

$${}^0_3T = \begin{bmatrix} C_{123} & -S_{123} & 0.0 & l_1C_1 + l_2C_{12} \\ S_{123} & C_{123} & 0.0 & l_1S_1 + l_2S_{12} \\ 0.0 & 0.0 & 1.0 & 0.0 \\ 0 & 0 & 0 & 1 \end{bmatrix} = \begin{bmatrix} C_\phi & -S_\phi & 0.0 & x \\ S_\phi & C_\phi & 0.0 & y \\ 0.0 & 0.0 & 1.0 & 0.0 \\ 0 & 0 & 0 & 1 \end{bmatrix} \quad (\text{A.4})$$

If we want to use the *analytic method*, then four on-linear equations are obtained from Eq. (A.4) which must be solved (see Eqns. (A.5) to (A.8)). Here, C_{123} stands for $\cos(\theta_1 + \theta_2 + \theta_3)$. A similar situation is suggested for the additional terms.

$$C_\phi = C_{123} \quad (\text{A.5})$$

$$S_\phi = S_{123} \quad (\text{A.6})$$

$$x = l_1C_1 + l_2C_{12} \quad (\text{A.7})$$

$$y = l_1 S_1 + l_2 S_{12} \quad (\text{A.8})$$

Squaring and adding Eqns. (A.7) and (A.8), we have:

$$x^2 + y^2 = l_1^2 + l_2^2 + 2 l_1 l_2 C_2 \quad (\text{A.9})$$

Solving for C_2 in Eq. (A.9):

$$C_2 = \frac{x^2 + y^2 - l_1^2 - l_2^2}{2 l_1 l_2} \quad (\text{A.10})$$

Assuming that the destiny is within the workspace, S_2 can be calculated as:

$$S_2 = \sqrt{1 - C_2^2} \quad (\text{A.11})$$

At last, θ_2 can be obtained as indicated by Eq. (A.12), where $atan2$ is the inverse tangential function of two arguments.

$$\theta_2 = atan2(S_2, C_2) \quad (\text{A.12})$$

After solving θ_2 we can write:

$$x = k_1 C_1 - k_2 S_1 \quad (\text{A.13})$$

$$y = k_1 S_1 - k_2 C_1 \quad (\text{A.14})$$

$$k_1 = l_1 + l_2 C_2 \quad (\text{A.15})$$

$$k_2 = l_2 S_2 \quad (\text{A.16})$$

Performing a change of variable:

$$r = +\sqrt{k_1^2 + k_2^2} \quad (\text{A.17})$$

$$\gamma = atan2(k_2, k_1) \quad (\text{A.18})$$

$$k_1 = r \cos(\gamma) \quad (\text{A.19})$$

$$k_2 = r \sin(\gamma) \quad (\text{A.20})$$

The Equations (A.13) and (A.13) can be written as:

$$\frac{x}{r} = \cos(\gamma) \cos(\theta_1) - \sin(\gamma) \sin(\theta_1) \quad (\text{A.21})$$

$$\frac{y}{r} = \cos(\gamma) \sin(\theta_1) + \sin(\gamma) \cos(\theta_1) \quad (\text{A.22})$$

Therefore,

$$\cos(\gamma + \theta_1) = \frac{x}{r} \quad (\text{A.23})$$

$$\sin(\gamma + \theta_1) = \frac{y}{r} \quad (\text{A.24})$$

Using the two-argument inverse tangential function:

$$\gamma + \theta_1 = \text{atan2}\left(\frac{y}{r}, \frac{x}{r}\right) = \text{atan2}(y, x) \quad (\text{A.25})$$

Therefore,

$$\theta_1 = \text{atan2}(y, x) - \text{atan2}(k_2, k_1) \quad (\text{A.26})$$

Finally we can solve for θ_3 from:

$$\theta_1 + \theta_2 + \theta_3 = \text{atan2}(S_\phi, C_\phi) = \phi \quad (\text{A.27})$$

In regard to the geometric method, we seek to decompose the spatial geometry of the arm in several sub-problems of plane geometry. As an example, look at Fig. (A.4) where a 3DOF arm is shown. Here, the figure shows the triangle formed by L_1 , L_2 and a line which binds the frame $\{0\}$ with the origin of the frame $\{3\}$. The dotted lines represent another possible configuration that leads to the same position. Considering the solid triangle, we can apply the cosine law and solve for θ_2 as shown in Eq. (A.28). Now, $\cos(180 + \theta_2) = -\cos(\theta_2)$ and obtain Eq. (A.29).

$$x^2 + y^2 = L_1^2 + L_2^2 - 2L_1L_2 \cos(180 + \theta_2) \quad (\text{A.28})$$

$$C_2 = \frac{x^2 + y^2 - L_1^2 - L_2^2}{2L_1L_2} \quad (\text{A.29})$$

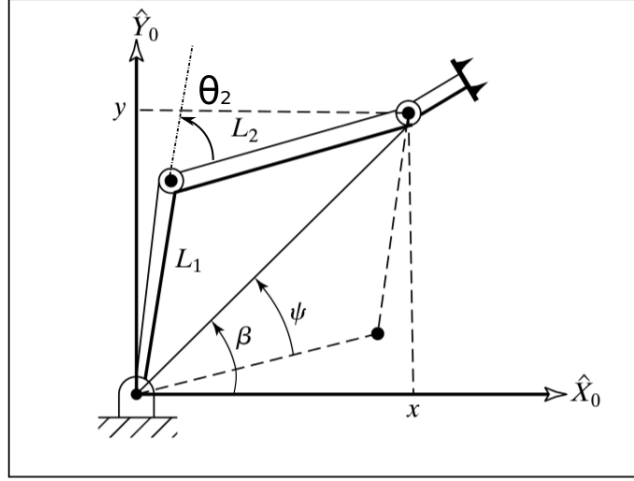


Figure A.4: Planar geometry associated with a 3 DOF robot

In order for the triangle to exist, the distance to the destiny point $\sqrt{x^2 + y^2}$ must be less or equal to the sum of the dimensions of $L_1 + L_2$. A computer software should check this issue. The other possible solution, can be found by symmetry when $\theta'_2 = -\theta_2$.

$$\beta = \text{atan2}(y, x) \quad (\text{A.30})$$

Again, we apply the cosine law to find ψ .

$$\cos(\psi) = \frac{x^2 + y^2 + L_1^2 - L_2^2}{2L_1\sqrt{x^2 + y^2}} \quad (\text{A.31})$$

$$\theta_1 = \beta \pm \psi \quad (\text{A.32})$$

We know that the angles in a plane are summed, that is why the orientation of the tool is given by $\theta_1 + \theta_2 + \theta_3$.

A.2 Trajectory Planning

The theory in the following subsection is taken from [Spong et al. (2006)]. A path from q_{init} to q_{final} is defined as a continuous map. A *trajectory* is a function of time $q(t)$ such that $q(t_0) = q_{init}$ and $q(t_f) = q_{final}$, where $q(t)$ could be referred to an angular or a Cartesian position (according to the particular case). Since the trajectory is parameterized by time, we can compute velocities and accelerations along the trajectories by differentiation.

A path planning algorithm will give only a sequence of points. In some cases, paths are specified by giving a sequence of end-effector poses; in this case, the inverse kinematics solution must be used to convert this to a sequence of joint configurations. A common way to specify paths for industrial robots is to physically lead the robot through the desired motion with a teach pendant: If no obstacles are present, the manipulator is essentially unconstrained: it is often the case that a manipulator motion can be decomposed into segments consisting of free motions, shown in Fig. A.5. During the free motion, the manipulator can move very fast since no obstacles are nearby. In some cases, there may be constraints on the trajectory (e.g. the robot must start and end with zero velocity). Nevertheless, it is easy to realize that there are infinitely many trajectories that will satisfy a finite number of constraints on the endpoints. It is common practice to choose trajectory from a finitely parameterizable family, for example, polynomials of degree n , with n dependent constraints to be satisfied.

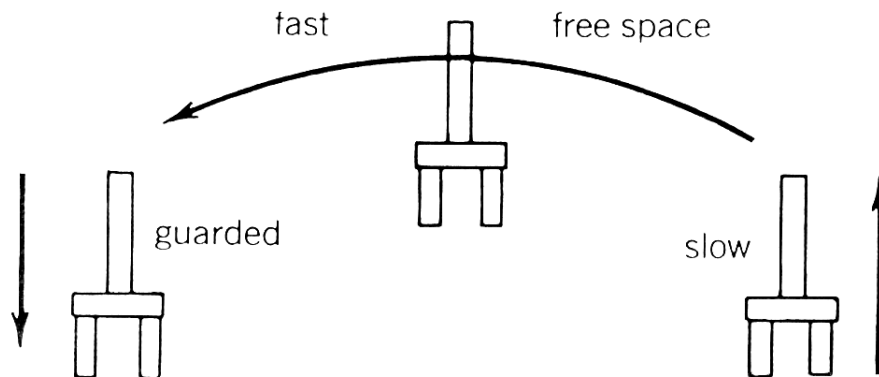


Figure A.5: Free motion

As described above, the problem here is to find a trajectory that connects an initial to a final configuration while satisfying other specified constraints (e.g. velocity and/or acceleration constraints).

Supposing that at time t_0 the joint variable satisfies

$$q(t_0) = q_0 \tag{A.33}$$

$$\dot{q}(t_0) = v_0 \tag{A.34}$$

and we wish to attain the values at t_f

$$q(t_f) = q_f \quad (\text{A.35})$$

$$\dot{q}(t_f) = v_f \quad (\text{A.36})$$

Figure A.6 shows a suitable trajectory for this motion. In addition, we may wish to specify the constraints on initial and final accelerations. In this case we have two additional equations.

$$\ddot{q}(t_0) = \alpha_0 \quad (\text{A.37})$$

$$\ddot{q}(t_f) = \alpha_f \quad (\text{A.38})$$

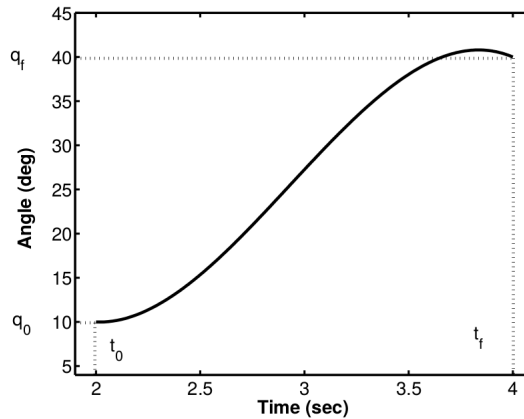


Figure A.6: Joint Space Trajectory

A.2.1 Cubic Polynomial Trajectories

Suppose that we wish to generate a trajectory between two configurations, and that we wish to specify the start and end velocities for the trajectory. One way to generate a smooth curve such as that shown in Figure A.6 is by a polynomial function of t . If we have four constraints to satisfy, such as (A.33) to (A.38), we require a polynomial with four independent coefficients that can be chosen to satisfy the constraints. Thus, we consider a cubic trajectory of the form

$$q(t) = a_0 + a_1t + a_2t^2 + a_3t^3 \quad (\text{A.39})$$

Then the desired velocity is given as

$$\dot{q}(t) = a_1 + 2a_2t + 3a_3t^2 \quad (\text{A.40})$$

Combining Eqns. (A.39) and (A.40) with four constraints yields four equations and four unknowns.

$$q_0 = a_0 + a_1t_0 + a_2t_0^2 + a_3t_0^3 \quad (\text{A.41})$$

$$v_0 = a_1 + 2a_2t_0 + 3a_3t_0^2 \quad (\text{A.42})$$

$$q_f = a_0 + a_1t_f + a_2t_f^2 + a_3t_f^3 \quad (\text{A.43})$$

$$v_f = a_1 + 2a_2t_f + 3a_3t_f^2 \quad (\text{A.44})$$

These four equations can be combined into a single matrix equation

$$\begin{bmatrix} 1 & t_0 & t_0^2 & t_0^3 \\ 0 & 1 & 2t_0 & 3t_0^2 \\ 1 & t_f & t_f^2 & t_f^3 \\ 0 & 1 & 2t_f & 3t_f^2 \end{bmatrix} \begin{bmatrix} a_0 \\ a_1 \\ a_2 \\ a_3 \end{bmatrix} = \begin{bmatrix} q_0 \\ v_0 \\ q_f \\ v_f \end{bmatrix} \quad (\text{A.45})$$

It can be shown that the determinant for the coefficient matrix in Eq. (A.45) always has a unique solution provided a nonzero time interval is allowed for the execution of the trajectory.

Writing Eq. (A.45) as

$$\mathbf{M}\mathbf{a} = \mathbf{b} \quad (\text{A.46})$$

The solution can be computed as

$$\mathbf{a} = \mathbf{M}^{-1}\mathbf{b} \quad (\text{A.47})$$

As an illustrative example, we may consider the special case that the initial and final velocities are zero (i.e., $v_0 = 0$ and $v_f = 0$). Suppose we take $t_0 = 0$ and $t_f = 1$. Thus, we want to go from the initial position q_0 to the final position q_f in 1 second, Then we obtain Eq. A.48.

$$\begin{bmatrix} 1 & 0 & 0 & 0 \\ 0 & 1 & 0 & 0 \\ 1 & 1 & 1 & 1 \\ 0 & 1 & 2 & 3 \end{bmatrix} \begin{bmatrix} a_0 \\ a_1 \\ a_2 \\ a_3 \end{bmatrix} = \begin{bmatrix} q_0 \\ 0 \\ q_f \\ 0 \end{bmatrix} \quad (\text{A.48})$$

Equation (A.48) can be solved to yield

$$a_0 = q_0 \quad (\text{A.49})$$

$$a_1 = 0 \quad (\text{A.50})$$

$$a_2 = 3(q_f - q_0) \quad (\text{A.51})$$

$$a_3 = -2(q_f - q_0) \quad (\text{A.52})$$

The required cubic polynomial function is therefore

$$q_i(t) = q_0 + 3(q_f - q_0)t^2 - 2(q_f - q_0)t^3 \quad (\text{A.53})$$

Figure A.7 shows this trajectory with $q_0 = 10^\circ$ and $q_f = -20^\circ$. The corresponding velocity and acceleration curves are given as well.

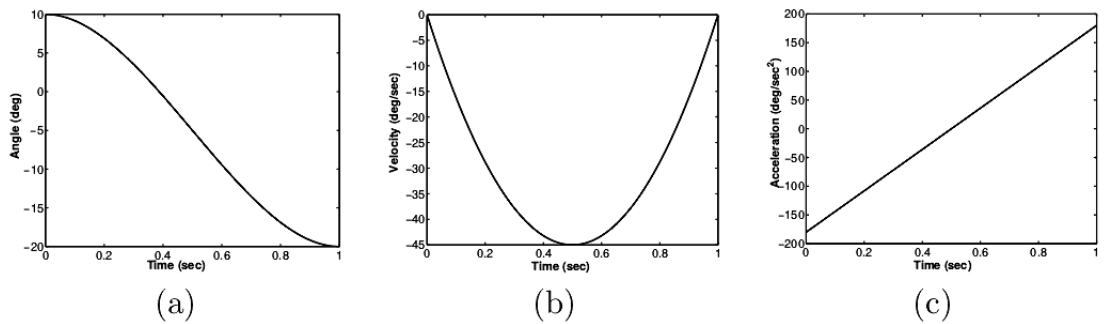


Figure A.7: (a) Cubic polynomial trajectory (b) Velocity profile (c) Acceleration profile

A.2.2 Quintic Polynomial Trajectories

As can be seen in Fig. A.7, a cubic trajectory gives continuous positions and velocities at the start and finish points, but it admits acceleration discontinuities. The derivative of the acceleration is called the *jerk*. A discontinuity in acceleration leads to an impulsive jerk, which may excite vibrational modes and reduce tracking accuracy. For this reason, one may wish to specify constraints on the acceleration as well as on the position and velocity. In this case, we have six constraints (one each for initial and final configurations, initial and final velocities, and initial and final accelerations). Therefore, we require a fifth order polynomial

$$q(t) = a_0 + a_1(t) + a_2(t)^2 + a_3(t)^3 + a_4(t)^4 + a_5(t)^5 \quad (\text{A.54})$$

Considering the initial conditions, such as the initial position $q(t_0)$, the initial velocity $v(t_0)$, and the initial acceleration $\alpha(t_0)$; as well as the final conditions, such as the final position $q(t_f)$, the final velocity $v(t_f)$, and the final acceleration $\alpha(t_f)$; and writing the appropriate number of derivatives, we obtain the Eqns. in (A.55); where t_0 and t_f refer to the initial and final time.

$$\begin{aligned} q(t_0) &= a_0 + a_1(t_0) + a_2(t_0)^2 + a_3(t_0)^3 + a_4(t_0)^4 + a_5(t_0)^5 \\ v(t_0) &= a_1 + 2a_2(t_0) + 3a_3(t_0)^2 + 4a_4(t_0)^3 + 5a_5(t_0)^4 \\ \alpha(t_0) &= 2a_2 + 6a_3(t_0) + 12a_4(t_0)^2 + 20a_5(t_0)^3 \\ q(t_f) &= a_0 + a_1(t_f) + a_2(t_f)^2 + a_3(t_f)^3 + a_4(t_f)^4 + a_5(t_f)^5 \\ v(t_f) &= a_1 + 2a_2(t_f) + 3a_3(t_f)^2 + 4a_4(t_f)^3 + 5a_5(t_f)^4 \\ \alpha(t_f) &= 2a_2 + 6a_3(t_f) + 12a_4(t_f)^2 + 20a_5(t_f)^3 \end{aligned} \quad (\text{A.55})$$

Equations in (A.55) can be written in matrix form as shown in Eq. (A.56).

$$\begin{bmatrix} 1 & t_0 & t_0^2 & t_0^3 & t_0^4 & t_0^5 \\ 0 & 1 & 2t_0 & 3t_0^2 & 4t_0^3 & 5t_0^4 \\ 0 & 0 & 2 & 6t_0 & 12t_0^2 & 20t_0^3 \\ 1 & t_f & t_f^2 & t_f^3 & t_f^4 & t_f^5 \\ 0 & 1 & 2t_f & 3t_f^2 & 4t_f^3 & 5t_f^4 \\ 0 & 0 & 2 & 6t_f & 12t_f^2 & 20t_f^3 \end{bmatrix} \begin{bmatrix} a_0 \\ a_1 \\ a_2 \\ a_3 \\ a_4 \\ a_5 \end{bmatrix} = \begin{bmatrix} q_0 \\ v_0 \\ \alpha_0 \\ q_f \\ v_f \\ \alpha_f \end{bmatrix} \quad (\text{A.56})$$

Figure A.8 shows a quintic polynomial trajectory with $q(0) = 0$, $q(2) = 20$ with zero initial and final velocities and accelerations.

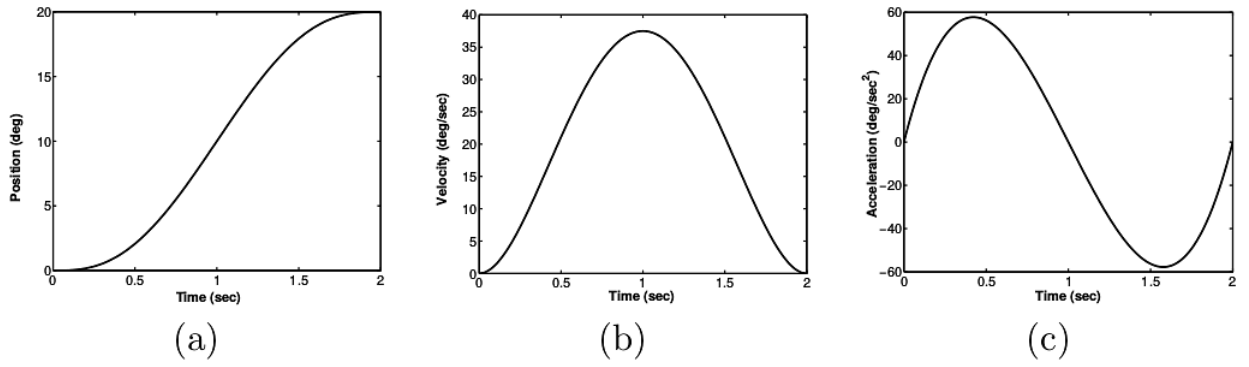


Figure A.8: (a) Quintic polynomial trajectory (b) Velocity profile (c) Acceleration profile

Appendix B

The Jacobian in Robotics

B.1 Inverse Kinematics Iterative Technique based in the Jacobian

As shown in [Jazar (2010)], the inverse kinematics problem can be interpreted as searching for the solution q_k of a set of non-linear algebraic equations

$${}^0T_n = \mathbf{T}(\mathbf{q}) = {}^0T_1(q_1) {}^1T_2(q_2) {}^2T_3(q_3) {}^3T_4(q_4) \cdots {}^{n-1}T_n(q_n)$$

The most common iterative method is the *Newton-Raphson method*. For variables \mathbf{q} , we start with an initial guess \mathbf{q}^* for the joint variables.

$$\mathbf{q}^* = \mathbf{q} + \delta\mathbf{q}$$

Using the forward kinematics, we can determine the configuration of the end-effector for the guessed joint variables.

$$\mathbf{T}^* = \mathbf{T}(\mathbf{q}^*)$$

The difference between the configuration calculated with the forward kinematics and the desired configuration \mathbf{T} represents an error $\delta\mathbf{T}$, which must be minimized.

$$\delta\mathbf{T} = \mathbf{T} - \mathbf{T}^*$$

A first Taylor expansion of the set of equations is:

$$\mathbf{T} = \mathbf{T}(\mathbf{q}^* - \delta\mathbf{q}) = \mathbf{T}(\mathbf{q}^*) + \frac{\partial\mathbf{T}}{\partial\mathbf{q}}\delta\mathbf{q} + O(\delta\mathbf{q}^2)$$

Assuming $\delta \mathbf{q} \ll \mathbf{I}$ allows for working with a set of linear equations

$$\delta \mathbf{T} = \mathbf{J} \delta \mathbf{q}$$

Where \mathbf{J} is the Jacobian matrix of the set of equations. The change in the joint variables can be written as

$$\delta \mathbf{q} = \mathbf{J}^{-1} \delta \mathbf{T}$$

Therefore, the unknown variables \mathbf{q} are:

$$\mathbf{q} = \mathbf{q}^* + \mathbf{J}^{-1} \delta \mathbf{T}$$

Which can be used as a new approximation to converge to a solution

$$\mathbf{q}^{(i+1)} = \mathbf{q}^{(i)} + \mathbf{J}^{-1}(\mathbf{q}^{(i)}) \delta \mathbf{T}(\mathbf{q}^{(i)})$$

References

- Abdolmaleki, A., GhasemAghaee, N., Reza, M., and Monadjemi, A. (2011). Robust humanoid turning-in-place using fourier series and genetic algorithm. In *2011 Fourth International Conference on Modeling, Simulation and Applied Optimization*. DOI: 10.1109/ICMSAO.2011.5775489.
- Aldebaran (2010). Aldebaran Robotics: Humanoid Robotics. <https://www.softbankrobotics.com/emea/en/nao>. Accessed: 8/April/2019.
- Almusawi, A. R., Dülger, L. C., and Kapucu, S. (2016). A new artificial neural network approach in solving inverse kinematics of robotic arm (Denso VP6242). *Computational intelligence and neuroscience*, 2016. DOI: 10.1155/2016/5720163.
- Craig, J. J. (2005). *Introduction to robotics: mechanics and control*, volume 3. Pearson Prentice Hall Upper Saddle River.
- ESI-Group (2019). Scilab [Computer Software]. <https://www.scilab.org/>. Accessed: 10/March/2019.
- Faraji, S. and Ijspeert, A. J. (2017). Singularity-Tolerant Inverse Kinematics for Bipedal Robots: An Efficient Use of Computational Power to Reduce Energy Consumption. *IEEE Robotics and Automation Letters*, 2(2):1132–1139. DOI:10.1109/lra.2017.2661810.
- Gouaillier, D., Hugel, V., Blazevic, P., Kilner, C., Monceaux, J., Lafourcade, P., Marnier, B., Serre, J., and Maisonnier, B. (2009). Mechatronic design of NAO humanoid. In *Robotics and Automation, 2009. ICRA'09. IEEE International Conference on*, pages 769–774. IEEE. DOI: 10.1109/ROBOT.2009.5152516.
- Graf, C., Härtl, A., Röfer, T., and Laue, T. (2009). A robust closed-loop gait for the standard platform league humanoid. In *Proceedings of the Fourth Workshop on Humanoid Soccer Robots*, pages 30–37.
- Graf, C. and Röfer, T. (2010). A closed-loop 3D-LIPM gait for the RoboCup Standard Platform League humanoid. In *Proceedings of the Fifth Workshop on Humanoid Soccer Robots*.
- Heo, J.-W. and Oh, J.-H. (2015). Biped walking pattern generation using an analytic method for a unit step with a stationary time interval between steps. *Industrial Electronics, IEEE Transactions on*, 62(2):1091–1100. DOI: 10.1109/TIE.2014.2359418.
- Hernández-Santos, C., Rodríguez-Leal, E., Soto, R., and Gordillo, J. (2012). Kinematics and dynamics of a new 16 DOF humanoid biped robot with active toe joint. *International Journal of Advanced Robotic Systems*, 9. DOI: 10.5772/52452.
- Ho, T., Kang, C.-G., and Lee, S. (2012). Efficient closed-form solution of inverse kinematics for a specific six-DOF arm. *International Journal of Control, Automation and Systems*, 10(3):567–573. DOI: 10.1007/s12555-012-0313-9.

- Ishida, T. (2004). Development of a small biped entertainment robot QRIO. In *Micro-Nanomechatronics and Human Science, 2004 and The Fourth Symposium Micro-Nanomechatronics for Information-Based Society, 2004. Proceedings of the 2004 International Symposium on*. DOI: 10.1109/MHS.2004.1421265.
- Jazar, R. N. (2010). *Theory of applied robotics: kinematics, dynamics, and control*. Springer Science & Business Media.
- Jiang, L., Sun, D., and Liu, H. (2009). An inverse-kinematics table-based solution of a humanoid robot finger with nonlinearly coupled joints. *IEEE/ASME Transactions on Mechatronics*, 14(3):273–281. DOI: 10.1109/TMECH.2008.2005581.
- Kajita, S., Hirukawa, H., Harada, K., and Yokoi, K. (2014). *Introduction to humanoid robotics*, volume 101. Springer.
- Kajita, S., Kanehiro, F., Kaneko, K., Fujiwara, K., Harada, K., Yokoi, K., and Hirukawa, H. (2003). Biped walking pattern generation by using preview control of zero-moment point. In *Robotics and Automation, 2003. Proceedings. ICRA'03. IEEE International Conference on*, volume 2, pages 1620–1626. IEEE. DOI: 10.1109/ROBOT.2003.1241826.
- Kajita, S., Kanehiro, F., Kaneko, K., Fujiwara, K., Yokoi, K., and Hirukawa, H. (2002). A realtime pattern generator for biped walking. In *Robotics and Automation, 2002. Proceedings. ICRA'02. IEEE International Conference on*, volume 1, pages 31–37. IEEE. DOI: 10.1109/ROBOT.2002.1013335.
- Kaneko, K., Kaminaga, H., Sakaguchi, T., Kajita, S., Morisawa, M., Kumagai, I., and Kanehiro, F. (2019). Humanoid Robot HRP-5P: An Electrically Actuated Humanoid Robot With High-Power and Wide-Range Joints. *IEEE Robotics and Automation Letters*, 4(2):1431–1438. DOI:10.1109/lra.2019.2896465.
- Kanoun, O., Laumond, J.-P., and Yoshida, E. (2010). Planning foot placements for a humanoid robot: A problem of inverse kinematics. *The International Journal of Robotics Research*. DOI: 10.1177/0278364910371238.
- Kaynov, D. (2010). *Open Motion Architecture for Humanoid Robots*. Lambert Academic Publishing.
- Kim, J.-Y., Lee, J., and Ho, J.-H. (2007). Experimental realization of dynamic walking for a human-riding biped robot, HUBO FX-1. *Advanced Robotics*, 21(3-4):461–484. DOI: 10.1163/156855307780132063.
- Kofinas, N., Orfanoudakis, E., and Lagoudakis, M. G. (2013). Complete analytical inverse kinematics for NAO. In *Autonomous Robot Systems (Robotica), 2013 13th International Conference on*, pages 1–6. IEEE. DOI: 10.1109/Robotica.2013.6623524.
- Kofinas, N., Orfanoudakis, E., and Lagoudakis, M. G. (2014). Complete analytical forward and inverse kinematics for the NAO humanoid robot. *Journal of Intelligent & Robotic Systems*, 77(2):251–264. DOI: 10.1007/s10846-013-0015-4.
- Li, T.-H. S., Ho, Y.-F., Kuo, P.-H., Ye, Y.-T., and Wu, L.-F. (2017). Natural Walking Reference Generation Based on Double-Link LIPM Gait Planning Algorithm. *IEEE Access*, 5:2459–2469. DOI:10.1109/access.2017.2669209.
- Liu, C., Zhang, T., Zhang, C., Liu, M., and Chen, Q. (2019). Foot Placement Compensator Design for Humanoid Walking Based on Discrete Control Lyapunov Function. *IEEE Transactions on Systems, Man, and Cybernetics: Systems*, pages 1–10. DOI:10.1109/tsmc.2019.2912417.

- Luo, R. C., Chang, P. H., Sheng, J., Gu, S. C., and Chen, C. H. (2013). Arbitrary biped robot foot gaiting based on variate COM height. In *Humanoid Robots (Humanoids), 2013 13th IEEE-RAS International Conference on*, pages 534–539. IEEE. DOI: 10.1109/HUMANOIDS.2013.7030025.
- Mandava, R. K. and Vundavilli, P. R. (2016). Forward and inverse kinematic based full body gait generation of biped robot. In *Electrical, Electronics, and Optimization Techniques (ICEEOT), International Conference on*, pages 3301–3305. IEEE. DOI: 10.1109/ICEEOT.2016.7755317.
- Maplesoft (2019). Maple [Computer Software]. <https://www.maplesoft.com/MapleEducation/>. Accessed: 10/March/2019.
- Missura, M. and Behnke, S. (2014). Balanced walking with capture steps. In *Robot Soccer World Cup*, pages 3–15. Springer. DOI: 10.1007/978-3-319-18615-3_1.
- Nakos, G., Joyner, D., and George Nakos, D. J. (1999). *Álgebra lineal con aplicaciones*. Thomson.
- Nunez, J. V., Briseno, A., Rodriguez, D. A., Ibarra, J. M., and Rodriguez, V. M. (2012). Explicit analytic solution for inverse kinematics of bioloid humanoid robot. In *Robotics Symposium and Latin American Robotics Symposium (SBR-LARS), 2012 Brazilian*, pages 33–38. IEEE. DOI: 10.1109/SBR-LARS.2012.62.
- Ogawa, T. and Kanada, H. (2010). Solution for ill-posed inverse kinematics of robot arm by network inversion. *Journal of Robotics*, 2010. DOI: 10.1155/2010/870923.
- Olvera, L. I., Nuñez, J. V., and Pámanes, J. A. (2009). Evaluacion experimental de patrones de marcha cicloidales en el robot humanoide bioloid. In *Proc. of 9º Congreso Iberoamericano de Ingeniería Mecánica*, pages 149–156.
- Park, H. A., Ali, M. A., and Lee, C. G. (2012). Closed-form inverse kinematic position solution for humanoid robots. *International Journal of Humanoid Robotics*, 9(03):28 pages. DOI: 10.1142/S0219843612500223.
- Park, H. A. and Lee, C. G. (2013). Cooperative-dual-task-space-based whole-body motion balancing for humanoid robots. In *Robotics and Automation (ICRA), 2013 IEEE International Conference on*, pages 4797–4802. IEEE. DOI: 10.1109/ICRA.2013.6631261.
- Park, I.-W., Kim, J.-Y., Lee, J., and Oh, J.-H. (2006a). Online free walking trajectory generation for biped humanoid robot KHR-3 (HUBO). In *Robotics and Automation, 2006. ICRA 2006. Proceedings 2006 IEEE International Conference on*, pages 1231–1236. DOI: 10.1109/ROBOT.2006.1641877.
- Park, I.-W., Kim, J.-Y., and Oh, J.-H. (2006b). Online biped walking pattern generation for humanoid robot khr-3 (KAIST Humanoid Robot-3: HUBO). In *Humanoid Robots, 2006 6th IEEE-RAS International Conference on*, pages 398–403. DOI: 10.1109/ICHR.2006.321303.
- Pieper, D. L. (1968). The kinematics of manipulators under computer control. Technical report, Stanford University.
- Robotis (2016). DARwin-OP: Open Platform Humanoid Project. http://www.robotis.com/xe/darwin_en. Accessed: 2016-Apr-6.
- Said, A., Rodriguez-Leal, E., Soto, R., Gordillo, J., and Garrido, L. (2015). Decoupled Closed-Form Solution for Humanoid Lower Limb Kinematics. *Mathematical Problems in Engineering*, 2015. DOI: 10.1155/2015/437979.

- Sakagami, Y., Watanabe, R., Aoyama, C., Matsunaga, S., Higaki, N., and Fujimura, K. (2002). The intelligent ASIMO: System overview and integration. In *Intelligent Robots and Systems, 2002. IEEE/RSJ International Conference on*, volume 3, pages 2478–2483. IEEE. DOI: 10.1109/IRDS.2002.1041641.
- Shin, H.-K. and Kim, B. K. (2015). Energy-efficient gait planning and control for biped robots utilizing vertical body motion and allowable ZMP region. *IEEE Transactions on Industrial Electronics*, 62(4):2277–2286. DOI: 10.1109/TIE.2014.2360152.
- Siciliano, B., Sciavicco, L., Villani, L., and Oriolo, G. (2009). *Robotics: modelling, planning and control*. Springer Science & Business Media.
- Spong, M. W., Hutchinson, S., and Vidyasagar, M. (2006). *Robot modeling and control*. John Wiley & Sons.
- Strom, J., Slavov, G., and Chown, E. (2010). Omnidirectional walking using zmp and preview control for the nao humanoid robot. In *RoboCup 2009: robot soccer world cup XIII*, pages 378–389. Springer. DOI: 10.1007/978-3-642-11876-0_33.
- Tay, A. J. S. B. (2009). Walking Nao omnidirectional bipedal locomotion. The University of New South Wales.
- Todd, D. J. (2013). *Walking machines: an introduction to legged robots*. Springer Science & Business Media.
- Vukobratovic, M., Borovac, B., Surla, D., and Stokic, D. (1990). *Biped locomotion: dynamics, stability, control and application*. Springer Science & Business Media.
- Wang, J., Liu, S., Zhang, B., and Yu, C. (2019). Inverse kinematics-based motion planning for dual-arm robot with orientation constraints. *International Journal of Advanced Robotic Systems*, 16(2):172988141983685. DOI:10.1177/1729881419836858.
- Wong, C. and Liu, C. (2013). FPGA realisation of inverse kinematics for biped robot based on CORDIC. *Electronics Letters*, 49(5):332–334. DOI: 10.1049/e1.2012.4280.
- Zannatha, J. I. and Limón, R. C. (2009). Forward and inverse kinematics for a small-sized humanoid robot. In *Electrical, Communications, and Computers, 2009. CONIELECOMP 2009. International Conference on*, pages 111–118. IEEE. DOI: 10.1109/CONIELECOMP.2009.50.
- Zorjan, M. and Hugel, V. (2013). Generalized humanoid leg inverse kinematics to deal with singularities. In *Robotics and Automation (ICRA), 2013 IEEE International Conference on*, pages 4791–4796. IEEE. DOI: 10.1109/ICRA.2013.6631260.

Vita



Alejandro Rodríguez Said was born in Veracruz, Veracruz, México, on January 17th, 1983. He earned the B.S. degree in Mechatronics in 2006 and the M.S. degree in Electronic Systems in 2009 at Tecnológico de Monterrey. He obtained the PhD in 2019 from same institution in Information Technologies and Electronics. His research interests are: Robotics, Power Electronics, Artificial Intelligence, Embedded Programming, Control Engineering, and Signal Processing. Until now, he has published three first-author journal articles.

This document was typed in using L^AT_EX 2_ε^a by Alejandro Rodríguez Said.

^aThe style file `phdThesisFormat.sty` used to set up this dissertation was prepared by the Center of Intelligent Systems of the Instituto Tecnológico y de Estudios Superiores de Monterrey, Monterrey Campus